INVESTIGATION OF THE OZONE FORMATION POTENTIALS OF EXXSOL® D95, ISOPAR-M®, AND THE EXXATE® FLUIDS

Report to
ExxonMobil Corporation

by

William P. L. Carter, Dongmin Luo, and Irina L. Malkina

October 31, 2000

College of Engineering
Center for Environmental Research and Technology
University of California
Riverside, California 92521

00-AP-RT3L-001-FR

ABSTRACT

A series of environmental chamber experiments and computer model simulations were carried out to assess the atmospheric ozone formation potentials of the Exxsol® D95, Isopar® M and the Exxate® fluids (These names are trademarks of ExxonMobil Chemical Company). D95 is a petroleum-derived mixture of C_{12}-C_{15} normal, branched, and cyclic alkanes, Isopar-M is a mixture of primarily C_{11}-C_{16} branched alkanes made using an isomerization process, and the Exxate fluids are acetates of various branched alcohol mixtures in narrow weight ranges from C_6 to $C_{\sim 13}$. The experiments consisted of determining the effects on NO oxidation, ozone formation and OH radical levels when adding D95, Isopar-M, or Exxate 1000 to varying simulated model photochemical smog systems. The reactivity characteristics of these materials were very similar to those for other alkane mixtures and individual higher molecular weight alkanes in this weight range that have been studied. They were found to be inhibitors of radical levels under all conditions and to inhibit rates of NO oxidation and O_3 formation in experiments that are sensitive to radical effects, but to have relatively small effects on ozone in experiments more representative of atmospheric conditions. The results were used to determine whether we could accurately simulate the effects of these compounds on ozone formation and other manifestations of photochemical smog. Compositional information provided by ExxonMobil were used to derive compositions in terms of individual representative compounds, though assumptions had to be made concerning the appropriate compounds to represent the complex mixtures of branched and cyclic constituents. The models using these compositions and the SAPRC-99 mechanisms for the constituents gave reasonably good simulations to the results of most of the experiments, though the Isopar-M experiments were not simulated as well as the others. The models were then used to calculate ozone impacts of these materials in various urban photochemical smog scenarios. The impacts were on peak ozone yields were variable, but generally were 20-40% those of an equal mass of VOC emissions from all sources. The relative impacts on maximum 8-hour average ozone levels were generally less than their relative impacts on peak ozone levels, especially in scenarios with relatively low NO_x conditions. However, making alternative assumptions concerning the appropriate compounds to represent the constituents of Isopar-M affected atmospheric ozone yield impacts by ~40%, even though they did not affect the simulations of the chamber data. Therefore, it is important that the types of compounds present in these fluids be represented as accurately as possible, even when environmental chamber data are available to test model predictions.

ACKNOWLEDGEMENTS

The authors acknowledge Mr. Dennis Fitz for assistance in administering this program, Mr. Kurt Bumiller for assistance in carrying out the environmental chamber experiments, and Dr. Peter Ellis of ExxonMobil Chemical Company for providing compositional information on the fluids studied and for other helpful discussions.

This work was funded by ExxonMobil Chemical Company. However, the opinions and conclusions expressed in this report are entirely those of the primary author, Dr. William P. L. Carter. Mention of trade names or commercial products does not constitute endorsement or recommendation for use. Exxsol, Isopar, and Exxate, and Exxal are trademarks of ExxonMobil Chemical Company.

TABLE OF CONTENTS

LIST OF TABLES

LIST OF FIGURES

INTRODUCTION

Ozone in photochemical smog is formed from the gas-phase reactions of volatile organic compounds (VOCs) and oxides of nitrogen (NO_x) in sunlight. Although Houston and Los Angeles currently have the worst ozone problems in the United States, other areas of the country also have episodes where ozone exceeds the federal air quality standard. Ozone control strategies in the past have focused primarily on VOC controls, though the importance of NO_x control has become recognized in recent years. VOC and NO_x controls have differing effects on ozone formation. NO_x is required for ozone formation, and if the levels of NO_x are low compared to the levels of reactive VOCs, then changing VOC emissions will have relatively little effect on ozone. Since NO_x is removed from the atmosphere more rapidly than VOCs, ozone in areas far downwind from the primary sources tend to be more NO_x limited, and thus less responsive to VOC controls. VOC controls tend to reduce the rate that O_3 is formed when NO_x is present, so VOC controls are the most beneficial in reducing O_3 in the urban source areas, where NO_x is relatively plentiful, and where O_3 yields are determined primarily by how rapidly it is being formed. Because of this, any comprehensive ozone control strategy should involve reduction of emissions of both NO_x and VOCs.

Many different types of VOC compounds are emitted into the atmosphere, each reacting at different rates and having different mechanisms for their reactions. Because of this, they can differ significantly in their effects on ozone formation, or their "reactivity". Some compounds, such as CFCs, do not react in the lower atmosphere at all, and thus make no contribution to ground-level ozone formation. Others, such as methane, react and contribute to ozone formation, but react so slowly that their practical effect on ozone formation in urban atmospheres is negligible. Obviously, it does not make sense to regulate such compounds as ozone precursors. In recognition of this, the EPA has exempted certain compounds from such regulations on the basis of having "negligible" effects on ozone formation. Although the EPA has no formal policy on what constitutes "negligible" reactivity, in practice it has used the ozone formation potential of ethane as the standard in this regard. This is because ethane is the most reactive of the compounds that the EPA has exempted to date. Therefore, the ozone formation potential of a compound relative to ethane is of particular interest when assessing whether it might be a likely candidate for exemption from regulation as an ozone precursor.

Many VOCs that would not be judged to have "negligible" reactivity under the current criterion might still have much lower ozone formation potential than average, and substituting emissions of highly reactive VOCs with such moderate-to-low reactivity VOCs would be expected to result in air quality improvements. Although the current EPA policies do not encourage such substitutions, it has been proposed to implement reactivity-based policies in consumer product regulations in California (CARB, 1999), and the EPA is currently re-evaluating its reactivity-based VOC policies (Dimitriades, 1999, RRWG, 1999). Mc.Bride et al (1977) showed that adopting reactivity-based VOC control policies could result in significant cost savings in ozone reduction strategies, though a number of difficult policy and enforcement issues need to be resolved (RRWG, 1999). Regulatory approaches that appropriately deal

with differences in VOC reactivity are still evolving, but it is clear that producers of solvent VOCs will need to know how their VOCs might be classified under any such system, so they can appropriately adapt to reactivity-based policies once they are implemented. This requires an ability to reliably estimated the ozone impacts of the VOCs of interest.

The ozone impacts of VOCs depend on the environmental conditions where they are emitted (NRC, 1991; Carter and Atkinson, 1989; Carter, 1994a). Because of this the only practical way to quantify their atmospheric ozone impacts is to use computer airshed models to simulate their reactions in various urban or regional atmospheres. This requires knowledge of the relevant atmospheric reactions of the VOCs and developing a chemical mechanism for these reactions that can accurately predict how their reactions affect ozone formation under various conditions. Because of the complexity of the atmospheric reactions of most VOCs and the reactive intermediates and products formed, the predictive capabilities of these mechanisms need to be experimentally verified. This generally involves conducting appropriate environmental chamber experiments with the VOCs to determine their actual effects on ozone and other measures of reactivity under various relevant conditions, and then determining whether the mechanisms give predictions that are consistent with the results obtained (Jeffries et al, 1992). This approach has been used to evaluate the mechanisms for a wide variety of VOCs that are emitted into the atmosphere (Gery et al, 1988; Carter and Lurmann, 1990, 1991; Carter, 1995; Carter, 2000, and references therein).

Many types of VOC products emitted into the atmosphere are complex mixtures of many compounds that are difficult or impossible to identify or speciate exactly. Examples include mineral spirits and other petroleum distillate products that are widely used as solvents and in cleaning applications, or solvents consisting of complex mixtures made by various oligomerization processes. Evaluating the ozone impacts of such products requires either determining an appropriate model for their composition in terms of species that are representative of the distribution of the constituents. This can then be used with mechanisms for these actual or representative constituents to predict the ozone impacts of the mixtures. The utility of this approach can be evaluated by conducting environmental chamber experiments with the whole VOC products and then determining whether the results are consistent with the predictions of the model using the assumed distribution of constituents and their chemical mechanisms.

This approach has been successfully employed in a recently completed two-phase study to evaluate the ozone impacts of several mineral spirits samples that was carried out for Safety-Kleen Corporation (Carter et al, 1997a, 2000a). The mineral spirits samples studied were complex mixtures of normal, branched and cyclic alkanes in the C_{10}-C_{14} range, with one sample being a recycled material that also contained ~8% aromatics and alkenes by weight. The branched and cyclic alkane constituents could not be identified, but carbon number fractionation combined with GC-MS type analysis allowed the distributions of the general types of alkanes to be identified, and selected were used compounds to represent the branched and cyclic alkanes with the various carbon numbers. The initial modeling analysis of the experiments with these samples was not successful (Carter et al, 1997a), a recent re-analysis using an updated mechanism gave very good simulations of the environmental chamber data obtained (Carter et

al, 2000a). However, the types of mineral spirits samples studied were highly limited, and the applicability of this approach to petroleum-derived samples with different molecular weight ranges, or to complex mixtures that are not derived from petroleum fractions, has not been assessed.

Exxsol® D95, Isopar® M, and the Exxate® fluids[1] are solvents marketed by ExxonMobil chemical company whose normal uses may result in their being emitted into the atmosphere, where their constituents may react and contribute to the formation of ground-level photochemical ozone. Knowledge of the actual ozone impacts of these compounds is therefore of interest to ExxonMobil Corporation. D95 is a petroleum-derived mixture of normal, branched, and cyclic alkanes that is similar to the all-alkane mineral spirits studied for Safety-Kleen (Carter et al, 1997a, 2000a), but it has a higher carbon number range of C_{12} - C_{15}. Isopar-M is also an all-alkane material with a similar (though somewhat broader) molecular weight range as D95, but it is not petroleum-derived, and consists primarily of branched alkanes formed from an oligomerization process. Therefore, each of these is different in potentially significant ways from the mineral spirits samples that have been previously studied. The Exxate fluids are chemically different from the other fluids of interest, consisting of acetates of mixtures of branched alcohols in various weight ranges, with the specific fluid chosen for study, Exxate 1000, being acetates of primarily C_{10} alcohols, and having a similar volatility range as D95 and Isopar-M. Although mechanisms for individual esters have been studied, no data are available to evaluate mechanisms for complex mixtures of esters of branched alcohols in these weight ranges.

Because of this, Exxon (now ExxonMobil) Chemical Company contracted with the College of Engineering Center for Environmental Research and Technology (CE-CERT) to carry out an experimental and modeling study of the ozone impacts of these fluids. This involves (1) conducting environmental chamber experiments to determine the effects of the representative fluids on O_3 formation and other measures of air quality under various conditions; (2) developing models for their chemical composition using information supplied by ExxonMobil and other considerations; (3) evaluating models using these compositions and existing or estimated chemical mechanisms for their constituents by comparing their predictions against the environmental chamber data; and, if the models are found to adequately simulate the data obtained (4) conducting model simulations to determine their ozone impacts of these fluids under various conditions representative of polluted urban atmospheres, so they can be compared with ozone impact predictions for other types of VOCs. The results of this program are documented in this report.

[1] Exxsol, Isopar, and Exxate are registered trademarks of ExxonMobil Chemical company.

EXPERIMENTAL AND DATA ANALYSIS METHODS

Environmental Chamber Experiments

Overall Experimental Approach

Most of the environmental chamber experiments for this program consisted of measurements of "incremental reactivities" of the three fluids under various conditions. These involve two types of irradiations of model photochemical smog mixtures. The first is a "base case" experiment where a mixture of reactive organic gases (ROGs) representing those present in polluted atmospheres (the "ROG surrogate") is irradiated in the presence of oxides of nitrogen (NO_x) in air. The second is the "test" experiment that consists of repeating the base case irradiation except that the VOC whose reactivity is being assessed is added. The differences between the results of these experiments provide a measure of the atmospheric impact of the test compound, and the difference relative to the amount added is a measure of its reactivity. To provide data concerning the reactivities of the test compound under varying atmospheric conditions, three types of base case experiments were carried out:

Mini-Surrogate Experiments. This base case employed a simplified ROG surrogate and relatively low ROG/NO_x ratios. Low ROG/NO_x ratios represent "maximum incremental reactivity" (MIR) conditions, which are most sensitive to VOC effects. This is useful because it provides a sensitive test for the model, and also because it is most important that the model correctly predict a VOC's reactivity under conditions where the atmosphere is most sensitive to the VOCs. The ROG mini-surrogate mixture employed consisted of ethene, n-hexane, and m-xylene. This surrogate was employed in our previous studies (Carter et al, 1993; 1995a-c, 1997b, 2000b), and was found to provide a more sensitive test of the mechanism than the more complex surrogates that more closely represent atmospheric conditions (Carter et al, 1995b). This high sensitivity to mechanistic differences makes the mini-surrogate experiments useful for mechanism evaluation. Most of the mini-surrogate experiments used the same composition as used in our previous studies, and the average initial reactant concentrations of these experiments were (in ppm): NO: 0.27, NO_2: 0.11, n-hexane: 0.46, ethene: 0.80, and m-xylene: 0.13. However, in one experiment with Isopar-M a "modified mini-surrogate" was employed where the m-xylene was replaced with 0.2 ppm of toluene and 0.05 ppm of 1,3,5-trimehtyl benzene. This modification was employed in an attempt to improve the precision of the integrated OH radical measurements, but it gave similar results as using the standard mini-surrogate mixture.

High NO_x Full Surrogate Experiments. This base case employed a more complex ROG surrogate under somewhat higher, though still relatively low, ROG/NO_x conditions. While less sensitive to the some aspects of the mechanism employed, experiments with a more representative ROG surrogate are needed to evaluate the mechanism under conditions that more closely resembling the atmosphere. The ROG surrogate employed was the same as the 8-component "lumped molecule" surrogate employed in our previous study (Carter et al. 1995b), and consists of n-butane, n-octane, ethene, propene, trans-2-butene, toluene, m-xylene, and formaldehyde. Calculations have indicated that use of this 8-component

mixture will give essentially the same results in incremental reactivity experiments as actual ambient mixtures (Carter et al. 1995b). The average initial reactant concentrations of these experiments were (in ppm): NO: 0.25, NO_2: 0.05, n-butane: 0.38, n-octane: 0.10, ethene: 0.07, propene: 0.06, trans-2-butene: 0.06, toluene: 0.09 and m-xylene: 0.09.

Low NO_x Full Surrogate Experiments. This base case employing the same 8-component "lumped molecule" surrogate as the full surrogate experiments described above, except that lower NO_x levels (higher ROG/NO_x ratios) were employed to represent NO_x-limited conditions. Such experiments are necessary to assess the ability of the model to properly simulate reactivities under conditions where NO_x is low. The initial ROG and NO_x reactant concentrations were comparable to those employed in our previous studies (Carter et al. 1995b, 1997b, 2000b). The average initial NO and NO_2 were 0.07 and 0.03 ppm, respectively, and the initial concentrations of the 8 ROG surrogate components were the same as in the high NO_x full surrogate experiments.

An appropriate set of control and characterization experiments necessary for assuring data quality and characterizing the conditions of the runs for mechanism evaluation were also carried out. These are discussed where relevant in the results or modeling methods sections (see also Carter et al, 1995c, 2000b).

Environmental Chamber

All experiments for this program were carried out using the CE-CERT "Dividable Teflon Chamber" (DTC) with a blacklight light source. This consists of two ~6000-liter 2-mil heat-sealed FEP Teflon reaction bags located adjacent to each other and fitted inside an 8' x 8' x 8' framework, and which uses two diametrically opposed banks of 32 Sylvania 40-W BL black lights as the light source. The lighting system in the DTC was found to provide so much intensity that only half the lights were used for irradiation. Four air blowers that are located in the bottom of the chamber were used to help cool the chamber as well as mix the contents of the chamber. The CE-CERT DTC is very similar to the SAPRC DTC which is described in detail elsewhere (Carter et al, 1995b,c).

The blacklight light source has the advantage of being relatively inexpensive to operate and provides a reasonably good simulation of natural sunlight in the region of the spectrum that is important in affecting most photolysis reactions of importance for non-aromatic VOCs (Carter et al, 1995c,d). This is therefore appropriate for studies of reactivities of compounds, such as these alkanes, which are not photoreactive or believed to form significant yields of photoreactive products whose action spectra are not well characterized.

The DTC is designed to allow simultaneous irradiations of experiments with and without added test reactants under the same reaction conditions. Since the chambers are actually two adjacent FEP Teflon reaction bags, two mixtures can be simultaneously irradiated using the same light source and with the same temperature control system. These two reaction bags are referred to as the two "sides" of the chambers (Side A and Side B) in the subsequent discussion. The sides are interconnected with two ports, each with a box fan, which rapidly exchange their contents to assure that base case reactants have equal

concentrations in both sides. In addition, a fan is located in each of the reaction bags to rapidly mix the reactants within each chamber. The ports connecting the two reactors can then be closed to allow separate injections on each side, and separate monitoring of each side.

Experimental Procedures

The reaction bags were flushed with dry air produced by an AADCO air purification system for 14 hours (6pm-8am) on the nights before experiments. The continuous monitors were connected prior to reactant injection and the data system began logging data from the continuous monitoring systems. The reactants were injected as described below (see also Carter et al, 1993, 1995c). The common reactants were injected in both sides simultaneously using a three-way (one inlet and two outlets connected to side A and B respectively) bulb of 2 liters in the injection line and were well mixed before the chamber was divided. The contents of each side were blown into the other using two box fans located between them. Mixing fans were used to mix the reactants in the chamber during the injection period, but these were turned off prior to the irradiation. The sides were then separated by closing the ports that connected them, after turning all the fans off to allow their pressures to equalize. After that, reactants for the different sides (the test fluid in the case of reactivity experiments) were injected and mixed. After the run, the contents of the chamber were emptied by allowing the bags to collapse, and then the chamber was flushed with purified air. The contents of the reactors were vented into a fume hood.

The procedures for injecting the various types of reactants were as follows. The NO and NO_2 were prepared for injection using a high vacuum rack. Known pressures of NO, measured with MKS Baratron capacitance manometers, were expanded into Pyrex bulbs with known volumes, which were then filled with nitrogen (for NO) or oxygen (for NO_2). The contents of the bulbs were then flushed into the chamber with nitrogen. The gaseous reactants were prepared for injection either using a high vacuum rack or a gas-tight syringes whose amounts were calculated to achieve the desired concentrations in the chamber. Sufficiently volatile liquid reactants (which included all the liquid ROG surrogate compounds used in this study, but not the test fluids) were injected using a micro syringe into a 1-liter Pyrex bulb equipped with stopcocks on each end and a port for the injection of the liquid. Then one end of the bulb was attached to the injection port of the chamber and the other to a nitrogen source. The stopcocks were then opened, and the contents of the bulb were flushed into the chamber with a combination of nitrogen and heat gun for approximately 5 minutes. For DTC767 and following runs the common gaseous and liquid reactants were injected in both sides simultaneously using a "Y"-shape glass tube.

The test fluids were injected into the chamber after the base ROG surrogate and NO_x has been injected into both sides and the contents of each side have been completely mixed. They were injected by measuring the desired amount of fluid with microsyringe into a tube wrapped with heat tape, then flushing the contents of the tube into the chamber with Aadco air at about 2 liters/minute for around 10 minutes, with the tube being heated to ~170^{o}C. The tube was wrapped with heat tape all the way to where it entered the chamber, to avoid condensation on the sides. Note that the heating tape failed during or before the test fluid injection for run DTC776, and a shorter tube without a completely heated line leading into the chamber was used for DTC776 the two test fluid runs that followed it. As discussed in the Results

section, somewhat less complete injection of the fluid constituents into the gas phase was observed for those later experiments.

A total carbon analyzer was used to determine the total amounts of gas-phase carbon in both sides of the chamber after the test fluid has been injected, but before the lights were turned on. The difference in gas-phase carbon in the side with the test fluid injected compared to the base case side without the test fluid is taken as the total carbon in the gas-phase test fluid constituents injected into the chamber.

Formaldehyde was prepared in a vacuum rack system by heating paraformaldehyde in an evacuated bulb until the pressure corresponded to the desired amount of formaldehyde. The bulb was then closed and detached from the vacuum system and its contents were flushed into the chamber with dry air through the injection port.

Analytical Methods

Ozone and nitrogen oxides (NO_x) were continuously monitored using commercially available continuous analyzers with Teflon sample lines inserted directly into the chambers. The sampling lines from each side of the chamber were connected to solenoids that switched from side to side every 10 minutes, so the instruments alternately collected data from each side. Ozone was monitored using a Dasibi 1003-AH UV photometric ozone analyzer and NO and total oxides of nitrogen (including organic nitrates and perhaps HNO_3) were monitored using a Teco Model 42 chemiluminescent NO/NO_x monitor. The output of these instruments, along with that from the temperature sensors and the formaldehyde instrument, were attached to a computer data acquisition system, which recorded the data at 10 minutes intervals for ozone, NOx and temperature (and at 15 minutes for formaldehyde), using 30 second averaging times. This yielded a sampling interval of 20 minutes for taking data from each side.

The Teco instrument and Dasibi CO analyzer were calibrated prior to each experiment using a certified NO and CO source and CSI 1700 gas-phase titration calibrator. The Dasibi ozone analyzer was calibrated against transfer standard ozone analyzer using transfer standard method in an interval of three months and was check with CSI ozone generator for each experiment to assure that the instrument worked properly. The details were discussed elsewhere (Carter et al, 1995c)

The base ROG surrogate organic reactants other than formaldehyde were measured by gas chromatography with FID detection as described elsewhere (Carter et al. 1993; 1995c). GC samples were taken for analysis at intervals from 20 minutes to 30 minutes either using 100 ml gas-tight glass syringes or by collecting the 100 ml sample from the chamber onto Tenax-GC solid adsorbent cartridge. These samples were taken from ports directly connected to the chamber after injection and before irradiation and at regular intervals after irradiation was started. The sampling method employed for injecting the sample onto the GC column depended on the volatility or “stickiness” of the compound. For analysis of the more volatile species, which includes all the base ROG surrogate and test compounds monitored in this study, the contents of the syringe were flushed through a 10 ml and 5 ml stainless steel or 1/8' Teflon tube loop and subsequently injected onto the column by turning a gas sample valve.

The calibrations for the GC analyses for most compounds were carried out by sampling from chambers or vessels of known volume into which known amounts of the reactants were injected, as described previously (Carter et al, 1995c).

Formaldehyde was monitored using an adaptation of the diffusion scrubber method developed by Dasgupta et al (1988, 1990), as described by Carter et al (1995c). It was calibrated using a formaldehyde diffusion tube whose weight loss was monitored over time. The system cycled between zero, calibrate, and sample modes to correct for zero and span drifts.

No attempt was made to monitor the constituents of the test fluids by GC because the individual fluid constituents were not resolved on the chromatographic columns employed in this study. Instead, the total amount of gas-phase carbon injected into the chamber was determined using a Ratfisch Model RS55CA total hydrocarbon analyzer. This operates using FID analysis and is calibrated using a prepared tank with a known amount (90 ppm) of propane, assuming equal per-carbon response for all gas-phase hydrocarbon species. Span checks were performed during each experiment, and the results were used to calibrate the measurement data obtained. The input to the analyzer alternated between each side of the chamber (after the reactants were injected but before the irradiation), zero air, and 90 ppm propane span gas.

Characterization Methods

Temperature

Two temperature thermocouples were used to monitor the chamber temperature, located in the sampling line of continuous analyzers to monitor the temperature in each side. The temperature range in these experiments was typically 25-30 C.

Blacklight Light Source

The light intensity in the DTC chamber was monitored by periodic NO_2 actinometry experiments utilizing the quartz tube method of Zafonte et al (1977), with the data analysis method modified as discussed by Carter et al. (1995c). The results of these experiments were tracked over time, and although there was a gradual decrease in light intensity over time during most of the operational lifetime of this chamber (Carter et al, 1995c, 2000b), the light intensity appeared to be relatively constant during the period of these experiments. Averages of results of actinometry experiments carried out during this period indicated an NO_2 photolysis rate of 0.161 min^{-1}. This was used when modeling all the experiments for this program.

The spectrum of the blacklight light source is periodically measured using a LiCor LI-1800 spectroradiometer, and found to be essentially the same as the general blacklight spectrum recommended by Carter et al (1995c) for use in modeling blacklight chamber experiments.

Dilution

The dilution of the chambers due to sampling is expected to be small because the flexible reaction bags can collapse as samples are withdrawn for analysis. Also, the chambers were designed to operate under slightly positive pressure, so any small leaks would result in reducing the bag volume rather than diluting the contents of the chamber. Information concerning dilution in an experiment can be obtained from relative rates of decay of added VOCs that react with OH radicals with differing rate constants (Carter et al. 1993; 1995c). Most experiments had a more reactive compound such as m-xylene and n-octane present either as a reactant or added in trace amounts to monitor OH radical levels. Trace amounts (~0.1 ppm) of n-butane were also added to experiments if needed to provide a less reactive compound for monitoring dilution. In addition, specific dilution check experiments such as CO irradiations were carried out. Based on these results, the dilution rate was found to be negligible in this chamber in most experiments, generally being less than 0.3% per hour.

Reactivity Data Analysis Methods

As indicated above, most of the experiments for this program consisted of simultaneous irradiation of a "base case" reactive organic gas (ROG) surrogate - NO_x mixture in one of the dual reaction chambers, together with an irradiation, in the other reactor, of the same mixture with added. The results were analyzed to yield two measures of VOC reactivity: the effect of the added VOC on the amount of NO reacted plus the amount of ozone formed, and integrated OH radical levels. These are discussed in more detail below.

The first measure of reactivity is the effect of the VOC on the change in the quantity $[O_3]$-[NO], or $\Delta([O_3]$-[NO]). As discussed elsewhere (e.g., Johnson, 1983; Carter and Atkinson, 1987; Carter and Lurmann, 1990, 1991, Carter et al, 1993, 1995a), this gives a direct measure of the amount of conversion of NO to NO_2 by peroxy radicals formed in the photooxidation reactions, which is the process that is directly responsible for ozone formation in the atmosphere. (Johnson calls it "smog produced" or "SP".) The incremental reactivity of the VOC relative to this quantity, which is calculated for each hour of the experiment, is given by

$$\mathrm{IR}[\Delta([O_3]-[NO])_t^{VOC}] = \frac{\Delta([O_3]-[NO])_t^{Test} - \Delta([O_3]-[NO])_t^{Base}}{[VOC]_0} \qquad \text{(I)}$$

where $\Delta([O3]\text{-}[NO])_t^{Test}$ is the $\Delta([O_3]$-[NO]) measured at time t from the experiment where the test VOC was added, $\Delta([O3]\text{-}[NO])_t^{Base}$ is the corresponding value from the corresponding base case run, and $[VOC]_0$ is the amount of test VOC added. An estimated uncertainty for IR[$\Delta([O_3]$-[NO])] is derived based on assuming an ~3% uncertainty or imprecision in the measured $\Delta([O_3]$-[NO]) values. This is consistent with the results of the side equivalency test, where equivalent base case mixtures are irradiated on each side of the chamber.

Note that reactivity relative to Δ([O3]-[NO]) is essentially the same as reactivity relative to O_3 in experiments where O_3 levels are high, because under such conditions $[NO]_t^{base}$. $[NO]_t^{test}$. 0, so a change in Δ([O3]-[NO]) caused by the test compound is due to the change in O_3 alone. However, Δ([O3]-[NO]) reactivity has the advantage that it provides a useful measure of the effect of the VOC on processes responsible for O_3 formation even in experiments where O_3 formation is suppressed by relatively high NO levels.

The second measure of reactivity is the effect of the VOC on integrated hydroxyl (OH) radical concentrations in the experiment, which is abbreviated as "IntOH" in the subsequent discussion. This is an important factor affecting reactivity because radical levels affect how rapidly all VOCs present, including the base ROG components, react to form ozone. If a compound is present in the experiment that reacts primarily with OH radicals, then the IntOH at time t can be estimated from

$$\mathrm{IntOH}_t = \frac{\ln([\mathrm{tracer}]_0/[\mathrm{tracer}]_t) - \mathrm{Dt}}{\mathrm{kOH}^{\mathrm{tracer}}} \qquad \text{(II)}$$

where $[tracer]_0$ and $[tracer]_t$ are the initial and time=t concentrations of the tracer compound, kOH^{tracer} its OH rate constant, and D is the dilution rate in the experiments. The latter was found to be small and was neglected in our analysis. The concentration of tracer at each hourly interval was determined by linear interpolation of the experimentally measured values. M-xylene was used as the OH tracer in most of these experiments because it is present as a surrogate component, its OH rate constant is known (the value used was 2.36×10^{-11} cm^3 $molec^{-1}$ s^{-1} [Atkinson, 1989]), and it reacts relatively rapidly. However, for one of the mini-surrogate experiments for Isopar-M the m-xylene was replaced with 1,3,5-trimethylbenzene, for which an OH radical rate constant of 5.75×10^{-11} cm^3 $molec^{-1}$ s^{-1} was used (Atkinson, 1989). This was used as an alternative tracer because it might serve as a more sensitive measurement of IntOH because of its higher OH radical rate constant.

The effect of the VOC on OH radicals can thus be measured by its IntOH incremental reactivity, which is defined as

$$\mathrm{IR[IntOH]}_t = \frac{\mathrm{IntOH}_t^{\mathrm{Test}} - \mathrm{IntOH}_t^{\mathrm{Base}}}{[\mathrm{VOC}]_0} \qquad \text{(III)}$$

where $IntOH^{Test}$ and $IntOH^{Base}$ are the IntOH values measured at time t in the added VOC and the base case experiment, respectively. The results are reported in units of 10^6 min. The uncertainties in IntOH and IR[IntOH] are estimated based on assuming an ~2% imprecision in the measurements of the m-xylene concentrations. This is consistent with the observed precision of results of replicate analyses of this compound.

CHEMICAL COMPOSITIONS OF THE FLUIDS

Information Provided by ExxonMobil Chemical Co.

The information about the chemical composition of the three fluids that were studied for this project as provided by Exxon (now ExxonMobil) Chemical Company is summarized in Table 1 and Table 2. The data on Table 1 were obtained as follows. The information on the boiling point range and specific gravities were obtained from the product information sheets on the ExxonMobil Chemical web site. The chemical composition data were provided by Dr. Peter Ellis of ExxonMobil Company in December, 1998. The carbon number distribution for hydrocarbon fluids were determined by the ASTM D2887 method, and the analysis for hydrocarbon isomer type (paraffin, cyclic and aromatic) was based on an Exxon Chemical Company mass spectroscopic method. The carbon number distribution for EXXATE 1000 Fluid was determined by Exxon Chemical gas chromatographic method. The elemental analysis was run by a third party laboratory using the ASTM D5291 method, with the stated results being based on single measurements.

Additional information was supplied about the Exxate fluids. These are acetates that are produced by reacting acetic acid with the corresponding Exxal® alcohols[2]. These alcohols are manufactured via propylene oligomerization, followed by carbonylation and hydrogenation. This process produces branched alcohols. Typical compositions for the lower molecular weight Exxal 6 through Exxal 9 alcohols that are used to produce Exxate 600 through Exxate 900 are shown on Table 2. Speciated information is not available for the higher Exxals, though carbon number distribution information is available, and is shown on Table 2. Since the process of making the Exxates from the Exxals should not affect the structure of the portion of the molecule derived from the alcohol, the information on Table 2 can be used to derive the compositions of the various Exxates that are of interest in this study.

The amount of linear alcohol is expected to be below 0.5 weight %, based on extrapolation of a single datum for another branched alcohol acetate. ExxonMobil has not tested for cyclics or aromatic components, but has no reason to expect these types of components.

Note that this information relates only to the specific material designated and may not be valid for such material used in combination with any other material or in any process. Such information is, to the best of the knowledge and belief of ExxonMobil Chemical Company, accurate and reliable as of the date compiled. However, no representation, warranty or guarantee is made as to its accuracy, reliability or completeness. ExxonMobil Chemical Company does not accept liability for any loss or damage that may occur from the use of this information nor do we offer any warranty against patent infringement. The values shown here are representative of a single sample analysis. These values do not represent any guarantee from ExxonMobil Chemical Company.

[2] Exxal is a registered trademark of ExxonMobil Chemical Company.

Table 1. Information provided by Exxon Chemical Company concerning Exxsol® D95, Isopar®-M and Exxate® 1000 Fluids.

	Exxsol® D95	Isopar®-M	Exxate® 1000
Derivation	Hydrogenated petroleum distillate	Oligomerization of propylene and isobutene and hydrogenation	Etherification of $C_{\sim 10}$ iso-alcohols produced by oligomerization of propylene and catalytic reaction with CO and H_2.
CAS Number			108419-35-7

Potentially proprietary information on this table has been deleted.
Contact ExxonMobil for this information.

The tables in the following section give the compositions that were used when analyzing and modeling the data for this project. These were based in part on the data in this table.

Table 2. Typical compositions of the Exxal 6 through Exxal 13 alcohols, based on information provided by ExxonMobil Chemical Company.

This table contains potentially proprietary information that has been deleted.
Contact ExxonMobil for this information.

The tables in the following section give the compositions that were used when analyzing and modeling the data for this project. These were based in part on the data in this table

Compositions Assumed for D95 and Isopar-M Fluids

The assumed composition used for the two hydrocarbon fluids as a basis for the model simulations given in this report is given Table 3. This is based on the carbon number and alkane type distribution data provided by Exxon Chemical, as summarized in the previous section, assuming that the alkane type distribution is the same for all carbon numbers. Note that the branched and cyclic components represent complex mixtures of many isomers whose exact structures could not be determined. These are represented in the model using selected compounds that are taken as representative of all the isomers with the same carbon number.

For D95 and the "standard" model for Isopar-M, the individual compounds chosen as representative are shown in the "standard representation" columns on Table 4 for the branched alkanes and on Table 5 for the cyclic alkanes. These were chosen based on results of GC-MS analyses of mineral spirits components, which indicate that compounds with relatively low degrees of branching tend to dominate (O'Donnell, Safety-Kleen Corp., private communication, 1996; Carter et al, 2000a). This representation is the same as used in our recent model simulations of the reactivities of representative all-alkane mineral spirits samples (Carter, 2000; Carter et al, 2000a). The main difference is that these fluids have a somewhat higher carbon number range and that Isopar-M has much higher fraction of branched relative to normal and cyclic alkanes.

Table 3. Compositions assumed when modeling ozone formation potentials of D95 and Isopar-M Fluids.

Constituent Types	Weight Percent	
	D95	Isopar-M
n-Undecane		0.001%
n-Dodecane	0.97%	0.02%
n-Tridecane	8.24%	0.04%
n-Tetradecane	12.86%	0.10%
n-Pentadecane	1.53%	0.03%
n-Hexadecane		0.01%
Branched C11 Alkanes		0.42%
Branched C12 Alkanes	1.38%	6.38%
Branched C13 Alkanes	11.73%	18.63%
Branched C14 Alkanes	18.31%	41.53%
Branched C15 Alkanes	2.18%	13.59%
Branched C16 Alkanes		3.36%
Cyclic C11 Alkanes		0.08%
Cyclic C12 Alkanes	1.75%	1.21%
Cyclic C13 Alkanes	14.94%	3.53%
Cyclic C14 Alkanes	23.33%	7.87%
Cyclic C15 Alkanes	2.78%	2.58%
Cyclic C16 Alkanes		0.64%

Table 4. Compounds used to represent branched alkanes when representing D95 and Isopar M Fluids in the model simulations.

Carbon No.	Standard Representation			Highly Branched Representation for Isopar M		
	Wt %	Compound	Model Name	Wt %	Compound	Model Name
11	50%	2,6-Dimethyl Nonane	26DM-C9	100%	2,3,4,6-Tetramethyl Heptane	2346TMC7
	25%	4-Methyl Decane	4-ME-C10			
	25%	3-Methyl Decane	3-ME-C10			
12	50%	3,6-Dimethyl Decane	36DM-C10	100%	2,3,5,7-Tetramethyl Octane	2357TMC8
	25%	5-Methyl Undecane	5-ME-C11			
	25%	3-Methyl Undecane	3-ME-C11			
13	50%	3,6-Dimethyl Undecane	36DM-C11	50%	2,4,6,8-Tetramethyl Nonane	2468TMC9
	25%	5-Methyl Dodecane	5-ME-C12	50%	2,3,6-Dimethyl 4-Isopropyl Heptane	236M4IC7
	25%	3-Methyl Dodecane	3-ME-C12			
14	50%	3,7-Dimethyl Dodecane	37DM-C12	50%	2,4,5,6,8-Pentamethyl Nonane	24568MC9
	25%	6-Methyl Tridecane	6-ME-C13			
	25%	3-Methyl Tridecane	3-ME-C13	50%	2-Methyl 3,5-Diisopropyl Heptane	2M35IPC7
15	50%	3,7-Dimethyl Tridecane	37DM-C13	100%	2,6,8-Trimethyl 4-Isopropyl Nonane	268M4IC9
	25%	6-Methyl Tetradecane	6-ME-C14			
	25%	3-Methyl Tetradecane	3-ME-C14			
16	50%	4,8-Dimethyl Tetradecane	48DM-C14	100%	2,7-Dimethyl 3,5-Diisopropyl Heptane	27M35IC8
	25%	7-Methyl Pentadecane	7-ME-C15			
	25%	3-Methyl Pentadecane	3-ME-C15			

The standard model for Isopar-M assumes that the branched alkanes in the Isopars are similar to those in hydrogenated petroleum-derived materials. This may not necessarily be the case because the Isopar fluids are made using a different process that may involve formation of much more highly branched isomers. To assess the effects of making alternative assumptions in this regard, model calculations were carried out using a separate "high branching" representation of the branched alkanes in this fluid, as shown on the "highly branched representation" columns on Table 4. Although the specific types of $C_{\geq 11}$ isomers that may in Isopar fluids are uncertain, the reactivity characteristics of these tetramethyl and/or isopropyl-substituted alkanes may be different than the monomethyl or dimethyl isomers used in the standard representation, at least to the extent that structural effects have any significance.

Exxate Fluids

As indicated above, since the Exxate fluids are produced by reacting acetic acid with the corresponding Exxal® alcohol to form the corresponding acetate, information about their structure can be obtained from the compositional information from the corresponding Exxals, as given in the previous section. Note that although nearly complete compositional information is available for the alcohols used

Table 5. Compounds used to represent cyclic alkanes when representing D95 and Isopar M Fluids in the model simulations.

Carbon No.	Representation	Compound	Model Name
11	34%	Pentyl Cyclohexane	C5-CYCC6
	33%	1,3-Diethyl-5-Methyl Cyclohexane	13E5MCC6
	33%	1-Ethyl-2-Propyl Cyclohexane	1E2PCYC6
12	34%	Hexyl Cyclohexane	C6-CYCC6
	33%	1,3,5-Triethyl Cyclohexane	135ECYC6
	33%	1-Methyl-4-Pentyl Cyclohexane	1M4C5CY6
13	34%	Heptyl Cyclohexane	C7-CYCC6
	33%	1,3-Diethyl-5-Pentyl Cyclohexane	13E5PCC6
	33%	1-Methyl-2-Hexyl-Cyclohexane	1M2C6CC6
14	34%	Octyl Cyclohexane	C8-CYCC6
	33%	1,3-Dipropyl-5-EthylCyclohexane	13P5ECC6
	33%	1-Methyl-4-Heptyl Cyclohexane	1M4C7CC6
15	34%	Nonyl Cyclohexane	C9-CYCC6
	33%	1,3,5-Tripropyl Cyclohexane	135PCYC6
	33%	1-Methyl-2-Octyl Cyclohexane	1M2C8CC6
16	34%	Decyl Cyclohexane	C10CYCC6
	33%	1,3-Propyl-5-Butyl Cyclohexane	13P5BCC6
	33%	1-Methyl-4-Nonyl Cyclohexane	1M4C9CY6

to produce Exxates 600 through 900, only carbon number distribution is available for the alcohols used to produce the higher Exxates, including the Exxate 1000 studied in this project. For these constituents, a set of representative isomers was chosen based on the types of isomers that were identified in the lower Exxals.

Based on this, a set of assumed compositions in terms of known or representative constituents was derived for each of the Exxate fluids for use when modeling their impacts. These are shown on Table 6. The second column indicates the compound or type of compounds in the corresponding Exxal that is being represented, the third and fourth give the specific compounds and model species that were used when deriving the mechanisms. Table 6 also gives the average molecular weights and the carbon numbers that were derived from these Exxate fluids from these compositions.

Table 6. Compositions assigned to the Exxate 600 through Exxate 1300 fluids for modeling their atmospheric reactions.

Wt %	Acetates of:	Represented by	Model Name
		Exxate 600 (Average Mwt = 144.5, Carbons = 8.02)	
37.0%	1-Hexanol	n-Hexyl Acetate	NC6-ACET
19.0%	2-Methyl-1-Pentanol	2-Methylpentyl Acetate	2MC5-ACT
23.0%	3-Methyl-1-Pentanol	3-Methylpentyl Acetate	3MC5-ACT
17.0%	4-Methyl-1-Pentanol	4-Methylpentyl Acetate	4MC5-ACT
1.5%	Other C6 Alcohols	2,3-Dimethylbutyl Acetate	23MC4ACT
2.5%	Branched C7 Alcohols	4-Methylhexyl Acetate	4MC6-ACT
		Exxate 700 (Average Mwt = 158.3, Carbons = 9.01)	
4.5%	C6 Alcohols	n-Hexyl Acetate	NC6-ACET
4.5%		3-Methylpentyl Acetate	3MC5-ACT
7.4%	2-Methyl Hexanol	2-Methylhexyl Acetate	2MC6-ACT
13.8%	3-Methyl Hexanol	3-Methylhexyl Acetate	3MC6-ACT
24.5%	4-Methyl Hexanol	4-Methylhexyl Acetate	4MC6-ACT
7.4%	5-Methyl Hexanol	5-Methylhexyl Acetate	5MC6-ACT
15.3%	Dimethyl Pentanols	2,4-Dimethylpentyl Acetate	24MC5ACT
4.6%	Ethyl Pentanols	3-Ethylpentyl Acetate	3EC5-ACT
6.6%	n-Heptyl Alcohol	n-Heptyl Acetate	NC7-ACET
	Other C7 Alcohols	(Represented by the C7 alcohol acetates above)	
11.5%	C8 Alcohols	3,4-Dimethylhexyl Acetate	34MC6ACT
		Exxate 800 (Average Mwt = 172.1, Carbons = 9.99)	
3.5%	C7 Alcohols	4-Methylhexyl Acetate	4MC6-ACT
17.5%	3,5-Dimethyl-1-Hexanol	3,5-Dimethylhexyl Acetate	35MC6ACT
13.5%	3-Ethyl-1-Hexanol	3-Ethylhexyl Acetate	3EC6-ACT
20.0%	3,4-Dimethyl-1-Hexanol	3,4-Dimethylhexyl Acetate	34MC6ACT
9.8%	4-Methyl-1-Heptanol	4-Methylheptyl Acetate	4MC7-ACT
9.8%	4,5-Dimethyl-1-Hexanol	4,5-Dimethylhexyl Acetate	45MC6ACT
8.0%	5-Methyl-1-Heptanol	5-Methylheptyl Acetate	5MC7-ACT
7.0%	3-Methyl-1-Heptanol	3-Methylheptyl Acetate	3MC7-ACT
7.0%	2,4-Dimethyl-1-Hexanol	2,4-Dimethylhexyl Acetate	24MC6ACT
1.5%	n-Octanol	n-Octyl Acetate	NC8-ACET
2.5%	C9 Alcohols	3,5-Dimethylheptyl Acetate	35MC7ACT
		Exxate 900 (Average Mwt = 188.5, Carbons = 11.16)	
3.5%	C8 Alcohols	3,4-Dimethylhexyl Acetate	34MC6ACT
2.0%	2,4-Dimethyl-1-Heptanol	2,4-Dimethylheptyl Acetate	24MC7ACT
2.0%	2-Methyl-1-Octanol	2-Methyloctyl Acetate	2MC8-ACT
9.3%	Other Methyl Octanols	4-Methyloctyl Acetate	4MC8-ACT
9.3%		5-Methyloctyl Acetate	5MC8-ACT
20.5%	3,5-Dimethyl-1-Heptanol	3,5-Dimethylheptyl Acetate	35MC7ACT
5.8%	3,6-Dimethyl-1-Heptanol	3,6-Dimethylheptyl Acetate	36MC7ACT
5.8%	4,6-Dimethyl-1-Heptanol	4,6-Dimethylheptyl Acetate	46MC7ACT
5.8%	4,5-Dimethyl-1-Heptanol	4,5-Dimethylheptyl Acetate	45MC7ACT
5.8%	3-Ethyl-1-Heptanol	3-Ethylheptyl Acetate	3EC7-ACT
1.5%	2,3-Dimethyl-1-Heptanol	2,3-Dimethylheptyl Acetate	23MC7ACT
3.8%	Other Dimethyl Heptanols	2,5-Dimethylheptyl Acetate	25MC7ACT

Table 6 (continued)

Wt %	Acetates of:	Represented by	Model Name
3.8%	or Trimethyl Hexanols	2,3,5-Teimethylhexyl Acetate	235M6ACT
0.5%	n-Nonanol	n-Nonyl Acetate	NC9-ACET
7.0%	C10 Alcohols	3,6-Dimethyloctyl Acetate	36MC8ACT
7.0%		4,6-Dimethyloctyl Acetate	46MC8ACT
7.0%		3-Isopropylheptyl Acetate	3IPC7ACT
		Exxate 1000 (Average Mwt = 199.5, Carbons = 11.94)	
0.8%	C8 Alcohols	3,4-Dimethylhexyl Acetate	34MC6ACT
3.4%	C9 Alcohols	3,5-Dimethylheptyl Acetate	35MC7ACT
3.4%		4,5-Dimethylheptyl Acetate	45MC7ACT
29.7%	C10 Alcohols	3,6-Dimethyloctyl Acetate	36MC8ACT
29.7%		4,6-Dimethyloctyl Acetate	46MC8ACT
29.7%		3-Isopropylheptyl Acetate	3IPC7ACT
3.2%	C11 Alcohols	3,5,7-Trimethyloctyl Acetate	357M8ACT
		Exxate 1200 (Average Mwt = 229.3, Carbons = 14.07)	
0.7%	C10 Alcohols	3,6-Dimethyloctyl Acetate	36MC8ACT
0.7%		4,6-Dimethyloctyl Acetate	46MC8ACT
0.7%		3-Isopropylheptyl Acetate	3IPC7ACT
4.7%	C11 Alcohols	3,5,7-Trimethyloctyl Acetate	357M8ACT
4.7%		4,7-Dimethylnonyl Acetate	47MC9ACT
4.7%		3-Ethyl-6-Methyloctyl Acetate	3E6M8ACT
19.3%	C12 Alcohols	3,6,8-Trimethylnonyl Acetate	368M9ACT
19.3%		3,5,7-Trimethylnonyl Acetate	357M9ACT
19.3%		2,3,5,7-Tetramethyloctyl Acetate	2357M8AC
8.0%	C13 Alcohols	2,4,6,8-Tetramethylnonyl Acetate	2468M8AC
8.0%		4,7,9-Trimethyldecyl Acetate	479M10AC
8.0%		3-Ethyl-6,7-Dimethylnonyl Acetate	3E67M9AC
0.7%	C14 Alcohols	3,5,7,9-Tetramethyldecyl Acetate	3579M10A
0.7%		5-Ethyl-3,6,8-Trimethylnonyl Acetate	5E368M9A
0.7%		2,3,5,6,8-Pentaamethylnonyl Acetate	23568M9A
		Exxate 1300 (Average Mwt = 239.4, Carbons = 14.79)	
0.3%	C10 Alcohols	3,6-Dimethyloctyl Acetate	36MC8ACT
0.3%		4,6-Dimethyloctyl Acetate	46MC8ACT
0.3%		3-Isopropylheptyl Acetate	3IPC7ACT
0.3%	C11 Alcohols	3,5,7-Trimethyloctyl Acetate	357M8ACT
0.3%		4,7-Dimethylnonyl Acetate	47MC9ACT
0.3%		3-Ethyl-6-Methyloctyl Acetate	3E6M8ACT
7.0%	C12 Alcohols	3,6,8-Trimethylnonyl Acetate	368M9ACT
7.0%		3,5,7-Trimethylnonyl Acetate	357M9ACT
7.0%		2,3,5,7-Tetramethyloctyl Acetate	2357M8AC
23.3%	C13 Alcohols	2,4,6,8-Tetramethylnonyl Acetate	2468M8AC
23.3%		4,7,9-Trimethyldecyl Acetate	479M10AC
23.3%		3-Ethyl-6,7-Dimethylnonyl Acetate	3E67M9AC
2.3%	C14 Alcohols	3,5,7,9-Tetramethyldecyl Acetate	3579M10A
2.3%		5-Ethyl-3,6,8-Trimethylnonyl Acetate	5E368M9A
2.3%		2,3,5,6,8-Pentaamethylnonyl Acetate	23568M9A

EXPERIMENTAL RESULTS

Summary of Experiments and Characterization Results

Table 7 gives a chronological listing of all the experiments carried out for this program. These consisted primarily of the experiments with the three fluids, whose results are summarized in the following section. In addition, several characterization runs were carried out to determine the chamber-dependent inputs needed for the model simulations of the experiments. Table 7 summarizes the purposes and relevant results from these runs. Except as indicated on the table, the results of most of these experiments were as expected based on our previous experience with these and similar chambers in our laboratories (Carter et al., 1995c and references therein; Carter et al, 2000b). A more detailed more discussion of the characterization results for these chambers during this time period, particularly with respect to light intensity and the chamber radical source, is given by Carter et al (2000b).

The results of these characterization experiments were taken into account when deriving the chamber dependent parameters used in the model simulations of these experiments, as discussed below and indicated on Table A-4 in Appendix A.

Reactivity Experiments

As indicated on Table 7, at least six incremental reactivity experiments were carried out for each of the three test fluids, consisting of at least two experiments for each compound using the three types of base case surrogate - NO_x mixtures. The initial reactant concentrations and results of these experiments are summarized on Table 8. Concentration-time plots of selected data are given in the following section, in conjunction with the discussion of the results of the model simulations of these and the mineral spirits experiments.

Results of Fluid Constituent Injections

Because the fluid constituents were not single compounds and the individual components could not be resolved by gas chromatography, the amount of fluid carbon injected into the gas phase was determined by total carbon analysis using an FID detector calibrated using propane. Table 8 gives the gas-phase carbon for the fluid constituents as determined by total carbon FID analysis and also as calculated from the volumes of liquid fluid injected[3], these quantities are plotted against each other on Figure 1. It can be seen that consistent results were obtained in all runs except for the last four of the program, where

[3] The amount injected was calculated from the volume of liquid fluid injected, the calculated volume of the reactor where the fluid was injected, the average molecular weights and carbon number distributions based on the data provided by ExxonMobil Co., as given in the previous section. The volume of the reactors were determined by comparing the known amounts of NO_x and base ROG surrogate reactants and the measured concentrations after they were injected and mixed. It was assumed that the two reactors had the same volume when making this calculation.

Table 7. Chronological listing of the environmental chamber experiments carried out to evaluate the ozone formation potentials of the three test fluids.

Run No.	Date	Title	Comments
DTC704	8/31/98	NO_2 Actinometry	NO_2 photolysis rate measured using the quartz tube method was 0.165 min^{-1}, in good agreement with the trend observed with the other such runs.
DTC706	9/2/98	Propene - NO_x	Standard propene - NO_x control run for comparison with other such runs in this and other chambers. Results in normal range.
DTC718	10/30/98	n-Butane - NO_x	Run to measure the rate of the chamber radical source, as discussed by Carter et al (1995c). The NO oxidation rate was slightly higher on Side A, but the results were in the normal range and were well simulated using the standard chamber model assigned to this series of experiments.
DTC719	11/4/98	Modified Mini-Surrogate + Isopar M	Mini-surrogate experiment with 2 ppmC of Isopar M added to Side A. The measured amount of added fluid was 75% the calculated amount injected. A modified mini-surrogate mixture was employed with toluene + 1,3,5-trimethyl benzene replacing the m-xylene. Conditions and results are summarized on Table 8, and plots of representative data are shown on Figure 3.
DTC720	11/5/98	Full Surrogate + Isopar M	High NO_x full surrogate experiment with 3 ppmC of Isopar M added to Side B. The measured amount of added fluid was 85% the calculated amount injected. Conditions and results are summarized on Table 8, and plots of representative data are shown on Figure 3.
DTC723	11/11/98	Low NO_x Full Surrogate + Isopar	Low NO_x full surrogate experiment with 4 ppmC of Isopar M added to Side A. The measured amount of added fluid was 80% the calculated amount injected. Conditions and results are summarized on Table 8, and plots of representative data are shown on Figure 3.
DTC724	11/12/98	Mini-Surrogate + Isopar M (B)	Standard mini-surrogate experiment with 4 ppmC of Isopar M added to Side B. The measured amount of added fluid was 81% the calculated amount injected. Conditions and results are summarized on Table 8, and plots of representative data are shown on Figure 3.
DTC727	11/17/98	Pure Air Irradiation	Control run to test for chamber background effects. Only about 10 ppb of O_3 was formed on both sides of the chamber, about half the amount predicted by the standard chamber wall model.

Table 7 (continued)

Run No.	Date	Title	Comments
DTC728	11/18/98	Full Surrogate + Isopar M	High NO_x full surrogate experiment with 4 ppmC of Isopar M added to Side A. The measured amount of added fluid was 82% the calculated amount injected. Conditions and results are summarized on Table 8, and plots of representative data are shown on Figure 3.
DTC731	11/21/98	Pure Air Irradiation	Pure air irradiation carried out to determine the results of improvements made to clean air system to reduce the background NO_x levels that have been periodically observed. Approximately 19 ppb of O_3 was observed on both sides after 6 hours of irradiation, compared to ~35 ppb of O_3 predicted by the standard chamber effects model. Therefore, the improvements reduced the background O_3 formed in these experiments. This should not effect results of experiments where NO_x is injected, as is the case for the mechanism evaluation runs for this program.
DTC735	11/29/98	Pure air run	Pure air irradiation to test for background effects after the improvements in the pure air system. Approximately 8 ppb of O_3 was found after 5 hours of irradiation on both sides, which was slightly less than was the case in run DTC731.
DTC736		NO_2 Actinometry	NO_2 photolysis rate measured using the quartz tube method was 0.162 min^{-1}, suggesting that the light intensity is becoming approximately constant during this period.
		Runs for other programs	
DTC751	12/22/98	n-Butane - Chlorine Actinometry	Run to measure the light intensity by determining the Cl_2 photolysis rate, as discussed by Carter et al (1995c). The results yielded a calculated NO_2 photolysis rate of 0.153 min-1, which is reasonably consistent with the results of the quartz tube Actinometry experiments carried out previously, which indicated an NO_2 photolysis rate of ~0.16 min-1.
DTC752	1/5/99	n-Butane - NO_x	Run to measure the rate of the chamber radical source, as discussed by Carter et al (1995c). Results are reasonably well simulated using the standard chamber model assigned to this series of experiments (see Table A-4), though Side B has a somewhat higher radical source than Side A.
DTC753	1/6/99	Mini-Surrogate + D95	Mini-surrogate experiment with 3 ppmC of D95 fluid added to Side A. The measured amount of added fluid was 82% the calculated amount injected. Conditions and results are summarized on Table 8, and plots of representative data are shown on Figure 2.
DTC754	1/7/99	Full Surrogate + D95	High NO_x full surrogate experiment with 3 ppmC of D95 fluid added to Side B. The measured amount of added fluid was 79% the calculated amount injected. Conditions and results are summarized on Table 8, and plots of representative data are shown on Figure 2.

Table 7 (continued)

Run No.	Date	Title	Comments
DTC756	1/11/99	Low NO_x Full Surrogate + D95	Low NO_x full surrogate experiment with 4 ppmC of D95 fluid added to Side B. The measured amount of added fluid was 82% the calculated amount injected. Conditions and results are summarized on Table 8, and plots of representative data are shown on Figure 2.
DTC757	1/12/99	Mini-Surrogate + D95	Mini-surrogate experiment with 1.5 ppmC of D95 fluid added to Side A. The measured amount of added fluid was 75% the calculated amount injected. Conditions and results are summarized on Table 8, and plots of representative data are shown on Figure 2.
DTC760	1/15/99	Mini-Surrogate + Exxate 1000	Mini-surrogate experiment with 2.5 ppmC of Exxate 1000 fluid added to Side B. The measured amount of added fluid was 77% the calculated amount injected. The initial NO and initial NO_2 was approximately equal in this run, unlike the usual experiments where the [NO]/[NO_2] ratio is approximately 3. Conditions and results are summarized on Table 8, and plots of representative data are shown on Figure 5. The model tended to underpredict the $\Delta([O_3]-[NO])$ formation rates in the base case experiment.
DTC761	1/20/99	Propene - NO_x	Standard propene - NO_x control run for comparison with other such runs in this and other chambers. Results in normal range.
DTC764	1/26/99	Acetaldehyde + air	Run to test for NO_x wall offgasing effects. Approximately 17 ppb of O_3 and 4 ppb of PAN formed after six hours of irradiation, with similar results on both sides. Results in good agreement with predictions of standard chamber wall model.
DTC767	2/8/99	n-Butane - NO_x	Run to measure the rate of the chamber radical source. Results are simulated very well using the standard chamber model assigned to this series of experiments (see Table A-4), and good side equivalency is observed. This indicates that that the magnitude of the chamber radical source is in the normal range, and that the side differences observed in DTC752 are no longer occurring.
DTC769	2/10/99	Full Surrogate + Exxate 1000	High NO_x full surrogate experiment with ~4 ppmC of Exxate 1000 fluid added to Side A. The measured amount of added fluid was 65% the calculated amount injected, slightly lower than the normal range of ~75%. No valid formaldehyde data for this experiment; so the initial formaldehyde concentrations were estimated. Conditions and results are summarized on Table 8, and plots of representative data are shown on Figure 5.

Table 7 (continued)

Run No.	Date	Title	Comments
DTC770	2/11/99	Low NO_x Full Surrogate + Exxate 1000	Low NO_x full surrogate experiment with ~4 ppmC of Exxate 1000 fluid added to Side B. The measured amount of added fluid was 74% the calculated amount injected. Conditions and results are summarized on Table 8, and plots of representative data are shown on Figure 5.
DTC771	2/12/99	Full Surrogate + Isopar M	High NO_x full surrogate experiment with 5 ppmC of Isopar M fluid added to Side A. The measured amount of added fluid was 82% the calculated amount injected. Conditions and results are summarized on Table 8, and plots of representative data are shown on Figure 3.
DTC772	2/16/99	Full Surrogate + D95	Mini-surrogate experiment with 5.5 ppmC of D95 fluid added to Side B. The measured amount of added fluid was 78% the calculated amount injected. Conditions and results are summarized on Table 8, and plots of representative data are shown on Figure 2.
DTC773	2/17/99	Mini-Surrogate + Exxate 1000	Mini-surrogate experiment with ~4 ppmC of Exxate 1000 fluid added to Side A. The measured amount of added fluid was 79% the calculated amount injected. Conditions and results are summarized on Table 8, and plots of representative data are shown on Figure 5.
DTC774	2/19/99	n-Butane - Chlorine Actinometry.	Run to measure the light intensity by determining the Cl_2 photolysis rate, as discussed by Carter et al (1995c). The results yielded a calculated NO_2 photolysis rate of 0.105 min^{-1}, which lower than indicated by the results of the quartz tube actinometry experiments, which indicate an NO_2 photolysis rate of ~0.16 min^{-1}. However, the results of these Cl_2 experiments in this chamber tend to be scattered, and this discrepancy is not outside of the range of this variability. The results were not used for assigning NO_2 photolysis rates for modeling.
DTC775	2/22/99	Low NO_x Full Surrogate + Isopar M	Low NO_x full surrogate experiment with 4 ppmC of Isopar M fluid added to Side B. The measured amount of added fluid was 64% the calculated amount injected, lower than the normal range of ~80%. It is possible that the heat tape on tube used to inject the test fluid was failing (see next run). Conditions and results are summarized on Table 8, and plots of representative data are shown on Figure 3.

Table 7 (continued)

Run No.	Date	Title	Comments
DTC776	2/23/99	Full Surrogate + Exxate 1000	High NO_x full surrogate experiment with nominal 4-5 ppmC of Exxate 1000 fluid added to Side A. However, it was found that the heat tape around the tube used to inject the test fluid had burned out, so an older tube with less complete heating was used instead. The injection procedure was not effective, since the gas-phase Exxate constituents were found to be only ~1 ppmC. Conditions and results are summarized on Table 8, and plots of representative data are shown on Figure 5.
DTC777	2/24/99	Low NO_x Full Surrogate + Exxate 1000	Low NO_x full surrogate experiment with 5 ppmC of Exxate 1000 fluid added to Side B. An attempt was made to improve the injection efficiency by placing the injection tube closer to the chamber, but the measured amount of added fluid was still only 53% the calculated amount injected, lower than the normal range of ~75%. Conditions and results are summarized on Table 8, and plots of representative data are shown on Figure 5.
DTC778	2/25/99	Low NO_x Full Surrogate + D95	Mini-surrogate experiment with 3 ppmC of D95 fluid added to Side A. The measured amount of added fluid was 69% the calculated amount injected, lower than the normal range of ~80%. Conditions and results are summarized on Table 8, and plots of representative data are shown on Figure 2.
DTC779	2/26/99	n-Butane - NO_x	Run to measure the chamber radical source. Somewhat different NO_x injection procedure employed. The NO oxidation rates on both sides were in good agreement with the predictions of the standard chamber model.

problems with the injection system were encountered. In particular, except for those runs the gas-phase fluid constituent concentrations as determined by FID analysis was consistently around 80% the calculated amounts injected for the runs with the hydrocarbon (D95 and Isopar) fluids, and around 74% for the runs with the Exxate fluid.

This less than 100% ratio for measured to calculated gas-phase carbon in the other experiments could be due either to the per-carbon response for the fluid constituents being only lower than that for propane, or to incomplete injection of the reactants also being a problem for those runs. The per-carbon response of FID detectors should be about the same for higher molecular weight alkanes as it is for propane, so for D95 and Isopar-M fluids the most likely explanation for the differences between measured and calculated gas-phase carbon is incomplete injection. Therefore, in the model simulations of these experiments, we assume that the total gas-phase carbon concentration as determined by the propane-calibrated FID analysis gives a reasonably good approximation of the actual gas-phase carbon concentrations of the hydrocarbon fluid constituents. This implies that no more than about 80% of the liquid constituents are being introduced into the gas phase in these experiments with these fluids.

However, for sensitivity purposes model simulations of these experiments are also carried out assuming that the per carbon FID response for these $C_{\geq 11}$ hydrocarbons are 80% that of propane. This is based on FID measurements of the initial gas-phase fluid carbon in the experiments with no apparent injection problems. This is done by correcting the FID-determined carbon by a factor of 1.25 when deriving the initial fluid constituent concentrations in the simulations of the chamber experiments. These simulations are referred "80% THC response" model in the presentation of the evaluation results, while those using no correction to the FID data are referred to as the "standard model".

Table 8 Summary of conditions and selected results of the environmental chamber experiments with the selected C_{10} cycloalkanes.

Run	Fluid (ppmC)		NO_x (ppm)	Surg. (ppmC)	6^{th} Hour $\Delta([O_3]-[NO])$ (ppm)			5^{th} Hour IntOH (10^{-6} min)		
	Calc.	Meas.			Base	Test	IR [a]	Base	Test	IR [a]
D95 Fluid										
Mini-Surrogate										
DTC753A	3.0	2.4	0.41	5.32	0.38	0.19	-0.076	10.7	5.1	-2.3
DTC757A	1.5	1.1	0.38	6.28	0.40	0.29	-0.106	11.0	6.5	-4.0
High NO_x Full Surrogate										
DTC754B	3.1	2.5	0.30	4.15	0.51	0.46	-0.019	21.4	10.8	-4.3
DTC772B	5.5	4.3	0.30	4.31	0.51	0.46	-0.012	21.0	8.4	-3.0
Low NO_x Full Surrogate										
DTC756B	4.7	3.8	0.13	4.12	0.38	0.36	-0.006	22.9	8.7	-3.7
DTC778A [b]	3.1	2.2	0.09	4.27	0.29	0.30	0.003	19.0	12.5	-3.0
Isopar-M Fluid										
Mini-Surrogate										
DTC719A [c]	2.0	1.5	0.40	6.16	0.41	0.33	-0.055	11.1	6.9	-2.9
DTC724B	3.9	3.1	0.33	5.16	0.36	0.18	-0.058	7.4	3.0	-1.4
High NO_x Full Surrogate										
DTC720B	3.2	2.7	0.32	4.18	0.52	0.49	-0.011	18.9	12.1	-2.5
DTC728A	4.3	3.5	0.28	4.10	0.43	0.45	0.005	12.4	8.8	-1.0
DTC771A	5.4	4.5	0.29	4.25	0.48	0.51	0.007	21.1	11.9	-2.1
Low NO_x Full Surrogate										
DTC723A	4.3	3.4	0.11	4.10	0.33	0.34	0.003	20.1	10.9	-2.7
DTC775B [b]	3.7	2.3	0.09	4.58	0.31	0.30	-0.004	19.3	12.4	-3.0
Exxate 1000 Fluid [d]										
Mini-Surrogate										
DTC760B	2.5	2.1	0.39	5.54	0.43	0.29	-0.066	13.3	6.4	-3.2
DTC773A	4.2	3.6	0.38	5.57	0.41	0.23	-0.049	11.6	4.1	-2.1
High NO_x Full Surrogate										
DTC769A	3.8	2.7	0.27	4.51	0.45	0.47	0.007	19.1	11.7	-2.7
DTC776A [b]	4.6	1.2	0.30	4.21	0.49	0.51	0.017	21.2	14.2	-5.8
Low NO_x Full Surrogate										
DTC770B	4.4	3.5	0.08	4.10	0.23	0.23	0.000	19.8	10.6	-2.6
DTC777B [b]	5.6	3.2	0.09	4.41	0.30	0.29	-0.001	19.0	8.0	-3.4

[a] IR = Incremental Reactivity = ([Test] - [Base]) / [Test Compound Added]

[b] Incomplete injection of fluid constituents considered likely in this experiment. See Table 7

[c] Modified mini-surrogate used, with m-xylene replaced by toluene and 1,3,5-trimethylbenzene.

[d] Carbon measured by FID corrected by a factor of 1.08 as discussed in the text.

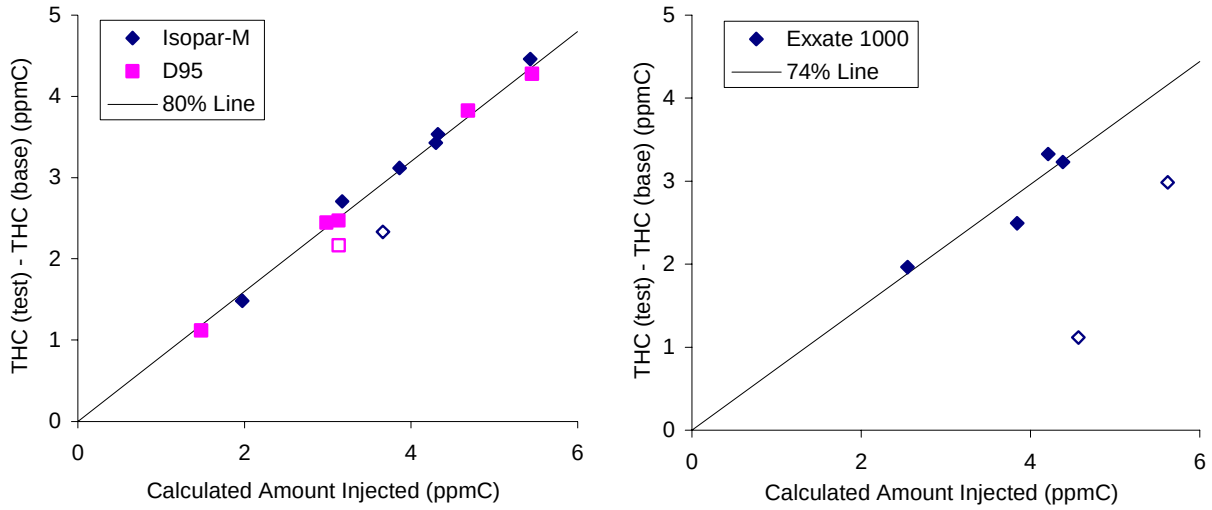

Figure 1. Plot of amounts of gas-phase carbon from test fluid constituents added in the reactivity experiments as measured by the total carbon analyzer against the calculated amount injected. Open symbols indicate runs carried out around the end of the program, using a less well heated injection system.

One might expect the per-carbon FID response to be somewhat lower in the case of the Exxate fluid because of the two oxygens in the molecule. The injection efficiencies for all three fluids should be about the same when the same injection procedure is used, since they all have very similar boiling point ranges (see Table 1). If this is assumed, then the differences between the FID-determined carbon / injected carbon ratios in the experiments without apparent injection problems suggest that the FID response for the Exxate fluid is about 92% obtained for the hydrocarbons. This is very close to the 90% response factor one would expect if the two carbons in the C_{10} ester molecules reduce the effective carbon number for FID analysis by one. In view of this, in the "standard model" calculations for Exxate 1000 we apply a factor of 1.09 to the FID total carbon analysis when determining the initial gas-phase carbon concentrations used for modeling the experiments with this fluid. However, for sensitivity purposes, "74% THC response" calculations are also carried out for the Exxate 1000 experiments based on the assumption that all the fluid is injected in the experiments without apparent injection problems, rather than the ~80% injection efficiency assumed in the standard model.

Reactivity Results

The results of these reactivity experiments are presented in more detail in the Mechanism Evaluation section, below. In general, the results indicate that the reactivity characteristics of these three fluids are very similar, and they are also similar to those for the higher alkane (Carter et al, 1996, 2000a, 2000c) and all-alkane mineral spirits samples (Carter et al, 2000a) we have studied previously. All these compounds and fluids inhibit OH radical levels in the experiments, and they also have negative effects on NO oxidation and O_3 formation rates in the mini-surrogate experiments. The magnitudes of the negative

IntOH and mini-surrogate $\Delta([O_3]-[NO])$ incremental reactivities are quite similar to each other, and also to the mineral spirits samples studied previously (Carter et al, 2000a). As with the higher alkanes and the mineral spirits samples, the effects of these fluids on NO oxidation and O_3 formation was less in the full surrogate experiments, with their negative effect on O_3 declining essentially to zero or becoming slightly positive by the end of the irradiations.

The fact that the reactivity characteristics between the D95 and Isopar-M fluids are so similar to those for the higher alkanes and the mineral spirits is not unexpected, given their similar chemical characteristics. Although one might expect more inhibiting characteristics for D95 than for the mineral spirits because of the higher carbon number range because inhibition characteristics tend to increase with the size of the molecule, the effect of size on inhibition characteristics tends to level off in the higher carbon number range. The similar results for Isopar-M relative to D95 and the all-alkane mineral spirits suggests that the high levels of branched alkanes, and the types of branching involved, for Isopar fluids does not significantly affect the reactivity characteristics.

The fact that the Exxate 1000 fluid has very similar reactivity characteristics to the hydrocarbon fluids in the same boiling point range may be surprising, given the different chemical nature of the constituents involved. Apparently the size of the molecules and the relatively large hydrocarbon-like portions of the molecules make the reactivity characteristics of these esters more like alkanes. The mechanistic implications of these results will be discussed further in the following section, in conjunction with the discussion of the model simulations of these experiments.

MECHANISM EVALUATION

Chemical Mechanism Employed

The chemical mechanism evaluated against the environmental chamber data and used in all of the atmospheric model simulations in this study is the "SAPRC-99" mechanism that is documented in detail by Carter (2000). This mechanism represents a complete update of the SAPRC-97 mechanism that was used in our previous study of mineral spirits reactivity (Carter et al, 1997a), and that is documented by Carter et al (1997b). It incorporates recent reactivity data from a wide variety of VOCs. The mechanism incorporates assignments for ~400 types of VOCs, and can be used to estimate reactivities for ~550 VOC categories. A condensed version, developed for use in regional models, is used to represent base case emissions in the atmospheric reactivity simulations discussed in this report. A unique feature of this mechanism is the use of a computerized system to estimate and generate complete reaction schemes for most non-aromatic hydrocarbons and oxygenates in the presence of NO_x, from which condensed mechanisms for the model can be derived. This was used to derive mechanisms for the constituents of the various fluids discussed in this report, including those whose mechanisms are not included in the tabulations of Carter et al (2000). The SAPRC-99 mechanism was evaluated against the results of almost 1700 environmental chamber experiments carried out at the University of California at Riverside, including experiments to test ozone reactivity predictions for over 80 types of VOCs (Carter, 2000).

Note that the mechanism as documented by Carter et al (2000) had a minor error that affects estimates mechanisms for the reactions of the esters that required regenerating the mechanisms for all the esters, including the Exxate constituents. The error concerned the method used to estimate the rate constant for the "ester rearrangement" reaction, which involves a shift of the hydrogen atom in the α-position of alkoxy radicals of the structure RCH(O·)OC(O)R', forming RC(O)· + R'C(O)OH. The activation energy for this rearrangement was estimated using $Ea = EaA + EaB \times \Delta H_r$,, where ΔH_r,, is the heat of reaction, and EaA and EaB = 0.35 being derived to be consistent with OH + methyl acetate product yields reported by Christensen et al (2000), OH +ethyl acetate yields of Tuazon et al (1998), and results of modeling n-butyl acetate reactivity chamber experiments. However, Carter (2000) had an error in the assumed product yields for the OH + methyl acetate reaction, with the net effect being that the rate constant assumed for the ester rearrangement for the $CH_3C(O)OCH_2O$· was about a factor of 3.5 higher than the value indicated by the data of Christensen et al (2000). When this is corrected, then corrected values of EaA = 9.11 kcal/mole and EaB = 0.20 are derived[4]. These were used when generating all the ester mechanisms in this work. However, the effect of this correction is small for most esters because the heats of reactions of reaction for most ester rearrangements involved are closer to those involved in the ethyl and n-butyl acetate systems, where the assumed rate constants were not changed. This change had very little effect on estimated mechanisms for the higher esters present in the Exxates because in most cases the competing 1,4-H shift isomerization are predicted to dominate over the ester rearrangement.

[4] The values derived by Carter (2000) were EaA = 20.23 kcal/mole and EaB = 0.35.

A listing of the portions of the SAPRC-99 mechanism used in the environmental chamber and atmospheric reactivity model simulations in this report is given in Appendix A. This consists of all the reactions and species used when representing the VOC - NO_x - air reactions of the base case experiments and base case ambient simulations, and the reactions of ethane used when calculating its ozone impacts for comparison purposes, and the reactions of the lumped species used to represent the various fluids assessed in this project. The latter were derived from the mechanisms used for the components of the test fluids, which are discussed below.

The detailed mechanisms for the atmospheric reactions of the $C_{\geq 11}$ alkane constituents of the hydrocarbon fluids were derived using the SAPRC-99 mechanism estimation and generation system as documented by Carter (2000) without any modifications. These mechanisms were found to give reasonably good simulations of results of reactivity experiments using a number of $C_{\geq 10}$ normal, branched and cyclic alkane mixtures and mineral spirits samples (Carter et al, 2000a,c; Carter, 2000). Note that the methods used to estimate nitrate yields in the reactions of peroxy radicals with NO were updated significantly compared to those used for previous versions of the SAPRC mechanisms, based on new data concerning nitrate yields from $C_{\geq 6}$ alkanes (Arey et al, 2000). This results in much better overall performance in the mechanisms in simulating reactivity experiments using mineral spirits and branched and cyclic alkanes (Carter et al, 2000a, Carter, 2000). These updates to the general alkane mechanisms are discussed in more detail elsewhere (Carter et al, 2000a,c, Carter, 2000).

The detailed mechanisms for the atmospheric reactions of the various high molecular weight acetates in the Exxate fluids were also generated using the SAPRC-99 mechanisms estimation generation system as documented by Carter (2000), corrected as indicated above. Because of the correction the mechanisms may be slightly different than those given by Carter (2000), though the differences for these higher molecular weight alkanes were generally insignificant. No adjustments or modifications to the ester mechanisms or estimation methods were made based on the data obtained in this study.

The detailed mechanisms derived using the mechanism generation system were then used to determine the overall effects of these reactions in the presence of NO_x in terms of overall effects on radical formation, NO to NO_2 conversions, and types of products ultimately formed. Various lumping rules" were applied to the comprehensive product lists to derive their representations in terms of SAPRC-99 model species (Carter, 2000). The resulting reactions of the individual alkane and ester species involved are listed in Table 9. Footnotes to the table indicate when measured rather than estimated OH radical rate constants were used.

Because of the relative large number of components in the fluids studied for this project, their constituents were represented using lumped model species whose rate constants and product yield parameters were derived by averaging those of the constituents they represented. The constituent mechanisms given in Table 9 and the assumed D95 and Isopar-M compositions given in Table 3 and the assumed Exxate compositions given in Table 4, above, were used for this purpose. These lumped mechanisms are given in Table 9 the fluids whose reactivities were assessed in this project.

Table 9. Representations of the constituents of D95, Isopar-M and the Exxate fluids in the SAPRC-99 mechanism.

Compound	k(298) [a] (cm^3 $molec^{-1}$ s^{-1})	Reactions and Products [b]
		Normal Alkanes
n-Undecane	1.29e-11 [c]	N-C11 + HO. = 0.553 RO2-R. + 0.447 RO2-N. + 0.771 R2O2. + 0.013 RCHO + 0.54 PROD2 + 5.038 XC
n-Dodecane	1.39e-11 [c]	N-C12 + HO. = 0.542 RO2-R. + 0.458 RO2-N. + 0.768 R2O2. + 0.011 RCHO + 0.53 PROD2 + 6.034 XC
n-Tridecane	1.60e-11 [c]	N-C13 + HO. = 0.535 RO2-R. + 0.465 RO2-N. + 0.766 R2O2. + 0.01 RCHO + 0.525 PROD2 + 7.03 XC
n-Tetradecane	1.80e-11 [c]	N-C14 + HO. = 0.53 RO2-R. + 0.47 RO2-N. + 0.765 R2O2. + 0.009 RCHO + 0.521 PROD2 + 8.027 XC
n-Pentadecane	2.10e-11 [c]	N-C15 + HO. = 0.527 RO2-R. + 0.473 RO2-N. + 0.764 R2O2. + 0.008 RCHO + 0.519 PROD2 + 9.025 XC
n-Hexadecane	2.30e-11 [c]	N-C16 + HO. = 0.525 RO2-R. + 0.475 RO2-N. + 0.763 R2O2. + 0.008 RCHO + 0.517 PROD2 + 10.023 XC
		Branched Alkanes used in the Standard Representation
2,6-Dimethyl Nonane	1.28e-11	26DM-C9 + HO. = 0.533 RO2-R. + 0.467 RO2-N. + 1.036 R2O2. + 0.001 CCHO + 0.221 RCHO + 0.12 ACET + 0.006 MEK + 0.376 PROD2 + 4.888 XC
4-Methyl Decane	1.29e-11	4-ME-C10 + HO. = 0.531 RO2-R. + 0.469 RO2-N. + 0.907 R2O2. + 0.001 CCHO + 0.08 RCHO + 0.003 MEK + 0.5 PROD2 + 4.932 XC
3-Methyl Decane	1.29e-11	3-ME-C10 + HO. = 0.526 RO2-R. + 0.474 RO2-N. + 0.917 R2O2. + 0.029 CCHO + 0.038 RCHO + 0.012 MEK + 0.489 PROD2 + 4.998 XC
3,6-Dimethyl Decane	1.45e-11	36DM-C10 + HO. = 0.494 RO2-R. + 0.506 RO2-N. + 1.079 R2O2. + 0.001 HCHO + 0.088 CCHO + 0.11 RCHO + 0.055 MEK + 0.458 PROD2 + 5.488 XC
5-Methyl Undecane	1.43e-11	5-ME-C11 + HO. = 0.524 RO2-R. + 0.476 RO2-N. + 0.867 R2O2. + 0.01 CCHO + 0.059 RCHO + 0.504 PROD2 + 5.923 XC
3-Methyl Undecane	1.43e-11	3-ME-C11 + HO. = 0.516 RO2-R. + 0.484 RO2-N. + 0.896 R2O2. + 0.025 CCHO + 0.033 RCHO + 0.011 MEK + 0.484 PROD2 + 5.997 XC
3,6-Dimethyl Undecane	1.60e-11	36DM-C11 + HO. = 0.488 RO2-R. + 0.512 RO2-N. + 1.046 R2O2. + 0.001 HCHO + 0.07 CCHO + 0.124 RCHO + 0.046 MEK + 0.442 PROD2 + 6.579 XC
5-Methyl Dodecane	1.57e-11	5-ME-C12 + HO. = 0.514 RO2-R. + 0.486 RO2-N. + 0.863 R2O2. + 0.009 CCHO + 0.044 RCHO + 0.498 PROD2 + 6.942 XC
3-Methyl Dodecane	1.57e-11	3-ME-C12 + HO. = 0.51 RO2-R. + 0.49 RO2-N. + 0.88 R2O2. + 0.023 CCHO + 0.03 RCHO + 0.009 MEK + 0.482 PROD2 + 6.997 XC
3,7-Dimethyl Dodecane	1.74e-11	37DM-C12 + HO. = 0.496 RO2-R. + 0.504 RO2-N. + 0.98 R2O2. + 0.055 CCHO + 0.11 RCHO + 0.03 MEK + 0.44 PROD2 + 7.772 XC
6-Methyl Tridecane	1.71e-11	6-ME-C13 + HO. = 0.512 RO2-R. + 0.488 RO2-N. + 0.852 R2O2. + 0.006 CCHO + 0.041 RCHO + 0.504 PROD2 + 7.909 XC
3-Methyl Tridecane	1.71e-11	3-ME-C13 + HO. = 0.506 RO2-R. + 0.494 RO2-N. + 0.871 R2O2. + 0.021 CCHO + 0.015 RCHO + 0.009 MEK + 0.493 PROD2 + 7.958 XC
3,7-Dimethyl Tridecane	1.88e-11	37DM-C13 + HO. = 0.487 RO2-R. + 0.513 RO2-N. + 0.98 R2O2. + 0.045 CCHO + 0.087 RCHO + 0.028 MEK + 0.44 PROD2 + 8.82 XC
6-Methyl Tetradecane	1.85e-11	6-ME-C14 + HO. = 0.51 RO2-R. + 0.49 RO2-N. + 0.843 R2O2. + 0.006 CCHO + 0.037 RCHO + 0.503 PROD2 + 8.918 XC

Table 9 (continued)

Compound	k(298) [a] (cm^3 $molec^{-1}$ s^{-1})	Reactions and Products [b]
3-Methyl Tetradecane	1.85e-11	3-ME-C14 + HO. = 0.505 RO2-R. + 0.495 RO2-N. + 0.861 R2O2. + 0.02 CCHO + 0.013 RCHO + 0.008 MEK + 0.493 PROD2 + 8.961 XC
4,8-Dimethyl Tetradecane	2.02e-11	48DM-C14 + HO. = 0.481 RO2-R. + 0.519 RO2-N. + 0.962 R2O2. + 0.001 CCHO + 0.071 RCHO + 0.003 MEK + 0.473 PROD2 + 9.82 XC
7-Methyl Pentadecane	2.00e-11	7-ME-C15 + HO. = 0.503 RO2-R. + 0.497 RO2-N. + 0.853 R2O2. + 0.022 RCHO + 0.5 PROD2 + 9.95 XC
3-Methyl Pentadecane	2.00e-11	3-ME-C15 + HO. = 0.504 RO2-R. + 0.496 RO2-N. + 0.853 R2O2. + 0.018 CCHO + 0.012 RCHO + 0.008 MEK + 0.493 PROD2 + 9.964 XC
	Branched Alkanes used in the "High Branching" Representation	
2,3,4,6-Tetramethyl Heptane	1.31e-11	2346TMC7 + HO. = 0.534 RO2-R. + 0.466 RO2-N. + 1.429 R2O2. + 0.036 HCHO + 0.256 CCHO + 0.076 RCHO + 0.446 ACET + 0.15 MEK + 0.492 PROD2 + 2.534 XC
2,3,5,7-Tetramethyl Octane	1.45e-11	2357TMC8 + HO. = 0.484 RO2-R. + 0.516 RO2-N. + 1.34 R2O2. + 0.033 HCHO + 0.076 CCHO + 0.289 RCHO + 0.379 ACET + 0.005 MEK + 0.358 PROD2 + 4.544 XC
2,4,6,8-Tetramethyl Nonane	1.59e-11	2468TMC9 + HO. = 0.457 RO2-R. + 0.543 RO2-N. + 1.24 R2O2. + 0.015 HCHO + 0.002 CCHO + 0.361 RCHO + 0.075 ACET + 0.001 MEK + 0.348 PROD2 + 6.322 XC
2,3,6-Dimethyl 4-Isopropyl Heptane	1.63e-11	236M4IC7 + HO. = 0.485 RO2-R. + 0.515 RO2-N. + 1.485 R2O2. + 0.015 HCHO + 0.269 CCHO + 0.306 RCHO + 0.593 ACET + 0.165 MEK + 0.282 PROD2 + 4.304 XC
2,4,5,6,8-Pentamethyl Nonane	1.76e-11	24568MC9 + HO. = 0.431 RO2-R. + 0.569 RO2-N. + 1.496 R2O2. + 0.022 HCHO + 0.094 CCHO + 0.089 RCHO + 0.064 ACET + 0.02 MEK + 0.847 PROD2 + 4.755 XC
2-Methyl 3,5-Diisopropyl Heptane	1.81e-11	2M35IPC7 + HO. = 0.459 RO2-R. + 0.541 RO2-N. + 1.318 R2O2. + 0.005 HCHO + 0.06 CCHO + 0.162 RCHO + 0.646 ACET + 0.001 MEK + 0.367 PROD2 + 5.996 XC
2,6,8-Trimethyl 4-Isopropyl Nonane	1.91e-11	268M4IC9 + HO. = 0.436 RO2-R. + 0.564 RO2-N. + 1.276 R2O2. + 0.009 HCHO + 0.001 CCHO + 0.284 RCHO + 0.265 ACET + 0.001 MEK + 0.346 PROD2 + 7.876 XC
2,7-Dimethyl 3,5-Diisopropyl Heptane	2.09e-11	27M35IC8 + HO. = 0.43 RO2-R. + 0.57 RO2-N. + 1.35 R2O2. + 0.005 HCHO + 0.003 CCHO + 0.234 RCHO + 0.562 ACET + 0.001 MEK + 0.329 PROD2 + 8.205 XC
	Cycloalkanes	
Pentyl Cyclohexane	1.63e-11	C5-CYCC6 + HO. = 0.557 RO2-R. + 0.443 RO2-N. + 0.808 R2O2. + 0.016 CCHO + 0.147 RCHO + 0.456 PROD2 + 5.135 XC
1,3-Diethyl-5-Methyl Cyclohexane	1.72e-11	13E5MCC6 + HO. = 0.429 RO2-R. + 0.566 RO2-N. + 1.371 R2O2. + 0.003 CCO-O2. + 0.002 RCO-O2. + 0.006 CO + 0.02 HCHO + 0.168 CCHO + 0.355 RCHO + 0.009 MEK + 0.09 PROD2 + 5.587 XC
1-Ethyl-2-Propyl Cyclohexane	1.70e-11	1E2PCYC6 + HO. = 0.461 RO2-R. + 0.539 RO2-N. + 1.199 R2O2. + 0.001 RCO-O2. + 0.007 HCHO + 0.031 CCHO + 0.186 RCHO + 0.349 PROD2 + 5.045 XC
Hexyl Cyclohexane	1.78e-11 [d]	C6-CYCC6 + HO. = 0.527 RO2-R. + 0.473 RO2-N. + 0.849 R2O2. + 0.093 RCHO + 0.461 PROD2 + 6.118 XC
1,3,5-Triethyl Cyclohexane	1.90e-11	135ECYC6 + HO. = 0.417 RO2-R. + 0.58 RO2-N. + 1.353 R2O2. + 0.003 RCO-O2. + 0.005 CO + 0.014 HCHO + 0.221 CCHO + 0.315 RCHO + 0.008 MEK + 0.116 PROD2 + 6.373 XC

Table 9 (continued)

Compound	k(298) [a] (cm^3 $molec^{-1}$ s^{-1})	Reactions and Products [b]
1-Methyl-4-Pentyl Cyclohexane	1.80e-11	1M4C5CY6 + HO. = 0.482 RO2-R. + 0.518 RO2-N. + 1.049 R2O2. + 0.001 CCO-O2. + 0.001 HCHO + 0.015 CCHO + 0.21 RCHO + 0.326 PROD2 + 6.274 XC
Heptyl Cyclohexane	1.91e-11	C7-CYCC6 + HO. = 0.515 RO2-R. + 0.485 RO2-N. + 0.855 R2O2. + 0.069 RCHO + 0.462 PROD2 + 7.108 XC
1,3-Diethyl-5-Pentyl Cyclohexane	2.05e-11	13E5PCC6 + HO. = 0.433 RO2-R. + 0.564 RO2-N. + 1.237 R2O2. + 0.003 RCO-O2. + 0.002 CO + 0.01 HCHO + 0.132 CCHO + 0.342 RCHO + 0.002 MEK + 0.188 PROD2 + 7.163 XC
1-Methyl-2-Hexyl-Cyclohexane	1.94e-11	1M2C6CC6 + HO. = 0.462 RO2-R. + 0.537 RO2-N. + 1.08 R2O2. + 0.001 RCO-O2. + 0.004 HCHO + 0.009 CCHO + 0.128 RCHO + 0.38 PROD2 + 7.092 XC
Octyl Cyclohexane	2.05e-11	C8-CYCC6 + HO. = 0.511 RO2-R. + 0.489 RO2-N. + 0.847 R2O2. + 0.063 RCHO + 0.463 PROD2 + 8.099 XC
1,3-Dipropyl-5-EthylCyclohexane	2.19e-11	13P5ECC6 + HO. = 0.445 RO2-R. + 0.553 RO2-N. + 1.158 R2O2. + 0.002 RCO-O2. + 0.001 CO + 0.007 HCHO + 0.06 CCHO + 0.376 RCHO + 0.234 PROD2 + 8.017 XC
1-Methyl-4-Heptyl Cyclohexane	2.08e-11	1M4C7CC6 + HO. = 0.455 RO2-R. + 0.544 RO2-N. + 1.059 R2O2. + 0.001 HCHO + 0.131 RCHO + 0.349 PROD2 + 8.242 XC
Nonyl Cyclohexane	2.20e-11	C9-CYCC6 + HO. = 0.509 RO2-R. + 0.49 RO2-N. + 0.838 R2O2. + 0.058 RCHO + 0.465 PROD2 + 9.091 XC
1,3,5-Tripropyl Cyclohexane	2.33e-11	135PCYC6 + HO. = 0.453 RO2-R. + 0.545 RO2-N. + 1.106 R2O2. + 0.002 RCO-O2. + 0.001 CO + 0.005 HCHO + 0.415 RCHO + 0.258 PROD2 + 8.923 XC
1-Methyl-2-Octyl Cyclohexane	2.22e-11	1M2C8CC6 + HO. = 0.462 RO2-R. + 0.538 RO2-N. + 1.035 R2O2. + 0.003 HCHO + 0.008 CCHO + 0.105 RCHO + 0.394 PROD2 + 9.08 XC
Decyl Cyclohexane	2.34e-11	C10CYCC6 + HO. = 0.508 RO2-R. + 0.492 RO2-N. + 0.834 R2O2. + 0.055 RCHO + 0.467 PROD2 + 10.085 XC
1,3-Propyl-5-Butyl Cyclohexane	2.47e-11	13P5BCC6 + HO. = 0.461 RO2-R. + 0.538 RO2-N. + 1.045 R2O2. + 0.001 RCO-O2. + 0.001 CO + 0.003 HCHO + 0.013 CCHO + 0.322 RCHO + 0.318 PROD2 + 9.863 XC
1-Methyl-4-Nonyl Cyclohexane	2.36e-11	1M4C9CY6 + HO. = 0.458 RO2-R. + 0.541 RO2-N. + 1.018 R2O2. + 0.001 HCHO + 0.113 RCHO + 0.367 PROD2 + 10.209 XC
		Exxate Constituents
n-Hexyl Acetate	7.47e-12	NC6-ACET + HO. = 0.683 RO2-R. + 0.309 RO2-N. + 0.805 R2O2. + 0.008 RCO-O2. + 0.058 RCHO + 0.647 PROD2 + 0.008 CCO-OH + 2.053 XC
2-Methylpentyl Acetate	7.73e-12	2MC5-ACT + HO. = 0.704 RO2-R. + 0.289 RO2-N. + 0.906 R2O2. + 0.006 RCO-O2. + 0.016 CO + 0.002 HCHO + 0.012 CCHO + 0.436 RCHO + 0.212 MEK + 0.253 PROD2 + 0.023 CCO-OH + 0.089 INERT + 2.397 XC
3-Methylpentyl Acetate	7.73e-12	3MC5-ACT + HO. = 0.732 RO2-R. + 0.259 RO2-N. + 0.877 R2O2. + 0.01 RCO-O2. + 0.001 HCHO + 0.179 CCHO + 0.386 RCHO + 0.31 MEK + 0.354 PROD2 + 0.01 CCO-OH + 0.001 INERT + 1.515 XC
4-Methylpentyl Acetate	7.45e-12	4MC5-ACT + HO. = 0.503 RO2-R. + 0.294 RO2-N. + 1.029 R2O2. + 0.203 RCO-O2. + 0.005 HCHO + 0.197 RCHO + 0.145 ACET + 0.178 MEK + 0.139 PROD2 + 0.203 CCO-OH + 0.01 INERT + 2.633 XC

Table 9 (continued)

Compound	k(298) [a] (cm^3 $molec^{-1}$ s^{-1})	Reactions and Products [b]
2,3-Dimethylbutyl Acetate	7.71e-12	23MC4ACT + HO. = 0.748 RO2-R. + 0.247 RO2-N. + 1.021 R2O2. + 0.005 RCO-O2. + 0.009 CO + 0.018 HCHO + 0.184 CCHO + 0.037 RCHO + 0.717 ACET + 0.549 MEK + 0.006 PROD2 + 0.013 CCO-OH + 0.2 INERT + 1.391 XC
4-Methylhexyl Acetate	9.15e-12	4MC6-ACT + HO. = 0.456 RO2-R. + 0.359 RO2-N. + 1.056 R2O2. + 0.185 RCO-O2. + 0.001 HCHO + 0.111 CCHO + 0.133 RCHO + 0.197 MEK + 0.196 PROD2 + 0.185 CCO-OH + 0.011 INERT + 3.325 XC
2-Methylhexyl Acetate	9.15e-12	2MC6-ACT + HO. = 0.631 RO2-R. + 0.364 RO2-N. + 0.922 R2O2. + 0.004 RCO-O2. + 0.004 CO + 0.001 HCHO + 0.045 CCHO + 0.143 RCHO + 0.107 MEK + 0.496 PROD2 + 0.008 CCO-OH + 0.082 INERT + 2.772 XC
3-Methylhexyl Acetate	9.15e-12	3MC6-ACT + HO. = 0.656 RO2-R. + 0.338 RO2-N. + 0.819 R2O2. + 0.006 RCO-O2. + 0.001 HCHO + 0.01 CCHO + 0.301 RCHO + 0.112 MEK + 0.446 PROD2 + 0.006 CCO-OH + 0.001 INERT + 2.891 XC
5-Methylhexyl Acetate	8.87e-12	5MC6-ACT + HO. = 0.629 RO2-R. + 0.365 RO2-N. + 0.821 R2O2. + 0.006 RCO-O2. + 0.005 CO + 0.008 HCHO + 0.089 RCHO + 0.013 ACET + 0.566 PROD2 + 0.011 CCO-OH + 0.003 INERT + 3.05 XC
2,4-Dimethylpentyl Acetate	9.13e-12	24MC5ACT + HO. = 0.587 RO2-R. + 0.397 RO2-N. + 1.291 R2O2. + 0.016 RCO-O2. + 0.008 CO + 0.153 HCHO + 0.02 CCHO + 0.267 RCHO + 0.048 ACET + 0.248 MEK + 0.193 PROD2 + 0.024 CCO-OH + 0.247 INERT + 2.979 XC
3-Ethylpentyl Acetate	9.56e-12	3EC5-ACT + HO. = 0.687 RO2-R. + 0.309 RO2-N. + 0.852 R2O2. + 0.004 RCO-O2. + 0.001 HCHO + 0.173 CCHO + 0.338 RCHO + 0.232 MEK + 0.398 PROD2 + 0.004 CCO-OH + 0.001 INERT + 2.448 XC
n-Heptyl Acetate	8.89e-12	NC7-ACET + HO. = 0.624 RO2-R. + 0.369 RO2-N. + 0.797 R2O2. + 0.006 RCO-O2. + 0.009 RCHO + 0.615 PROD2 + 0.006 CCO-OH + 3.034 XC
3,4-Dimethylhexyl Acetate	1.08e-11	34MC6ACT + HO. = 0.594 RO2-R. + 0.374 RO2-N. + 1.064 R2O2. + 0.031 RCO-O2. + 0.008 HCHO + 0.309 CCHO + 0.109 RCHO + 0.274 MEK + 0.51 PROD2 + 0.031 CCO-OH + 0.011 INERT + 2.478 XC
3,5-Dimethylhexyl Acetate	1.06e-11	35MC6ACT + HO. = 0.576 RO2-R. + 0.419 RO2-N. + 1.103 R2O2. + 0.005 RCO-O2. + 0.097 HCHO + 0.014 CCHO + 0.337 RCHO + 0.041 ACET + 0.008 MEK + 0.484 PROD2 + 0.005 CCO-OH + 3.263 XC
3-Ethylhexyl Acetate	1.10e-11	3EC6-ACT + HO. = 0.624 RO2-R. + 0.374 RO2-N. + 0.82 R2O2. + 0.003 RCO-O2. + 0.001 HCHO + 0.043 CCHO + 0.276 RCHO + 0.546 PROD2 + 0.003 CCO-OH + 0.001 INERT + 3.551 XC
4-Methylheptyl Acetate	1.06e-11	4MC7-ACT + HO. = 0.444 RO2-R. + 0.408 RO2-N. + 0.984 R2O2. + 0.148 RCO-O2. + 0.001 HCHO + 0.001 CCHO + 0.086 RCHO + 0.114 MEK + 0.309 PROD2 + 0.148 CCO-OH + 0.009 INERT + 4.232 XC
4,5-Dimethylhexyl Acetate	1.06e-11	45MC6ACT + HO. = 0.524 RO2-R. + 0.397 RO2-N. + 1.117 R2O2. + 0.079 RCO-O2. + 0.005 HCHO + 0.087 CCHO + 0.134 RCHO + 0.323 ACET + 0.102 MEK + 0.312 PROD2 + 0.079 CCO-OH + 0.012 INERT + 3.371 XC
5-Methylheptyl Acetate	1.06e-11	5MC7-ACT + HO. = 0.585 RO2-R. + 0.409 RO2-N. + 0.836 R2O2. + 0.005 RCO-O2. + 0.005 CO + 0.001 HCHO + 0.044 CCHO + 0.058 RCHO + 0.012 MEK + 0.544 PROD2 + 0.01 CCO-OH + 0.003 INERT + 3.929 XC
3-Methylheptyl Acetate	1.06e-11	3MC7-ACT + HO. = 0.583 RO2-R. + 0.412 RO2-N. + 0.843 R2O2. + 0.005 RCO-O2. + 0.001 HCHO + 0.034 CCHO + 0.079 RCHO + 0.561 PROD2 + 0.005 CCO-OH + 3.834 XC

Table 9 (continued)

Compound	k(298) [a] (cm^3 $molec^{-1}$ s^{-1})	Reactions and Products [b]
2,4-Dimethylhexyl Acetate	1.08e-11	24MC6ACT + HO. = 0.506 RO2-R. + 0.48 RO2-N. + 1.388 R2O2. + 0.014 RCO-O2. + 0.003 CO + 0.012 HCHO + 0.286 CCHO + 0.132 RCHO + 0.173 MEK + 0.297 PROD2 + 0.017 CCO-OH + 0.271 INERT + 3.319 XC
n-Octyl Acetate	1.03e-11	NC8-ACET + HO. = 0.585 RO2-R. + 0.409 RO2-N. + 0.784 R2O2. + 0.005 RCO-O2. + 0.008 RCHO + 0.577 PROD2 + 0.005 CCO-OH + 4.03 XC
3,5-Dimethylheptyl Acetate	1.23e-11	35MC7ACT + HO. = 0.492 RO2-R. + 0.504 RO2-N. + 1.242 R2O2. + 0.004 RCO-O2. + 0.005 HCHO + 0.227 CCHO + 0.266 RCHO + 0.012 MEK + 0.451 PROD2 + 0.004 CCO-OH + 3.941 XC
2,4-Dimethylheptyl Acetate	1.23e-11	24MC7ACT + HO. = 0.48 RO2-R. + 0.508 RO2-N. + 1.282 R2O2. + 0.012 RCO-O2. + 0.001 CO + 0.008 HCHO + 0.003 CCHO + 0.303 RCHO + 0.045 MEK + 0.411 PROD2 + 0.013 CCO-OH + 0.229 INERT + 4.089 XC
2-Methyloctyl Acetate	1.20e-11	2MC8-ACT + HO. = 0.538 RO2-R. + 0.459 RO2-N. + 0.931 R2O2. + 0.003 RCO-O2. + 0.002 CO + 0.002 CCHO + 0.077 RCHO + 0.041 MEK + 0.476 PROD2 + 0.005 CCO-OH + 0.042 INERT + 4.929 XC
4-Methyloctyl Acetate	1.20e-11	4MC8-ACT + HO. = 0.47 RO2-R. + 0.439 RO2-N. + 0.919 R2O2. + 0.091 RCO-O2. + 0.01 CCHO + 0.064 RCHO + 0.455 PROD2 + 0.091 CCO-OH + 0.005 INERT + 4.966 XC
5-Methyloctyl Acetate	1.20e-11	5MC8-ACT + HO. = 0.559 RO2-R. + 0.437 RO2-N. + 0.831 R2O2. + 0.004 RCO-O2. + 0.004 CO + 0.001 CCHO + 0.087 RCHO + 0.003 MEK + 0.531 PROD2 + 0.008 CCO-OH + 0.002 INERT + 4.884 XC
3,6-Dimethylheptyl Acetate	1.20e-11	36MC7ACT + HO. = 0.519 RO2-R. + 0.477 RO2-N. + 1.16 R2O2. + 0.004 RCO-O2. + 0.012 HCHO + 0.006 CCHO + 0.251 RCHO + 0.148 ACET + 0.494 PROD2 + 0.004 CCO-OH + 3.934 XC
4,6-Dimethylheptyl Acetate	1.20e-11	46MC7ACT + HO. = 0.425 RO2-R. + 0.452 RO2-N. + 1.123 R2O2. + 0.123 RCO-O2. + 0.037 HCHO + 0.009 CCHO + 0.178 RCHO + 0.022 ACET + 0.007 MEK + 0.374 PROD2 + 0.123 CCO-OH + 0.007 INERT + 4.739 XC
4,5-Dimethylheptyl Acetate	1.23e-11	45MC7ACT + HO. = 0.522 RO2-R. + 0.431 RO2-N. + 1.136 R2O2. + 0.047 RCO-O2. + 0.003 HCHO + 0.21 CCHO + 0.08 RCHO + 0.235 MEK + 0.472 PROD2 + 0.047 CCO-OH + 0.01 INERT + 3.736 XC
3-Ethylheptyl Acetate	1.24e-11	3EC7-ACT + HO. = 0.556 RO2-R. + 0.442 RO2-N. + 0.849 R2O2. + 0.002 RCO-O2. + 0.049 CCHO + 0.074 RCHO + 0.536 PROD2 + 0.002 CCO-OH + 4.8 XC
2,3-Dimethylheptyl Acetate	1.23e-11	23MC7ACT + HO. = 0.569 RO2-R. + 0.429 RO2-N. + 1.066 R2O2. + 0.002 RCO-O2. + 0.007 CO + 0.002 HCHO + 0.068 CCHO + 0.071 RCHO + 0.289 MEK + 0.528 PROD2 + 0.009 CCO-OH + 0.089 INERT + 3.631 XC
2,5-Dimethylheptyl Acetate	1.23e-11	25MC7ACT + HO. = 0.534 RO2-R. + 0.463 RO2-N. + 1.235 R2O2. + 0.003 RCO-O2. + 0.032 CO + 0.003 HCHO + 0.162 CCHO + 0.089 RCHO + 0.217 MEK + 0.45 PROD2 + 0.035 CCO-OH + 0.107 INERT + 3.84 XC
2,3,5-Teimethylhexyl Acetate	1.22e-11	235M6ACT + HO. = 0.541 RO2-R. + 0.457 RO2-N. + 1.288 R2O2. + 0.002 RCO-O2. + 0.007 CO + 0.04 HCHO + 0.063 CCHO + 0.058 RCHO + 0.063 ACET + 0.376 MEK + 0.484 PROD2 + 0.009 CCO-OH + 0.131 INERT + 3.162 XC
n-Nonyl Acetate	1.17e-11	NC9-ACET + HO. = 0.561 RO2-R. + 0.435 RO2-N. + 0.777 R2O2. + 0.004 RCO-O2. + 0.007 RCHO + 0.554 PROD2 + 0.004 CCO-OH + 5.025 XC

Table 9 (continued)

Compound	k(298) [a] (cm^3 $molec^{-1}$ s^{-1})	Reactions and Products [b]
3,6-Dimethyloctyl Acetate	1.37e-11	36MC8ACT + HO. = 0.522 RO2-R. + 0.474 RO2-N. + 1.101 R2O2. + 0.004 RCO-O2. + 0.002 HCHO + 0.107 CCHO + 0.187 RCHO + 0.071 MEK + 0.514 PROD2 + 0.004 CCO-OH + 4.987 XC
4,6-Dimethyloctyl Acetate	1.37e-11	46MC8ACT + HO. = 0.429 RO2-R. + 0.495 RO2-N. + 1.158 R2O2. + 0.076 RCO-O2. + 0.003 HCHO + 0.136 CCHO + 0.194 RCHO + 0.013 MEK + 0.395 PROD2 + 0.076 CCO-OH + 0.004 INERT + 5.371 XC
3-Isopropylheptyl Acetate	1.38e-11	3IPC7ACT + HO. = 0.548 RO2-R. + 0.449 RO2-N. + 0.958 R2O2. + 0.003 RCO-O2. + 0.001 HCHO + 0.012 CCHO + 0.117 RCHO + 0.247 ACET + 0.503 PROD2 + 0.003 CCO-OH + 5.16 XC
3,5,7-Trimethyloctyl Acetate	1.51e-11	357M8ACT + HO. = 0.463 RO2-R. + 0.534 RO2-N. + 1.185 R2O2. + 0.003 RCO-O2. + 0.008 HCHO + 0.006 CCHO + 0.368 RCHO + 0.041 ACET + 0.001 MEK + 0.394 PROD2 + 0.003 CCO-OH + 6.168 XC
		Lumped Species Representing Entire Fluids
Exxal® D95 Fluid	1.85e-11	D95 + HO. = #.496 RO2-R. + #.504 RO2-N. + #.938 R2O2. + #.002 HCHO + #.026 CCHO + #.106 RCHO + #.007 MEK + #.429 PROD2
Isopar®-M Fluid (Standard Representation)	1.76e-11	ISOPAR-M + HO. = #.497 RO2-R. + #.503 RO2-N. + #.949 R2O2. + #.001 HCHO + #.035 CCHO + #.089 RCHO + #.017 MEK + #.45 PROD2
Isopar®-M Fluid (High Branching Representation)	1.80e-11	ISOPARMB + HO. = #.456 RO2-R. + #.544 RO2-N. + #1.314 R2O2. + #.013 HCHO + #.07 CCHO + #.211 RCHO + #.291 ACET + #.022 MEK + #.449 PROD2
Exxate® 600 Fluid	7.62e-12	OC6-ACET + HO. = #.664 RO2-R. + #.291 RO2-N. + #.888 R2O2. + #.045 RCO-O2. + #.003 CO + #.002 HCHO + #.049 CCHO + #.231 RCHO + #.036 ACET + #.155 MEK + #.398 PROD2 + #.048 CCO-OH + #.022 INERT
Exxate® 700 Fluid	9.16e-12	OC7-ACET + HO. = #.59 RO2-R. + #.355 RO2-N. + #.985 R2O2. + #.054 RCO-O2. + #.002 CO + #.025 HCHO + #.084 CCHO + #.182 RCHO + #.008 ACET + #.165 MEK + #.38 PROD2 + #.056 CCO-OH + #.048 INERT
Exxate® 800 Fluid	1.07e-11	OC8-ACET + HO. = #.558 RO2-R. + #.403 RO2-N. + #1.024 R2O2. + #.039 RCO-O2. + #.001 CO + #.02 HCHO + #.114 CCHO + #.17 RCHO + #.039 ACET + #.098 MEK + #.451 PROD2 + #.039 CCO-OH + #.024 INERT
Exxate® 900 Fluid	1.24e-11	OC9-ACET + HO. = #.51 RO2-R. + #.462 RO2-N. + #1.083 R2O2. + #.027 RCO-O2. + #.002 CO + #.007 HCHO + #.102 CCHO + #.155 RCHO + #.028 ACET + #.062 MEK + #.472 PROD2 + #.029 CCO-OH + #.018 INERT
Exxate® 1000 Fluid	1.36e-11	OC10ACET + HO. = #.5 RO2-R. + #.473 RO2-N. + #1.084 R2O2. + #.027 RCO-O2. + #.002 HCHO + #.094 CCHO + #.172 RCHO + #.074 ACET + #.036 MEK + #.468 PROD2 + #.027 CCO-OH + #.002 INERT
Exxate® 1200 Fluid	1.68e-11	OC12ACET + HO. = #.457 RO2-R. + #.527 RO2-N. + #1.176 R2O2. + #.016 RCO-O2. + #.001 CO + #.015 HCHO + #.055 CCHO + #.198 RCHO + #.014 ACET + #.088 MEK + #.421 PROD2 + #.017 CCO-OH + #.021 INERT
Exxate® 1300 Fluid	1.79e-11	OC13ACET + HO. = #.445 RO2-R. + #.53 RO2-N. + #1.175 R2O2. + #.025 RCO-O2. + #.001 CO + #.013 HCHO + #.06 CCHO + #.163 RCHO + #.014 ACET + #.09 MEK + #.417 PROD2 + #.026 CCO-OH + #.024 INERT

Table 9 (continued)

[a] OH Radical rate constant at 298^{o}K. Rate constant estimated using the group-additivity method of Kwok and Atkinson (1995) unless indicated otherwise. No temperature dependence information is available for any of these rate constants, so temperature dependence is ignored in the model simulations.

[b] See Table A-1 in Appendix A for a description of the SAPRC-99 model species used to represent the products formed. The reactant name indicates the model species name used for this compound.

[c] Rate constant recommended by Atkinson (1997).

[d] Rate constant measured by Carter et al (2000c).

As discussed above, there is an uncertainty concerning the most appropriate representative compounds to use when representing the branched alkanes in the Isopar-M fluid, so model calculations were carried out using two different branched alkane representations. In the "standard" model the Isopar-M fluid is represented by the lumped model species ISOPAR-M, whose parameters were derived using the "standard representation" species shown on Table 4. In the "high branching" model, Isopar-M is represented by the lumped model species "ISOPARMB", whose parameters are derived using the "highly branched representation" species on that table. The main differences between these representations in terms of the overall Isopar-M mechanisms is that using the high branching representation causes the nitrate yield to increase by ~8%, the number of NO to NO_2 conversions to increase by ~40%, and the total yield of aldehyde products to increase by about 0.16 moles (with isobutyraldehyde, $CH_3CH(CH_3)CHO$, being the major contributor), and significant formation of acetone is predicted. The higher nitrate yields would tend to result in a lower reactivity mechanism, but the higher number of NO to NO_2 conversions and the higher yields of aldehydes would have the opposite effect on overall reactivity. As discussed later, the predicted differences in aldehyde yields are of particular concern in terms of effects on atmospheric reactivity predictions.

Methods

The environmental chamber modeling methods used in this work are based on those discussed in detail by Carter and Lurmann (1990, 1991), updated as discussed by Carter et al. (1995c; 1997b, 2000b). Model simulations of environmental chamber experiments requires including in the model appropriate representations of chamber-dependent effects such as wall reactions and characteristics of the light source. The photolysis rates were derived from results of NO_2 actinometry experiments and measurements of the relative spectra of the light source. In the case of the xenon arc lights used in the CTC, the spectra were derived from those measured during the individual experiments, assuming continuous linear changes in relative intensity at the various wavelengths, as discussed by Carter et al. (1997b, 2000b). The thermal rate constants were calculated using the temperatures measured during the experiments, with the small variations in temperature with time during the experiment being taken into account. The computer programs and modeling methods employed are discussed in more detail elsewhere (Carter et al, 1995c). The specific values of the chamber-dependent parameters used in the model simulations of the experiments for this study are given in Table A-4 in Appendix A.

As indicated in the Experimental Results section, above, there is some uncertainty concerning the amounts of fluid constituents injected into the gas phase, depending on what assumptions are made concerning injection efficiencies or FID response factors for the fluid constituents. Therefore, for each experiment separate simulations were carried out using the two assumptions in this regard. The "standard model" calculations assumed that FID total hydrocarbon detector calibrated by propane gave a 100% response to the hydrocarbon constituents and a 92% response to the Exxate 1000 constituents, which meant that no more than ~80% of the liquid constituents were being injected into the gas phase. The "80% THC response" or (for Exxate) "74% THC response" calculations are based on the assumption that all the constituents are injected into the gas phase in the runs without apparent injection problems. Therefore, these calculations had initial gas phase fluid constituent concentrations that were 25% higher than used in the standard model.

In the case of Isopar-M, the effects of making alternative assumptions about the model species used to represent the branched alkanes were also assessed in the simulations of the chamber experiments. In these simulations, the calculations labeled "standard model" used not only the standard model in terms of 100% FID response, but also used the "standard representation" in terms of the branched alkane species, i.e., used the "ISOPAR-M" model species on Table 9. The calculations labeled "80% THC response" also used the "standard" branched alkane representation (i.e., the ISOPAR-M species), so comparing these two show only effects of alternative assumptions regarding initial concentrations. The calculations labeled "high branching" use the standard model with regard to FID response, so comparing the "high branching" and the "standard model" show only the effects of alternative assumptions concerning the branched alkane representation.

Results

D95 Fluid

The results of the model simulations of the experiments with D95 fluid are shown in Figure 2, which gives plots of the experimental and calculated $\Delta([O_3]\text{-}[NO])$ data and $\Delta([O_3]\text{-}[NO])$ and IntOH incremental reactivities for the experiments using this solvent. The solid lines show model calculations using the standard representation in terms of THC response, the dotted lines show the calculations assuming 80% THC response and thus 25% higher initial concentrations, and the points show the experimental data. The error bars in the $\Delta([O3]\text{-}[NO])$ and IntOH change data are based on an assumed 3% and 2% variabilities in the $\Delta([O_3]\text{-}[NO])$ and m-xylene (or 1,3,5-trimethylbenzene) OH tracer measurements, respectively. These may underestimate the actual variability of the data, but are used in this consistency with our previous presentations of our data (e.g., Carter et al, 1997a,b, 2000a-c; Carter, 2000).

Figure 2 shows that the model gives reasonably good simulations of the results of the experiments with the D95 fluid, correctly predicting how the $\Delta([O_3]\text{-}[NO])$ reactivity characteristics vary with experimental condition, and giving reasonably good simulations of the $\Delta([O_3]\text{-}[NO])$ and IntOH inhibition effects in the mini-surrogate experiments. The model may have a slight bias towards

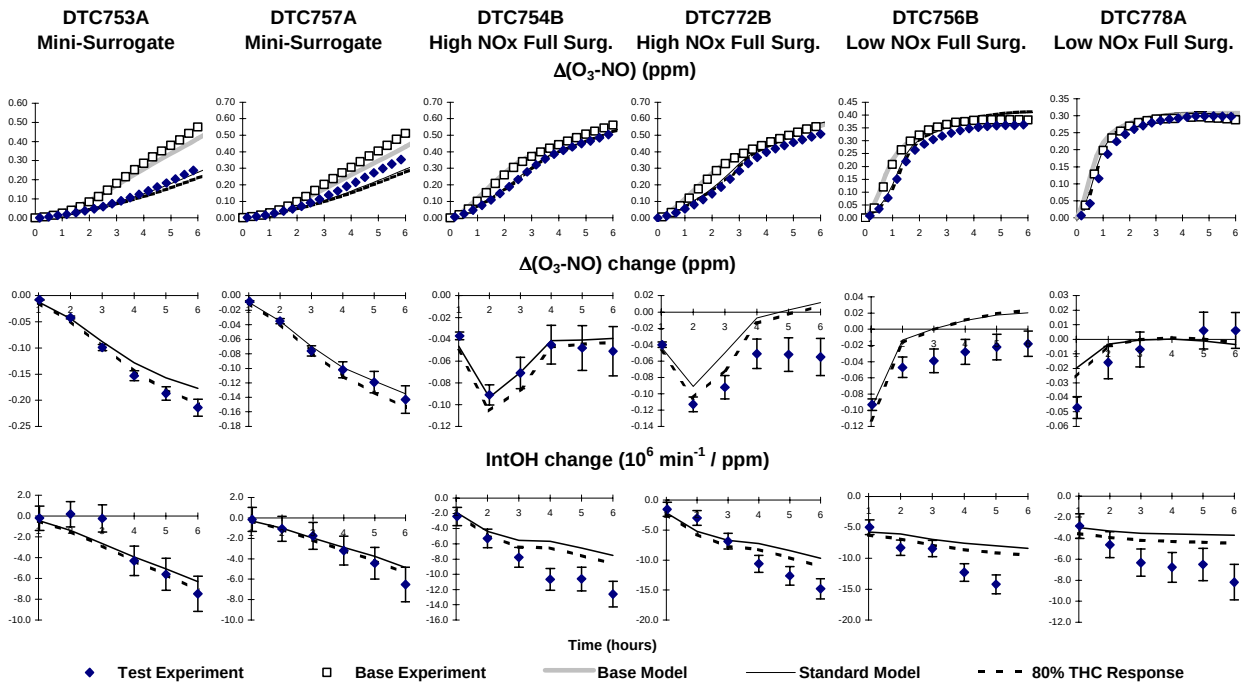

Figure 2. Selected experimental and calculated results of the incremental reactivity experiments with D95 Fluid.

underpredicting IntOH inhibition in the full surrogate experiments, and towards overpredicting $\Delta([O_3]-[NO])$ reactivities in two of the four full surrogate experiments. However, the changes in $\Delta([O_3]-[NO])$ caused by adding the D95 in the full surrogate experiments are small, and the biases may not be significant compared to experimental variability. In addition, underprediction of IntOH reactivities in the low NO_x full surrogate experiments is seen for many VOCs (Carter, 2000), and may be due at least in part to problems with the base mechanism rather than the mechanisms for the test compounds. Overall, the model performance is comparable to what was obtained in simulations of the all-alkane mineral spirits samples studied for Safety-Kleen (Carter et al, 2000a), which are similar to composition to D95 but have somewhat lower molecular weight range.

Figure 2 also shows that the ~25% uncertainty concerning the amount of gas-phase fluid constituents injected in the experiments is of minor consequence in terms of assessing model performance in simulating these experiments. In particular, the results of the two sets of simulations differ by less than the 25% variation in the input concentrations, indicating that the effects of adding these fluids changes in less than a liner manner when the amount added is increased. The calculations assuming the 80% THC response give a slightly better fit to the data in most cases, but the differences are much too small compared to experimental uncertainty to make any conclusions with regard to THC response in this basis.

Isopar-M

The results of the model simulations of the experiments with Isopar-M are shown in Figure 3. The format of the data is the same as used for the simulations of the D95 experiments, above, except that Figure 3 also shows model calculations using the "high branching" representation for the branched alkanes in the mixture.

The model gives fair simulations of the results of the experiments with the Isopar-M fluid, correctly predicting the overall reactivity characteristics observed. The overall performance is not quite as good as the model performance seen with D96 and with the mineral spirits samples studied by Carter et al (2000a) because of its consistent bias in underpredicting $\Delta([O_3]\text{-}[NO])$ reactivities in the high NO_x full surrogate runs. However, the effects of Isopar-M on $\Delta([O_3]\text{-}[NO])$ in the full surrogate experiments are relatively small, and no bias is observed in the simulations of one of the three high NO_x full surrogate runs. In addition, the model performs better in simulating IntOH reactivities in the high NO_x full experiments than it does for D95.

As with D95, making alternative assumptions concerning the amounts of Isopar-M injected in these experiments has only very small effects on the model simulations of the results, so this uncertainty does not affect conclusions concerning overall model performance.

Figure 3 shows that making alternative assumptions concerning the degree of branching of the branched alkane constituents has almost no effects on the model simulations of the $\Delta([O3]\text{-}[NO])$ and IntOH data in these experiments. This is despite the fact that the more branched representation involves higher nitrate yields, more NO to NO_2 conversions, and higher total aldehyde yields in the overall reactions of the constituents. Apparently the reactivity enhancing effects caused by the extra NO to NO_2 conversions and the additional aldehyde formation offsets the inhibiting effects caused by the increased nitrate yields, at least under the conditions of these experiments. This means that the $\Delta([O3]\text{-}[NO])$ and IntOH data in these experiments cannot be used as a basis for determining which set of compounds is the more representative in terms of the branched alkane mixtures actually present in Isopar fluids.

However, the branching representations also affect the predictions of the products that can be formed. As indicated in Table 9, above, the more branched representation predicts somewhat higher yields of formaldehyde and acetaldehyde, and considerably higher yields of higher aldehydes and acetone formed from Isopar-M than does the standard representation. Although a comprehensive product study was beyond the scope of this study, formaldehyde, acetaldehyde and acetone data were taken during the course of the reactivity experiments. The experimental and calculated data for formaldehyde and acetone are shown on Figure 4. Both models give reasonably good fits to the formaldehyde data, with no significant differences seen between the two different models. Similar results were obtained with the acetaldehyde data, and those results were not shown. On the other hand, the models differed significantly in acetone predictions, with the model predictions for the base case experiments and the standard Isopar-M model models predicting no acetone formation, while the high branching Isopar model predicts that measurable acetone levels are formed.

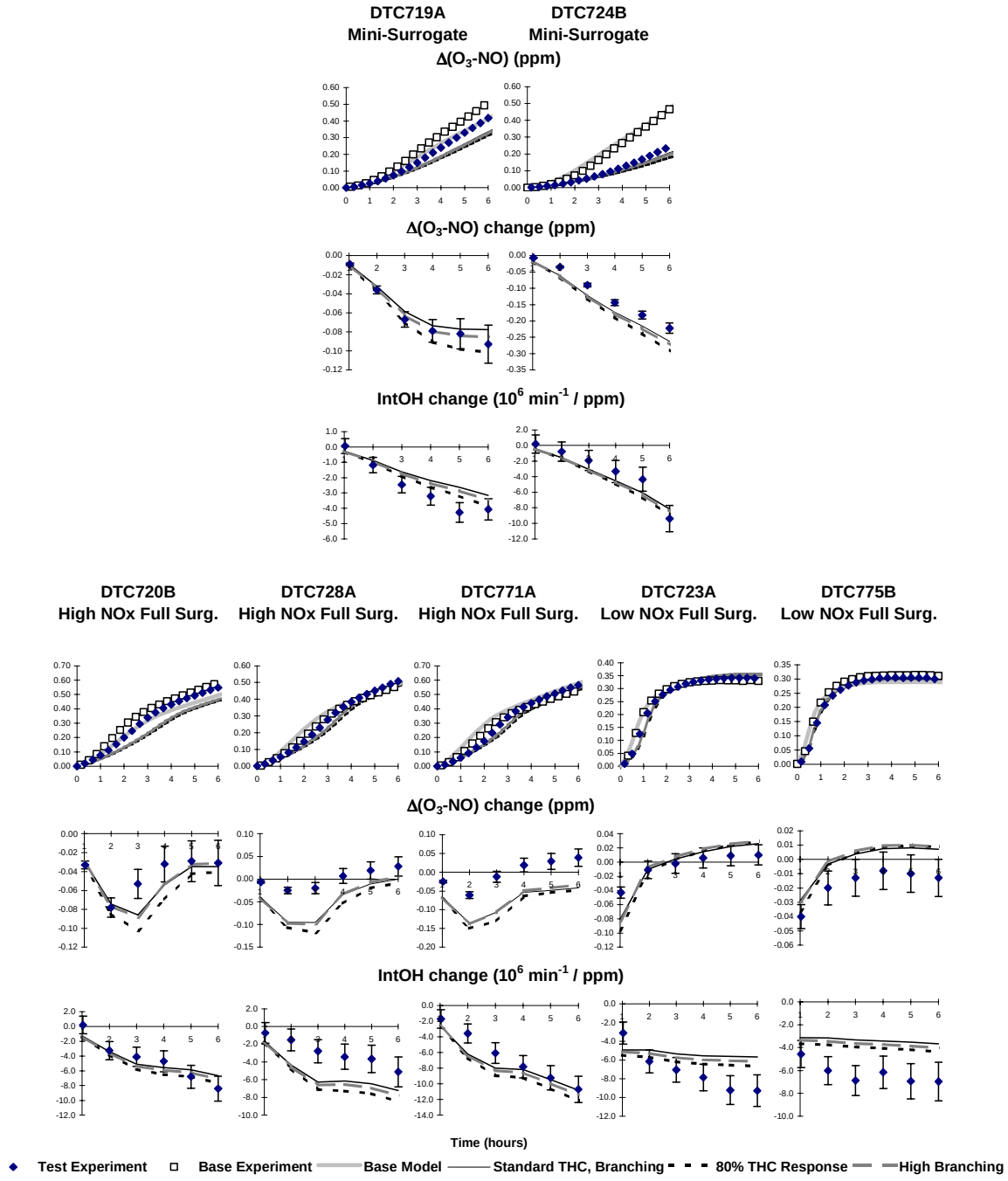

Figure 3. Selected experimental and calculated results of the incremental reactivity experiments with Isopar-M.

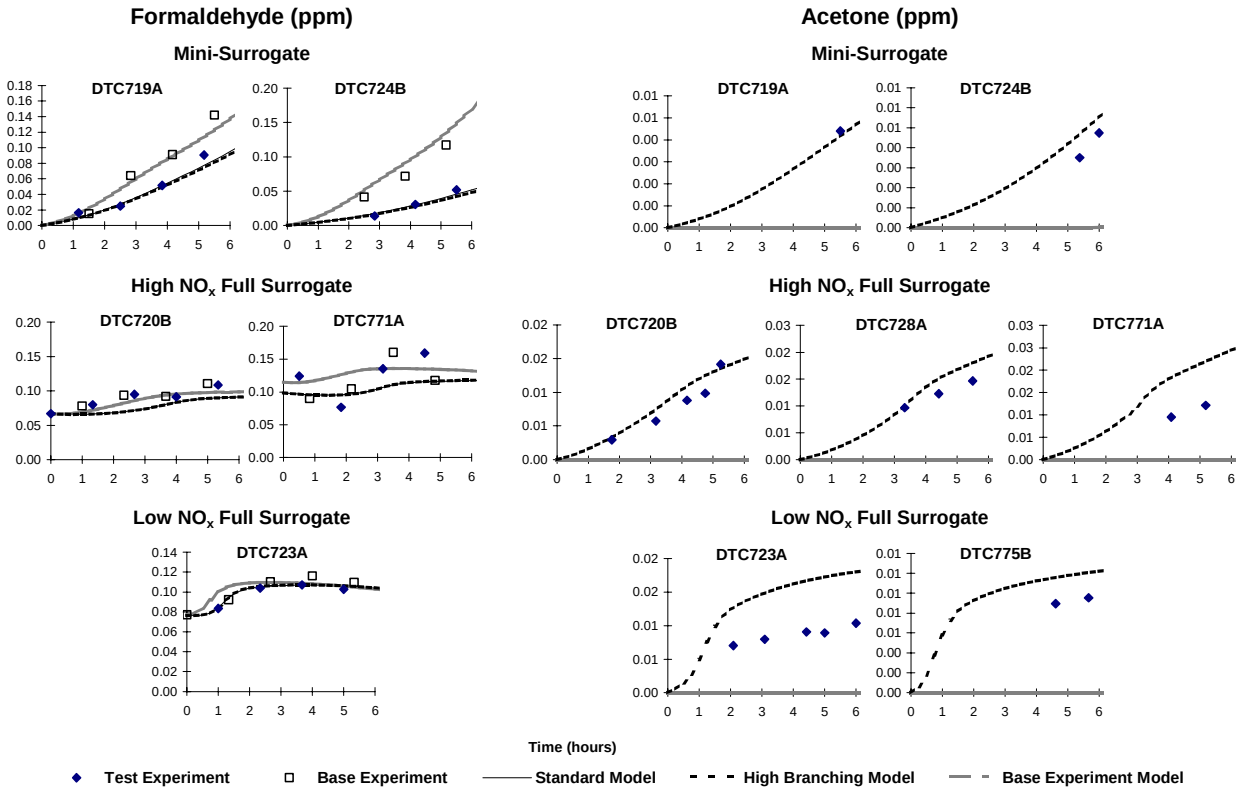

Figure 4. Experimental and calculated concentration-time plots for formaldehyde and acetone observed in the reactivity experiments with Isopar-M. Experiments without valid acetone or formaldehyde data are not shown.

The data on Figure 4 shows that acetone is indeed formed in the Isopar-M experiments, in approximately the yields predicted by the high branching model, though it is somewhat overpredicted in some of the experiments. This suggests that the highly branched compounds used in the high branching representation may be better approximation to the actual constituents of Isopar-M fluid, at least in terms of structures whose reactions tend to form acetone, than the standard representation that includes no acetone precursors. Because of the low reactivity of acetone its formation is not a significant factor affecting a VOC's overall reactivity, but these results suggest that the highly branched representation may give better predictions of the more reactive products as well.

Exxate-1000

The results of the model simulations of the experiments with Exxate-100 are shown in Figure 5. The format of the data is the same as used for the simulations of the D95 experiments, above. As with the other two mixtures, the effects of making alternative assumptions concerning the amounts of fluid injected are small, and do not affect assessments of overall model performance.

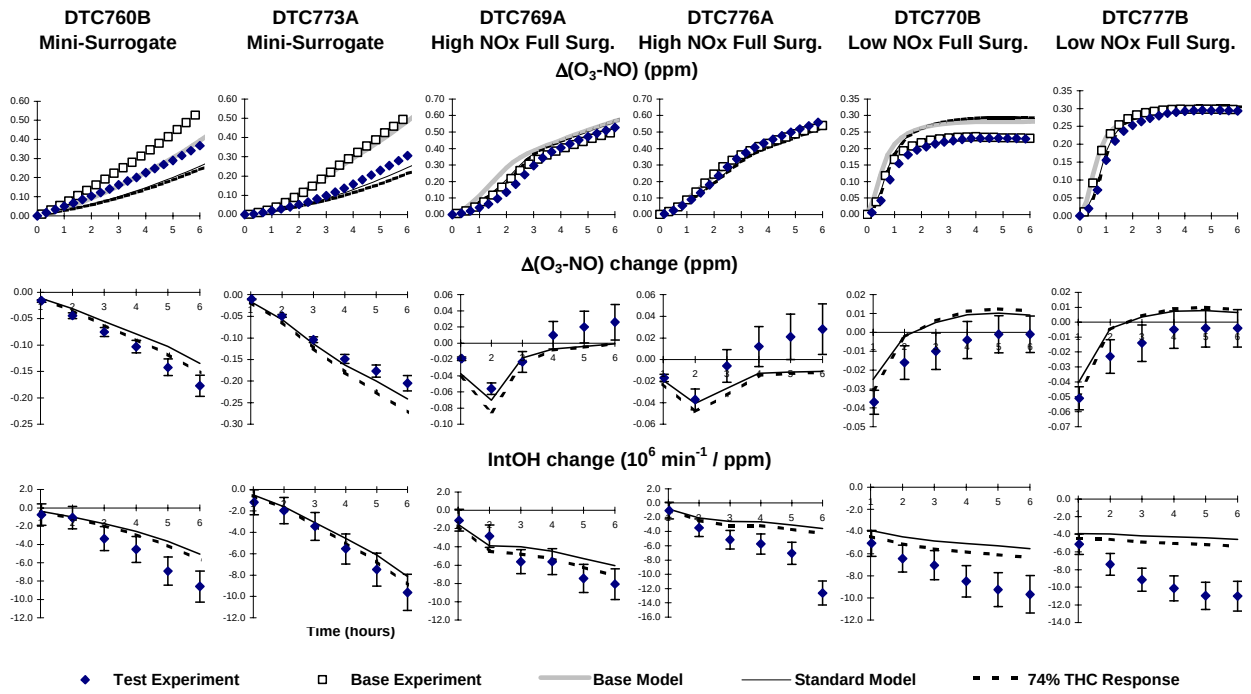

Figure 5. Selected experimental and calculated results of the incremental reactivity experiments with Exxate-1000 Fluid.

The performance of the model in simulating the experiments with the Exxate 1000 fluid is generally satisfactory, and is comparable to the model performance in simulating the experiments with the hydrocarbon fluids. As with D95, there may be a slight bias in underpredicting inhibition of IntOH, but as indicated above an underprediction of IntOH reactivities in low NO_x full surrogate runs is seen for many VOCs (Carter, 2000). There do not appear to be significant overall biases in the model simulations of the $\Delta([O_3]-[NO])$ reactivities in these experiments.

Note that if the "ester rearrangement" (Tuazon et al, 1998) is not predicted to be important for these high molecular weight esters because 1,4-H shift isomerizations, giving rise to the same types of radicals and products as formed in higher alkane photooxidations, are predicted to dominate. For example, Reaction (1) below shows an ester rearrangement, and Reaction (2) is the competing 1,4-H-shift isomerization that is predicted to dominate.

$$CH_3C(O)OCH(O\cdot)CH_2CH_2CH_2R \rightarrow CH_3C(O)\cdot + RCH_2CH_2CH_2C(O)OH \quad (1)$$

$$CH_3C(O)OCH(O\cdot)CH_2CH_2CH_2R \rightarrow CH_3C(O)OCH(OH)CH_2CH_2CH(\cdot)R \quad (2)$$

The ester rearrangement is relatively more important in the lower molecular weight esters where the competing 1,4-H shift isomerizations are not important. These reactions would results in different predicted reactivity characteristics because of the predicted formation of the acetyl radicals, which can react with NO_2 to form PAN, in yields depending on the NO to NO_2 ratio.

$$CH_3C(O)\cdot + O_2 \rightarrow CH_3C(O)OO\cdot$$
$$CH_3C(O)OO\cdot + NO_2 \rightarrow CH_3C(O)OONO_x$$
$$CH_3C(O)OO\cdot + NO \rightarrow \rightarrow CH_3\cdot + CO_2 + NO_2$$

This results in significant differences in results in model simulations of environmental chamber experiments, as can be seen in the model simulations of the ethyl acetate experiments of Carter et al (2000b). The fact that the current mechanism gives reasonably good simulations of these data therefore support the estimate that the ester rearrangement reaction is not an important factor in the reactions of the Exxate constituents, at least for Exxate 1000.

ATMOSPHERIC REACTIVITY CALCULATIONS

Incremental reactivities of VOCs have been shown to be highly dependent on environmental conditions, so reactivities measured in environmental chamber experiments cannot necessarily be assumed to be the same as those under atmospheric conditions (Carter and Atkinson, 1989; Carter et al, 1995b). Because of this, the only method available to obtain quantitative estimates of incremental reactivities of VOCs in ambient air pollution episodes is to conduct airshed model simulations of the episodes. Since these simulations cannot be any more reliable than the chemical mechanisms, the major objective of our studies of the mineral spirits samples and representative constituent compounds has been to assess the reliability of the mechanisms for the compounds and mixtures of interest for use in such calculations. The results of this study suggest that our compositional estimates and the SAPRC-99 mechanism serves as an appropriate basis for estimating the effects of Exxsol D95, Isopar-M, and Exxate 1000 fluids on ozone formation under atmospheric conditions. Since the SAPRC-99 mechanism also performs reasonably well in simulating chamber experiments for the individual esters that were studied, these results also suggest that the model should be appropriate for estimating reactivities of the other Exxate fluids as well. Therefore, atmospheric reactivity estimates for D95, Isopar-M and the Exxate fluids were carried out as part of this project, and the methods and results of this analysis are discussed in this section. The results are compared with atmospheric reactivity estimates for the mineral spirits samples studied for Safety-Kleen (Carter et al, 1997a, 2000a), as well as those for ethane, the $C_{\geq 8}$ normal alkanes, and the mixture used to represent VOC emissions from all sources.

Scenarios Used for Reactivity Assessment

The set of airshed scenarios employed to assess the reactivities for this study is the same as those used for calculating the MIR and other reactivity scales in our previous work (Carter, 1994a), and also in the update using the SAPRC-99 mechanism (Carter, 2000). These scenarios, and the reasons for using them, are briefly described below.

The objective is to use a set of scenarios that represents, as much as possible, a comprehensive distribution of the environmental conditions where unacceptable levels of ozone are formed. Although a set of scenarios has not been developed for the specific purpose of VOC reactivity assessment, the EPA developed an extensive set of scenarios for conducting analyses of effects of ROG and NO_x controls on ozone formation using the EKMA modeling approach (Gipson et al. 1981; Gipson and Freas, 1983; EPA, 1984; Gery et al. 1987; Baugues, 1990). The EKMA approach involves the use of single-cell box models to simulate how the ozone formation in one day episodes is affected by changes in ROG and NO_x inputs. Although single-cell models cannot represent realistic pollution episodes in great detail, they can represent dynamic injection of pollutants, time-varying changes of inversion heights, entrainment of pollutants from aloft as the inversion height raises, and time-varying photolysis rates, temperatures, and humidities (Gipson and Freas, 1981; EPA, 1984; Gipson, 1984; Hogo and Gery, 1988). Thus, they can be used to simulate a wide range of the chemical conditions which affect ozone formation from ROG and

NO_x, and which affect VOC reactivity. Therefore, at least to the extent they are suitable for their intended purpose, an appropriate set of EKMA scenarios should also be suitable for assessing reactivities over a wide range of conditions.

Base Case Scenarios

The set of EKMA scenarios used in this study were developed by the United States EPA for assessing how various ROG and NO_x control strategies would affect ozone nonattainment in various areas of the country (Baugues, 1990). The characteristics of these scenarios and the methods used to derive their input data are described in more detail elsewhere (Baugues, 1990; Carter, 1994b). Briefly, 39 urban areas in the United States were selected based on geographical representativeness of ozone nonattainment areas and data availability, and a representative high ozone episode was selected for each. The initial non-methane organic carbon (NMOC) and NO_x concentrations, the aloft O_3 concentrations, and the mixing height inputs were based on measurement data for the various areas, the hourly emissions in the scenarios were obtained from the National Acid Precipitation Assessment Program emissions inventory (Baugues, 1990), and biogenic emissions were also included. Table 10 gives a summary of the urban areas represented and other selected characteristics of the scenarios.

Several changes to the scenario inputs were made based on discussions with the California ARB staff and others (Carter, 1994a,b). Two percent of the initial NO_x and 0.1% of the emitted NO_x in all the scenarios was assumed to be in the form of HONO. The photolysis rates were calculated using solar light intensities and spectra calculated by Jeffries (1991) for 640 meters, the approximate mid-point of the mixed layer during daylight hours. The composition of the non-methane organic pollutants entrained from aloft was based on the analysis of Jeffries et al. (1989). The composition of the initial and emitted reactive organics was derived as discussed below. Complete listings of the input data for the scenarios are given elsewhere (Carter, 1994b).

This set of 39 EKMA scenarios are referred to as “base case” to distinguish them from the scenarios derived from them by adjusting NO_x inputs to yield standard conditions of NO_x availability as discussed below. No claim is made as to the accuracy of these scenarios in representing any real episode, but they are a result of an effort to represent, as accurately as possible given the available data and the limitations of the formulation of the EKMA model, the range of conditions occurring in urban areas throughout the United States. When developing general reactivity scales it is more important that the scenarios employed represent a realistic distribution of chemical conditions than accurately representing the details of any one particular episode.

The Base ROG mixture is the mixture of reactive organic gases used to represent the chemical composition of the initial and emitted anthropogenic reactive organic gases from all sources in the scenarios. Consistent with the approach used in the original EPA scenarios, the same mixture was used for all scenarios. The speciation for this mixture was derived by Croes (1991) based on an analysis of the EPA database (Jeffries et al. 1989) for the hydrocarbons and the 1987 Southern California Air Quality Study (SCAQS) database for the oxygenates (Croes et al. 1994; Lurmann and Main. 1992). This mixture

Table 10. Summary of the conditions of the scenarios used for atmospheric reactivity assessment.

	Scenario	Max O_3 (ppb)	Max 8-Hr Avg O_3 (ppb)	ROG / NO_x	NO_x / MOIR NO_x	Height (kM)	Init., Emit ROG (m. mol m^{-2})	O_3 aloft (ppb)	Integrated OH (ppt-min)
Avg.	MIR	187	119	3.1	1.5	1.8	15	70	128
Cond.	MOIR	239	165	4.5	1.0	1.8	15	70	209
	EBIR	227	172	6.4	0.7	1.8	15	70	210
Base	Atlanta, GA	179	132	7.3	0.7	2.1	12	63	200
Case	Austin, TX	175	144	9.3	0.5	2.1	11	85	179
	Baltimore, MD	334	215	5.2	1.1	1.2	17	84	186
	Baton Rouge, LA	241	173	6.8	0.9	1.0	11	62	186
	Birmingham, AL	244	202	6.9	0.5	1.8	13	81	208
	Boston, MA	197	167	6.5	0.6	2.6	14	105	262
	Charlotte, NC	143	126	7.8	0.3	3.0	7	92	212
	Chicago, IL	278	226	11.6	0.5	1.4	25	40	164
	Cincinnati, OH	205	153	6.4	0.7	2.8	17	70	220
	Cleveland, OH	252	179	6.6	0.9	1.7	16	89	187
	Dallas, TX	208	141	4.7	1.2	2.3	18	75	176
	Denver, CO	204	139	6.3	1.1	3.4	29	57	143
	Detroit, MI	246	177	6.8	0.7	1.8	17	68	235
	El Paso, TX	182	135	6.6	1.0	2.0	12	65	138
	Hartford, CT	172	144	8.4	0.5	2.3	11	78	220
	Houston, TX	312	217	6.1	0.9	1.7	25	65	225
	Indianapolis, IN	212	148	6.6	0.9	1.7	12	52	211
	Jacksonville, FL	155	115	7.6	0.6	1.5	8	40	206
	Kansas City, MO	159	126	7.1	0.6	2.2	9	65	233
	Lake Charles, LA	286	209	7.4	0.6	0.5	7	40	233
	Los Angeles, CA	568	406	7.6	1.0	0.5	23	100	134
	Louisville, KY	212	155	5.5	0.8	2.5	14	75	260
	Memphis, TN	229	180	6.8	0.6	1.8	15	58	249
	Miami, FL	132	111	9.6	0.4	2.7	9	57	181
	Nashville, TN	167	138	8.0	0.4	1.6	7	50	225
	New York, NY	365	294	8.1	0.7	1.5	39	103	159
	Philadelphia, PA	247	169	6.2	0.9	1.8	19	53	227
	Phoenix, AZ	277	193	7.6	1.0	3.3	40	60	153
	Portland, OR	166	126	6.5	0.7	1.6	6	66	233
	Richmond, VA	242	172	6.2	0.8	1.9	16	64	217
	Sacramento, CA	204	142	6.6	0.8	1.1	7	60	209
	St Louis, MO	324	209	6.1	1.1	1.6	26	82	176
	Salt Lake City, UT	186	150	8.5	0.6	2.2	11	85	182
	San Antonio, TX	133	98	3.9	1.0	2.3	6	60	192
	San Diego, CA	193	150	7.1	0.9	0.9	8	90	146
	San Francisco, CA	229	126	4.8	1.8	0.7	25	70	61
	Tampa, FL	230	153	4.4	1.0	1.0	8	68	211
	Tulsa, OK	231	160	5.3	0.9	1.8	15	70	264
	Washington, DC	283	209	5.3	0.8	1.4	13	99	239

consists of 52% (by carbon) alkanes, 15% alkenes, 27% aromatics, 1% formaldehyde, 2% higher aldehydes, 1% ketones, and 2% acetylene. The detailed composition of this mixture is given elsewhere (Carter, 1994b; Carter, 2000).

Adjusted NO_x scenarios

Incremental reactivities in the base case scenarios are expected to vary widely because incremental reactivities depend on the ROG/NO_x ratio, and that ratio varies widely among the base case scenarios. To obtain reactivity scales for specified NO_x conditions, separate scenarios, designated MIR (for maximum incremental reactivity), MOIR (for maximum ozone incremental reactivity), and EBIR (for Equal Benefit Incremental Reactivity) were developed (Carter, 1994a). In the MIR scenarios, the NO_x inputs were adjusted so the base ROG mixture (and most VOCs) has its highest incremental reactivity. This is representative of the highest NO_x conditions of relevance to VOC reactivity assessment because at higher NO_x levels O_3 yields become significantly suppressed, it is also the condition where O_3 is most sensitive to VOC emissions. In the MOIR scenarios, the NO_x inputs were adjusted to yield the highest ozone concentration. In the EBIR scenarios, the NO_x inputs were adjusted so that the relative effects of NO_x reductions and total ROG reductions on peak ozone levels were equal. This represents the lowest NO_x condition of relevance for VOC reactivity assessment, because O_3 formation becomes more sensitive to NO_x emissions than VOC emissions at lower NO_x levels. As discussed by Carter (1994a) the MIR and EBIR ROG/NO_x ratios are respectively ~1.5 and ~0.7 times those for the MOIR scenarios in all cases.

NO_x Conditions in the Base Case Scenarios

The variability of ROG/NO_x ratios in the base case scenarios suggests a variability of reactivity characteristics in those scenarios. However, as discussed previously (Carter, 1994a), the ROG/NO_x ratio is also variable in the MIR or MOIR scenarios, despite the fact that the NO_x inputs in these scenarios are adjusted to yield a specified reactivity characteristic. Thus, the ROG/NO_x ratio, by itself, is not necessarily a good predictor of reactivity characteristics of a particular scenario. The NO_x/NO_x^{MOIR} ratio is a much better predictor of this, with values greater than 1 indicating relatively high NO_x conditions where ozone formation is more sensitive to VOCs, and values less than 1 indicating NO_x-limited conditions. NO_x/NO_x^{MOIR} ratios less than 0.7 represent conditions where NO_x control is a more effective ozone control strategy than ROG control (Carter, 1994a). These rations are shown on Table 10 for the various base case scenarios. Note that more than half of the base case scenarios represent NO_x-limited conditions, and ~25% of them represent conditions where NO_x control is more beneficial than VOC control. A relatively small number of scenarios represent MIR or near MIR conditions. However, as discussed elsewhere (Carter, 1994a), this set of scenarios is based on near-worst-case conditions for ozone formation in each of the airsheds. Had scenarios representing less-than-worst-case conditions been included, one might expect a larger number of MIR or near MIR scenarios. This is because NO_x is consumed more slowly on days with lower light intensity or temperature, and thus the scenario is less likely to become NO_x-limited.

Quantification of Atmospheric Reactivity

The reactivity of a VOC in an airshed scenario is measured by its incremental reactivity. For ambient scenarios, this is defined as the change in ozone caused by adding the VOC to the emissions, divided by the amount of VOC added, calculated for sufficiently small amounts of added VOC that the incremental reactivity is independent of the amount added[5].

$$IR(VOC, Scenario) = \lim_{VOC \to 0} \left[\frac{O_3(\text{Scenario with VOC added}) - O_3(\text{Base Scenario})}{\text{Amount of VOC Added}} \right] \qquad \text{(IV)}$$

The specific calculation procedure is discussed in detail elsewhere (Carter, 1994a,b).

Incremental reactivities derived as given above tend to vary from scenario to scenario because they differ in their overall sensitivity of O_3 formation to VOCs. These differences can be factored out to some extent by using "relative reactivities", which are defined as ratios of incremental reactivities to the incremental reactivity of the base ROG mixture, which is used to represent emissions of reactive VOCs from all sources.

$$RR(VOC, Scenario) = \frac{IR(VOC, Scenario)}{IR\ (\text{Base ROG}, Scenario)} \qquad \text{(V)}$$

These relative reactivities can also be thought of as the relative effect on O_3 of controlling emissions of the particular VOC by itself, compared to controlling emissions from all VOC sources equally. Thus, they are more meaningful in terms of control strategy assessment than absolute reactivities, which can vary greatly depending on the episode and local meteorology.

In addition to depending on the VOC and the scenario, the incremental and relative reactivities depend on how the amounts of VOC added are quantified. In this work, this is quantified on a mass basis, since this is how VOCs are regulated, and generally approximates how VOC substitutions are made in practice. Note that relative reactivities will be different if they are quantified on a molar basis, with VOCs with higher molecular weight having higher reactivities on a mole basis than a gram basis.

Relative reactivities can also depend significantly on how ozone impacts are quantified (Carter, 1994a). Two different ozone quantification methods are used in this work, as follows:

"Ozone Yield" reactivities measure the effect of the VOC on the total amount of ozone formed in the scenario at the time of its maximum concentration. Incremental reactivities are quantified as grams O_3 formed per gram VOC added. Most previous recent studies of ozone reactivity (Dodge, 1984; Carter and Atkinson, 1987, 1989, Chang and Rudy, 1990; Jeffries and Crouse, 1991) have been based on this quantification method. The MIR, MOIR, and EBIR scales of Carter (1994a) also use this quantification.

[5] Note that this differs from how the term "incremental reactivity" is used in the context of chamber experiments. In that case, the incremental reactivity refers to the relative change observed in the individual experiments, which in general depends on the amount added.

"Maximum 8 Hour Average Ozone" reactivities measure the effect of the VOC on the average ozone concentration during the 8-hour period when the average ozone concentration was the greatest, which in these one-day scenarios was the last 8 hours of the simulation. This provides a measure of ozone impact that is more closely related to the new Federal ozone standard that is given in terms of an 8 hour average. This quantification is used for relative reactivities in this work.

In previous reports, we have reported reactivities in terms of integrated O_3 over a standard concentration of 0.09 or 0.12 ppm. This provides a measure of the effect of the VOC on exposure to unacceptable levels of ozone. This is replaced by the maximum 8 hour average reactivities because it is more representative of the proposed new Federal ozone standard and because reactivities relative to integrated O_3 over a standard tend to be between those relative to ozone yield and those relative to 8-hour averages. Therefore, presenting both ozone yield and maximum 8-hour average relative reactivities should be sufficient to provide information on how relative reactivities vary with ozone quantification method. Incremental reactivities are quantified as ppm O_3 per milligram VOC emitted per square meter, but maximum 8 hour average reactivities are usually quantified as relative reactivities quantified on a mass basis.

Note that incremental reactivities are calculated for a total of 156 scenarios, consisting of the 39 base case scenarios and the three adjusted NO_x scenarios for each of the 39 base case scenarios. However, the incremental reactivities in the MIR, MOIR, or EBIR) scales are reported as averages of the incremental reactivities in the corresponding adjusted NO_x scenarios, because adjusting the NO_x conditions reduces the scenario variability, and this allows for a derivation single reactivity scales representing each type of NO_x condition. On the other hand, the individual scenario results for the base case scenarios give an indication of the scenario-to-scenario variability of the calculated reactivity results.

Results

Table 11 lists the ozone yield incremental reactivities calculated for the set of ExxonMobil fluids of interest in this program, together with, for comparison purposes, the mineral spirits samples studied for Safety-Kleen, ethane, the C_8-C_{16} normal alkanes, and base ROG mixture that represents VOC emissions from all sources. Table 12 shows both the ozone yield and maximum 8-hour average ozone reactivities for these compounds and mixtures relative to the base ROG mixture, and plots of these relative reactivities against carbon number are shown on Figure 6. Note that the values given are averages of the incremental or relative reactivities calculated for the various adjusted NO_x and the base case scenarios. Note also that the relative reactivities on Table 12 and Figure 6 can be thought of as the relative ozone benefits resulting from regulating emissions of these compounds or mixtures alone, compared to regulating VOC emissions from all sources equally.

The ozone impacts calculated for D95 and the other all-alkane petroleum-based substances, for the $C_{\geq 10}$ Exxate materials, and those calculated Isopar-M using the standard representation tend to follow those for the normal alkanes reasonably closely. Although their impacts tend to be about 15-25% higher than those for the normal alkanes in the same carbon number ranges, they tend to have about the same

Table 11. Atmospheric incremental calculated for representative ExxonMobil commercial products, mineral spirits samples, and normal alkanes..

Compound or Mixture	Ozone Yield Incremental Reactivities (grams O_3 / grams VOC or mixture)			
	MIR	MOIR	EBIR	Average Base Case
Normal Alkanes				
Ethane	0.31	0.20	0.15	0.15
n-Octane	1.11	0.71	0.41	0.43
n-Nonane	0.96	0.61	0.33	0.34
n-Decane	0.83	0.54	0.28	0.28
n-Undecane	0.74	0.48	0.24	0.24
n-Dodecane	0.66	0.43	0.21	0.21
n-Tridecane	0.62	0.41	0.20	0.20
n-Tetradecane	0.59	0.38	0.19	0.19
n-Pentadecane	0.56	0.37	0.19	0.18
Mineral Spirits Samples Studied for Safety-Kleen				
Mineral Spirits "A" (Type I-B, 91% Alkanes)	1.27	0.65	0.35	0.39
Mineral Spirits "B" (Type II-C, 100% Alkanes)	0.78	0.48	0.25	0.26
Mineral Spirits "C" (Type II-C, 100% Alkanes)	0.78	0.48	0.26	0.26
Mineral Spirits "D" (Type II-C, 100% Alkanes)	0.79	0.49	0.26	0.26
Hydrocarbon Fluids Studied for This Project				
Exxsol® D95	0.67	0.42	0.22	0.23
Isopar®-M (Standard Representation)	0.65	0.41	0.22	0.22
Isopar®-M (High Branching)	0.92	0.54	0.30	0.31
Exxate® Fluids				
Exxate® 600	1.03	0.61	0.38	0.40
Exxate® 700	0.97	0.57	0.34	0.36
Exxate® 800	0.96	0.56	0.33	0.35
Exxate® 900	0.85	0.50	0.28	0.30
Exxate® 1000	0.83	0.49	0.28	0.29
Exxate® 1200	0.72	0.43	0.24	0.24
Exxate® 1300	0.67	0.40	0.22	0.23
Mixture Representing VOC Emissions from all Sources				
Base ROG Mixture	3.71	1.46	0.85	1.03

Table 12. Atmospheric relative reactivities calculated for the C_8 - C_{15} alkanes, the mineral spirits samples, and ethane. Reactivities are relative to the base ROG mixture, quantified on an ozone formed per unit mass basis.

Compound or Mixture	Ozone Yield Relative Reactivities				Maximum 8-Hour Average Relative Reactivities			
	MIR	MOIR	EBIR	Average Base	MIR	MOIR	EBIR	Average Base
				Normal Alkanes				
Ethane	0.08	0.14	0.17	0.15	0.07	0.09	0.10	0.09
n-Octane	0.30	0.49	0.48	0.41	0.24	0.26	0.22	0.20
n-Nonane	0.26	0.42	0.39	0.33	0.20	0.20	0.15	0.14
n-Decane	0.22	0.37	0.33	0.27	0.17	0.16	0.10	0.09
n-Undecane	0.20	0.33	0.29	0.24	0.15	0.13	0.06	0.06
n-Dodecane	0.18	0.30	0.25	0.21	0.13	0.11	0.04	0.03
n-Tridecane	0.17	0.28	0.23	0.19	0.12	0.10	0.03	0.02
n-Tetradecane	0.16	0.26	0.22	0.18	0.11	0.08	0.01	0.01
n-Pentadecane	0.15	0.25	0.22	0.18	0.10	0.07	0.01	0.00
				Mineral Spirits Samples Studied for Safety-Kleen				
Mineral Spirits "A"	0.34	0.45	0.42	0.37	0.29	0.27	0.20	0.19
Mineral Spirits "B"	0.21	0.33	0.30	0.25	0.15	0.13	0.06	0.05
Mineral Spirits "C"	0.21	0.33	0.30	0.25	0.16	0.14	0.06	0.06
Mineral Spirits "D"	0.21	0.33	0.30	0.26	0.16	0.14	0.07	0.06
				Hydrocarbon Fluids Studied for This Project				
Exxsol® D95	0.18	0.29	0.26	0.22	0.13	0.11	0.04	0.03
Isopar®-M (Std.)	0.18	0.28	0.26	0.21	0.13	0.11	0.04	0.04
(High Branching)	0.25	0.37	0.36	0.30	0.19	0.17	0.10	0.09
				Exxate® Fluids				
Exxate® 600	0.28	0.42	0.44	0.39	0.23	0.25	0.24	0.23
Exxate® 700	0.26	0.39	0.40	0.35	0.22	0.23	0.20	0.19
Exxate® 800	0.26	0.38	0.38	0.33	0.21	0.21	0.18	0.17
Exxate® 900	0.23	0.35	0.33	0.29	0.18	0.17	0.13	0.12
Exxate® 1000	0.22	0.34	0.32	0.28	0.17	0.17	0.11	0.11
Exxate® 1200	0.19	0.29	0.28	0.24	0.15	0.13	0.07	0.07
Exxate® 1300	0.18	0.28	0.26	0.22	0.14	0.12	0.06	0.06

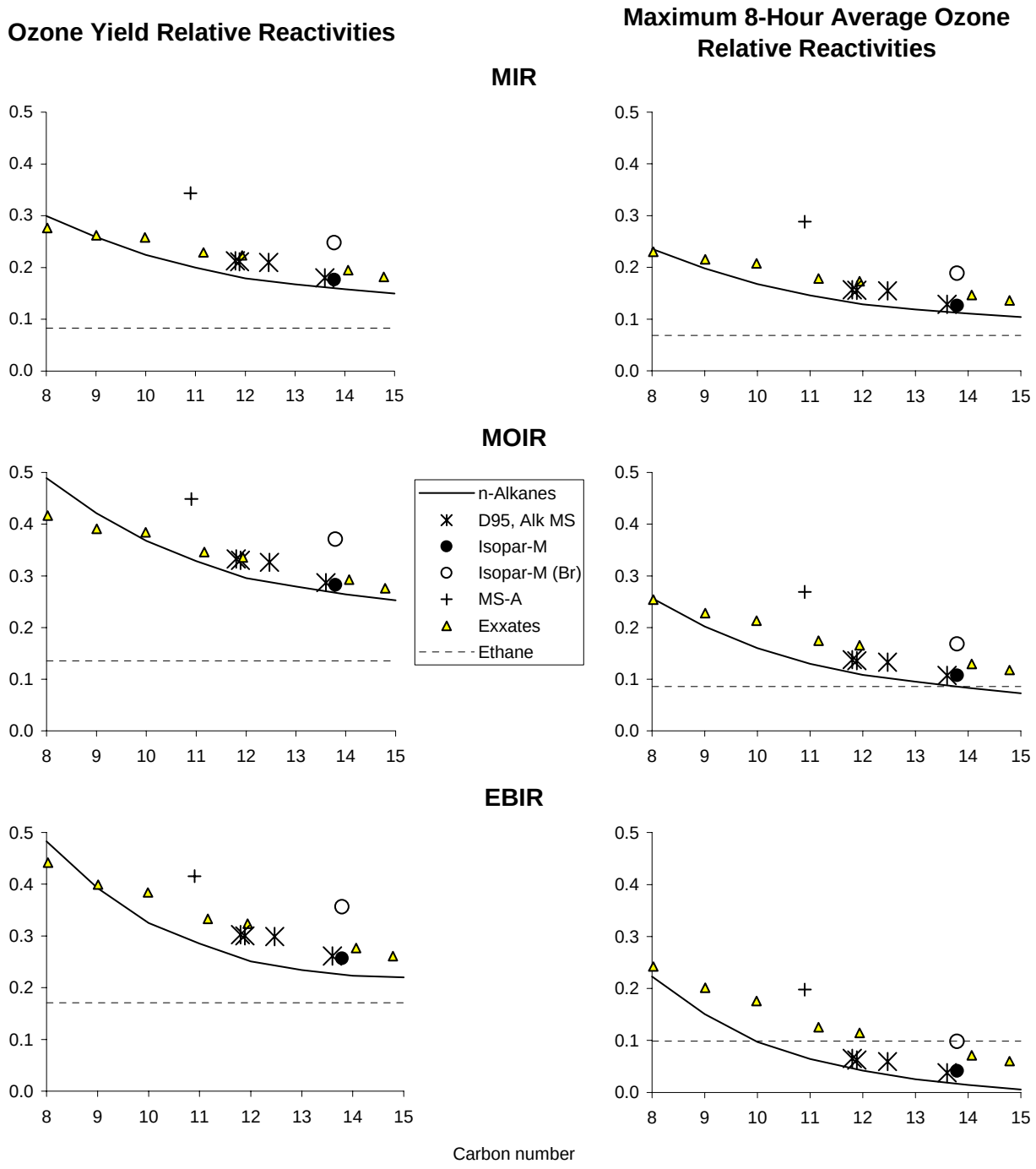

Figure 6. Plots of MIR and EBIR ozone yield and maximum 8-hour average ozone relative reactivities against carbon number. Reactivities are relative to the base ROG mixture, quantified on a mass basis. Relative reactivities of ethane are shown for comparison.

apparent dependence on carbon number, scenario conditions, and how ozone impacts are quantified. This indicates that the aspects of their mechanisms that affect ozone formation are very similar. The ozone impacts of these materials are relatively low compared to the emissions of VOCs from all sources, indicating that regulating their emissions is less effective than regulating emissions of VOCs from all sources equally. Their relative impacts tend to decrease with carbon number because of the increasing importance of radical inhibition due to nitrate formation in the reactions of higher molecular weight compounds, this tends to level off at the highest molecular weight range. Their relative impacts on maximum 8-hour average ozone tend to be less than their impacts on peak ozone yields, particularly in scenarios with lower NO_x levels, such as the EBIR scenarios or many of the base case scenarios. Their relative impacts on peak ozone yields tend to be less dependent on NO_x conditions than their impacts on maximum 8-hour average ozone. The ozone yield reactivities relative to the base ROG are in the 20-30% range, while their 8-hour average ozone relative reactivities decline from ~15% in the MIR scenarios to ~6% in the lower NO_x EBIR and average base case scenarios.

The ozone impact for Safety-Kleen mineral spirits sample "A" is higher than the range observed for the other materials because of the ~6% aromatic and ~1% alkene content (by weight) of this recycled material. Although these percentages are relatively low, the aromatics and alkenes are much more reactive than the alkanes in this molecular weight range, so their presence has a significant impact on the net calculated ozone impact. Many commercial mineral spirits contain aromatics, and such materials would be expected to have similar or greater reactivities than mineral spirits sample "A", depending on their aromatic content. However, the ability of the current mechanism and composition assignment methods to predict ozone impacts for commercial aromatics-containing mineral spirits has not been assessed.

It is interesting to note that the ozone yield reactivities calculated for Isopar-M increase by about 40% higher when the "highly branched" representation is used for the branched alkane constituents, rather than the standard representation considered to be appropriate for mineral spirits samples. The effects on calculated maximum 8-hour average reactivities are somewhat greater, ranging from a 50% increase for the MIR scenarios to a factor of 2.5 or greater increase for the low NO_x scenarios. This is despite the fact that making alternative assumptions in this regard had almost no effect on the model simulations of the chamber experiments. This is unfortunate, because it means that the set of environmental chamber experiments employed in our study is not sufficient to assess composition or mechanistic differences that have non-negligible effects on predictions of atmospheric reactivity.

Sensitivity calculations and a "pure mechanism species" analysis such as carried out by Carter and Atkinson (1998) indicate that the major factor affecting the differences results with the two Isopar-M representations is due to the differences in predicted yields of aldehyde products (see Table 9, above). In particular, the standard representation predicts a total aldehyde yield of 0.125 moles of aldehyde per mole of lumped Isopar model species reacting, while the highly branched representation predicts a yield of 0.294. The reactivity simulations were found to have much higher sensitivity to differences in reactive product yields than is the case for simulations of environmental chamber, so this difference in aldehyde yields has relatively little effect on the chamber simulations but a significant effect on the atmospheric

reactivity predictions. This is because the integrated radical levels are much higher in the atmospheric simulations than in the chamber experiments, because of the longer reaction time combined with the lower NO_x concentrations once the inversion height has reached its maximum. The contributions of the products to overall atmospheric reactivity simulations are also high on a percentage basis for these compounds. This is because the negative effects on reactivity caused by nitrate formation and the positive effects caused by NO to NO_2 conversions tend to cancel each other out, making the net total reactivity relatively low.

Another interesting result of these calculations is that the Exxate fluids are quite similar in reactivity to the all-alkane fluids in the same molecular weight range, at least for carbon numbers of 10 or greater (i.e., Exxate 800 and higher). This is because most of the reaction is at the hydrocarbon portions of the molecule, and the presence of the acetate groups do not significantly affect the net effect of the overall reactions. As discussed above, the "ester rearrangement", which if important would result in different reactivity characteristics for these materials, does not appear to be important in the higher Exxate fluids. However, the model also predicts that the ozone yield reactivities of the lower molecular weight Exxates tend to be somewhat less than the n-alkanes with the same carbon number, though the 8-hour average reactivities are about the same or slightly higher.

As is the case with the higher molecular weight alkanes (Carter, 2000a,c), the relative reactivities of these high molecular weight materials are highly variable from scenario to scenario. This is shown on Figure 7, which shows distribution plots of reactivities of D95 and Exxate 1000 relative to the base ROG mixture for the base case scenarios and the three types of adjusted NO_x scenarios. The relative reactivities for ethane, the compound used by the EPA to define "negligible" reactivity, are also shown. It can be seen that the relative reactivities of these materials are quite varied even in the adjusted NO_x scenarios, especially the maximum 8-hour average relative reactivities and the relative reactivities in the lower NO_x scenarios. Note, however, that there are not many differences between the distribution of reactivities of D95 and Exxate 1000, despite their quite different chemical compositions. The relative reactivities of ethane (and many other types of VOCs) are much less varied in the adjusted NO_x scenarios. This shows that the ozone impacts of these higher molecular weight mixtures are significantly affected by environmental factors other than NO_x conditions. A systematic assessment of the other scenario conditions that may be important has not been carried out.

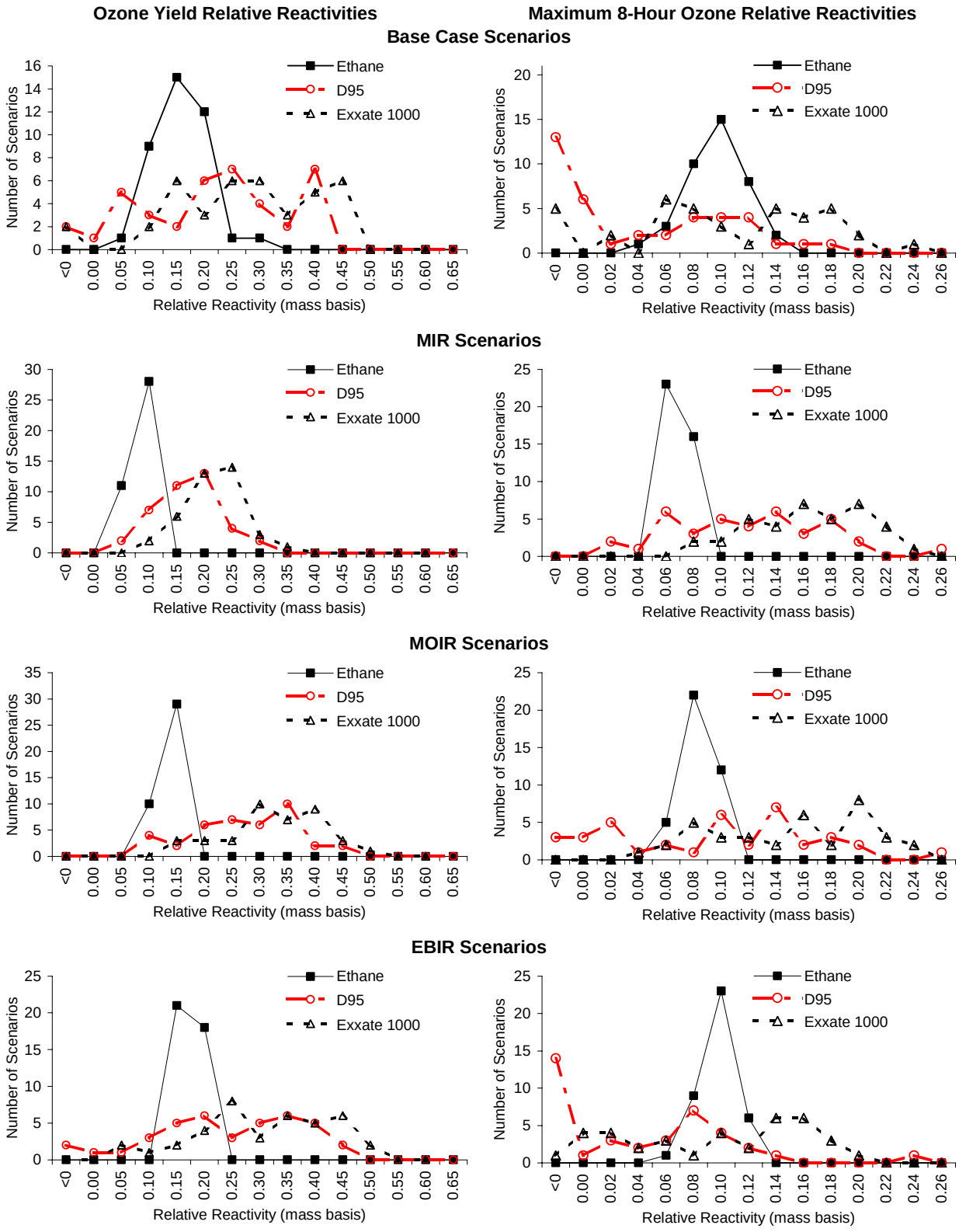

Figure 7. Distribution plots of relative reactivities of ethane and two representative all-alkane mineral spirits samples in the various types of scenarios. Reactivities are relative to the base ROG mixture.

CONCLUSIONS

This program has achieved its objectives in providing data needed to reduce uncertainties in estimates of atmospheric ozone impacts of Exxsol D95, Isopar-M and the Exxate fluids. Models using estimated compositions for these materials based on data provided by ExxonMobil, and chemical mechanisms for the assumed constituents derived using the SAPRC-99 mechanism estimation methods, were able to give reasonably good simulations of results of environmental chamber experiments representing different chemical conditions. This gives us some confidence on the ability of these models to estimate the ozone impacts of these materials in the atmosphere. However, the results also showed that the types of chamber experiments employed are not sufficient to test all aspects of the representations and mechanisms for these materials that may affect predictions of atmospheric reactivity.

The data obtained with the D95 and the Isopar fluids have broader utility than just predictions of the ozone impacts of these particular products. They provide a useful supplement to experiments carried out under separate funding on individual high molecular weight normal, branched, and cyclic alkanes, and on representative mineral spirits samples. These are representative of a wide variety of materials that consist of complex mixtures of varying amounts of normal, branched, and cyclic alkanes, and that are used in relatively large volumes in a number of applications. The experiments with the individual normal, branched, and cyclic alkanes provide tests for the mechanisms for the individual compounds, and the experiments with the actual commercial samples provide tests for our ability to characterize their compositions for reactivity modeling purposes. The latter also indirectly test mechanisms for constituent compounds for which individual compound data are not available. The data with D95 extends the data base because it has a higher molecular weight range than the mineral spirits samples studied previously, and the data for Isopar-M is important because it provides a separate test for our mechanisms for complex mixtures of high molecular weight branched alkanes. Overall, the data available prior to this program tended to support the validity of the estimates and the mechanisms currently used (Carter, 2000; Carter et al, 2000a,c), and the data obtained in this program tended to provide additional confirmation in this regard.

However, this does not mean that there are not potentially significant uncertainties involved in our estimates of atmospheric ozone impacts of these higher molecular weight hydrocarbon materials. The fact that two quite different representations of the branched alkanes in the Isopar-M fluid gave no significant differences in reactivity predictions in the chamber experiments but gave 40% or greater differences in atmospheric reactivity predictions is clearly of concern. This is because environmental chamber experiments do not provide good tests of how well the model is representing the reactive products formed from these types of compounds, even though the reactive products can have non-negligible effects on predictions of their overall reactivity in the atmosphere. This indicates the importance of using an appropriate representation for the structure of the compounds present in these complex mixtures, which can affect the types of products that are formed when they are predicted to

react. It also indicates that there is a need to develop new types of experiments that are more sensitive to mechanism differences in yields of reactive products that are derived.

In the case of the petroleum-derived fluids such as mineral spirits and the Exxsols, the available GC-MS data, though limited and inconclusive, tend to suggest that less branched compounds may be relatively more important. This serves as a basis for the representation we used in our current representation of the constituents of these fluids. However, additional speciated analysis studies to confirm this assumption, and to provide data to refine our choices of compounds used to represent high molecular weight branched and cyclic alkane constituents, would reduce uncertainties in atmospheric reactivity estimates for these hydrocarbon fluids.

In the case of the Isopars, the acetone data in the Isopar-M experiments suggests that a more branched representation may be more appropriate for these substances. Although analytical data were not provided, one might expect more branched compounds to be formed based on the type of process used to manufacture this material. This tends to be supported by the acetone levels observed in our experiments, which are more consistent with the assumption that compounds with higher degrees of branching are presented than indicated by the GC-MS analyses of petroleum-derived substances. However, acetone formation has an insignificant effect on reactivity, it is differences in predicted aldehyde yields that are important. Obtaining yields of isobutyraldehyde and other higher aldehydes formed in the photooxidations of this material would have been of more direct utility. Unfortunately, the more extensive product analyses required were beyond the scope of the present project.

Although experimental data has become available concerning the atmospheric reactivities of various lower molecular weight esters (Carter et al, 2000b, Carter, 2000 and references therein), until this program there has been no information concerning atmospheric ozone impacts of complex mixtures of higher molecular weight esters such as the Exxates. The data from this program indicated that the mechanisms generated using the SAPRC-99 mechanism estimation methods provide good simulations of results of environmental chamber experiments with Exxate 1000, as they generally do in simulating chamber experiments with the individual esters that have been studied (Carter, 2000). The reasonably good model simulations of the experiments with Exxate 1000 combined with the results with the individual esters suggests that the model is probably representing the other Exxates reasonably well, even though the model was only evaluated for Exxate 1000. Although the exact distribution of compounds present in Exxate 1000 and higher is unknown, the more comprehensive compositional data provided for the lower Exxates gave a reasonable basis for estimating the types of compounds likely to be present. The results of the experiments tended to confirm the predictions of the mechanism that the reactivity characteristics of these Exxates are generally similar to those of all-alkane mixtures such as all-alkane hydrocarbon materials of similar molecular weight range.

The atmospheric ozone impacts calculated for these materials were calculated to be relatively low, with the effect on peak ozone yields being 20-40% that of VOC emissions from all sources, on a mass basis. This means that regulating emissions of these materials is less effective in reducing ozone than reducing emissions of VOCs from all sources equally. The impacts of the Exxates decrease with

increasing molecular weight, but are comparable to all-alkane materials in the same molecular weight range. The impacts of Isopar-M are either similar to or about 40% higher than those of the petroleum-based alkane mixtures in the same weight range, depending on what assumptions are made concerning the representation of the branched alkane constituents, but the higher reactivity range is probably more likely. All these materials tend to have less of an impact on maximum 8-hour average ozone yields than on peak ozone yields, particularly in lower NO_x scenarios. Ozone impacts relative to ethane are of current interest because the EPA has used that compound as the standard to define "negligible" reactivity. Although the mass-based ozone impacts of these materials are calculated to be somewhat greater than those of ethane on the average, they approach or become less than those of ethane in terms of impacts on maximum 8-hour average ozone in the lower NO_x scenarios. However, the relative impacts of these materials were found to be quite variable from scenario to scenario. This means that it is important that the model appropriately represent scenario conditions in assessments of relative ozone impacts of mineral spirits emissions.

REFERENCES

Arey, J., S. M. Aschmann, E. S. C. Kwok, and R. Atkinson (2000): Alkyl nitrate, hydroxyalkyl nitrate, and hydroxycarbonyl formation from the NO_x-air photooxidations of C_5-C_{10} n-alkanes. J. Phys. Chem. A, to be submitted for publication.

Atkinson, R. (1989): "Kinetics and Mechanisms of the Gas-Phase Reactions of the Hydroxyl Radical with Organic Compounds," J. Phys. Chem. Ref. Data, Monograph no 1.

Atkinson, R. (1997): "Gas Phase Tropospheric Chemistry of Volatile Organic Compounds: 1. Alkanes and Alkenes," J. Phys. Chem. Ref. Data, 26, 215-290.

Baugues, K. (1990): "Preliminary Planning Information for Updating the Ozone Regulatory Impact Analysis Version of EKMA," Draft Document, Source Receptor Analysis Branch, Technical Support Division, U. S. Environmental Protection Agency, Research Triangle Park, NC, January.

CARB (1999) California Air Resources Board, Proposed Regulation for Title 17, California Code of Regulations, Division 3, Chapter 1, Subchapter 8.5, Article 3.1, sections 94560- 94539.

Carter, W. P. L. (1994a): "Development of Ozone Reactivity Scales for Volatile Organic Compounds," J. Air & Waste Manage. Assoc., 44, 881-899.

Carter, W. P. L. (1994b): "Calculation of Reactivity Scales Using an Updated Carbon Bond IV Mechanism," Report Prepared for Systems Applications International Under Funding from the Auto/Oil Air Quality Improvement Research Program, April 12. Available at http://helium.ucr.edu/~carter/absts.htm#cb4rct.

Carter, W. P. L. (1995): "Computer Modeling of Environmental Chamber Measurements of Maximum Incremental Reactivities of Volatile Organic Compounds," Atmos. Environ., 29, 2513-2517.

Carter, W. P. L. (2000): "Documentation of the SAPRC-99 Chemical Mechanism for VOC Reactivity Assessment," Report to the California Air Resources Board, Contracts 92-329 and 95-308, May 8. Available at http://helium.ucr.edu/~carter/absts.htm#saprc99.

Carter, W. P. L. and R. Atkinson (1987): "An Experimental Study of Incremental Hydrocarbon Reactivity," Environ. Sci. Technol., 21, 670-679

Carter, W. P. L. and R. Atkinson (1989): "A Computer Modeling Study of Incremental Hydrocarbon Reactivity", Environ. Sci. Technol., 23, 864.

Carter, W. P. L., and F. W. Lurmann (1990): "Evaluation of the RADM Gas-Phase Chemical Mechanism," Final Report, EPA-600/3-90-001.

Carter, W. P. L. and F. W. Lurmann (1991): "Evaluation of a Detailed Gas-Phase Atmospheric Reaction Mechanism using Environmental Chamber Data," Atm. Environ. 25A, 2771-2806.

Carter, W. P. L., J. A. Pierce, I. L. Malkina, D. Luo and W. D. Long (1993): "Environmental Chamber Studies of Maximum Incremental Reactivities of Volatile Organic Compounds," Report to Coordinating Research Council, Project No. ME-9, California Air Resources Board Contract No. A032-0692; South Coast Air Quality Management District Contract No. C91323, United States Environmental Protection Agency Cooperative Agreement No. CR-814396-01-0, University Corporation for Atmospheric Research Contract No. 59166, and Dow Corning Corporation. April 1. Available at http://helium.ucr.edu/~carter/absts.htm#rct1rept.

Carter, W. P. L., J. A. Pierce, D. Luo, and I. L. Malkina (1995a): "Environmental Chamber Studies of Maximum Incremental Reactivities of Volatile Organic Compounds," Atmos. Environ. 29, 2499-2511.

Carter, W. P. L., D. Luo, I. L. Malkina, and J. A. Pierce (1995b): "Environmental Chamber Studies of Atmospheric Reactivities of Volatile Organic Compounds. Effects of Varying ROG Surrogate and NO_x," Final report to Coordinating Research Council, Inc., Project ME-9, California Air Resources Board, Contract A032-0692, and South Coast Air Quality Management District, Contract C91323. March 24. Available at http://helium.ucr.edu/~carter/absts.htm#rct2rept.

Carter, W. P. L., D. Luo, I. L. Malkina, and D. Fitz (1995c): "The University of California, Riverside Environmental Chamber Data Base for Evaluating Oxidant Mechanism. Indoor Chamber Experiments through 1993," Report submitted to the U. S. Environmental Protection Agency, EPA/AREAL, Research Triangle Park, NC., March 20. Available at http://helium.ucr.edu/ ~carter/absts.htm#databas.

Carter, W. P. L., D. Luo, I. L. Malkina, and J. A. Pierce (1995d): "Environmental Chamber Studies of Atmospheric Reactivities of Volatile Organic Compounds. Effects of Varying Chamber and Light Source," Final report to National Renewable Energy Laboratory, Contract XZ-2-12075, Coordinating Research Council, Inc., Project M-9, California Air Resources Board, Contract A032-0692, and South Coast Air Quality Management District, Contract C91323, March 26.

Carter, W. P. L., D. Luo, and I. L. Malkina (1996): "Investigation of Atmospheric Ozone Formation Potentials of C_{12} - C_{16} n-Alkanes," Report to the Aluminum Association, October 28. Available at http://cert.ucr.edu/~carter/absts.htm#alkrept.

Carter, W. P. L., D. Luo, and I. L. Malkina (1997a): "Investigation of the Atmospheric Ozone Formation Potentials of Selected Mineral Spirits Mixtures," Report to Safety-Kleen Corporation, July 25. Available at http://cert.ucr.edu/~carter/absts.htm#msrept.

Carter, W. P. L., D. Luo, and I. L. Malkina (1997b): "Environmental Chamber Studies for Development of an Updated Photochemical Mechanism for VOC Reactivity Assessment," Final report to the California Air Resources Board, the Coordinating Research Council, and the National Renewable Energy Laboratory, November 26. Available at http://helium.ucr.edu/~carter/absts.htm#rct3rept.

Carter, W. P. L., D. Luo, and I. L. Malkina (2000a): "Investigation of the Atmospheric Ozone Formation Potentials of Selected Branched Alkanes and Mineral Spirits Samples," Draft Report to Safety-Kleen Corporation, August 18.

Carter. W. P. L., D. Luo and I. L. Malkina (2000b): "Investigation of Atmospheric Reactivities of Selected Consumer Product VOCs," Report to California Air Resources Board, May 30. Available at http://helium.ucr.edu/~carter/absts.htm#cpreport.

Carter, W. P. L., D. Luo, and I. L. Malkina (2000c): "Investigation of the Atmospheric Ozone Formation Potentials of Selected $C_{\geq 12}$ Normal and Cyclic Alkanes," Draft Report to the Aluminum Association, August 9.

Chang, T. Y. and S. J. Rudy (1990): "Ozone-Forming Potential of Organic Emissions from Alternative-Fueled Vehicles," Atmos. Environ., 24A, 2421-2430.

Christensen, L. K., J. C. Ball and T. J. Wallington (2000): "Atmospheric Oxidation Mechanism of Methyl Acetate," J. Phys. Chem. A, 104, 345-351.

Croes, B. E., Technical Support Division, California Air Resources Board, personal communication (1991).

Croes, B. E., et al. (1994): "Southern California Air Quality Study Data Archive," Research Division, California Air Resources Board.

Dasgupta, P. K, Dong, S. and Hwang, H. (1988): "Continuous Liquid Phase Fluorometry Coupled to a Diffusion Scrubber for the Determination of Atmospheric Formaldehyde, Hydrogen Peroxide, and Sulfur Dioxide," Atmos. Environ. 22, 949-963.

Dasgupta, P.K, Dong, S. and Hwang, H. (1990): Aerosol Science and Technology 12, 98-104

Dimitriades, B. (1999): "Scientific Basis of an Improved EPA Policy on Control of Organic Emissions for Ambient Ozone Reduction," J. Air & Waste Manage. Assoc. 49, 831-838

Dodge, M. C. (1984): "Combined effects of organic reactivity and NMHC/NOx ratio on photochemical oxidant formation -- a modeling study," Atmos. Environ., 18, 1657.

EPA (1984): "Guideline for Using the Carbon Bond Mechanism in City-Specific EKMA," EPA-450/4-84-005, February.

Gery, M. W., R. D. Edmond and G. Z. Whitten (1987): "Tropospheric Ultraviolet Radiation. Assessment of Existing Data and Effects on Ozone Formation," Final Report, EPA-600/3-87-047, October.

Gery, M. W., G. Z. Whitten, and J. P. Killus (1988): "Development and Testing of the CBM-IV For Urban and Regional Modeling,", EPA-600/ 3-88-012, January.

Gipson, G. L., W. P. Freas, R. A. Kelly and E. L. Meyer (1981): "Guideline for Use of City-Specific EKMA in Preparing Ozone SIPs, EPA-450/4-80-027, March.

Gipson, G. L. and W. P. Freas (1983): "Use of City-Specific EKMA in the Ozone RIA," U. S. Environmental Protection Agency, July.

Hogo, H. and M. W. Gery (1988): "Guidelines for Using OZIPM-4 with CBM-IV or Optional Mechanisms. Volume 1. Description of the Ozone Isopleth Plotting Package Version 4", Final Report for EPA Contract No. 68-02-4136, Atmospheric Sciences Research Laboratory, Research Triangle Park, NC. January.

Johnson, G. M. (1983): "Factors Affecting Oxidant Formation in Sydney Air," in "The Urban Atmosphere -- Sydney, a Case Study." Eds. J. N. Carras and G. M. Johnson (CSIRO, Melbourne), pp. 393-408.

Jeffries, H. E. (1991): “UNC Solar Radiation Models,” unpublished draft report for EPA Cooperative Agreements CR813107, CR813964 and CR815779”.

Jeffries, H. E., K. G. Sexton, J. R. Arnold, and T. L. Kale (1989): “Validation Testing of New Mechanisms with Outdoor Chamber Data. Volume 2: Analysis of VOC Data for the CB4 and CAL Photochemical Mechanisms,” Final Report, EPA-600/3-89-010b.

Jeffries, H. E. and R. Crouse (1991): “Scientific and Technical Issues Related to the Application of Incremental Reactivity. Part II: Explaining Mechanism Differences,” Report prepared for Western States Petroleum Association, Glendale, CA, October.

Jeffries, H. E., M. W. Gery and W. P. L. Carter (1992): “Protocol for Evaluating Oxidant Mechanisms for Urban and Regional Models,” Report for U. S. Environmental Protection Agency Cooperative Agreement No. 815779, Atmospheric Research and Exposure Assessment Laboratory, Research Triangle Park, NC.

Kwok, E. S. C., and R. Atkinson (1995): “Estimation of Hydroxyl Radical Reaction Rate Constants for Gas-Phase Organic Compounds Using a Structure-Reactivity Relationship: An Update,” Atmos. Environ 29, 1685-1695.

Lurmann, F. W. and H. H. Main (1992): “Analysis of the Ambient VOC Data Collected in the Southern California Air Quality Study,” Final Report to California Air Resources Board Contract No. A832-130, February.

NRC (1991): “Rethinking the Ozone Problem in Urban and Regional Air Pollution,” National Research Council Committee on Tropospheric Ozone Formation and Measurement. National Academy Press, Washing, DC.

RRWG (1999): “VOC Reactivity Policy White Paper,” Prepared by the Reactivity Research Work Group Policy Team, October 1. Available at http://www.cgenv.com/Narsto/reactinfo.html.

Tuazon, E. C., S. M. Aschmann, R. Atkinson, and W. P. L. Carter (1998): “The reactions of Selected Acetates with the OH radical in the Presence of NO: Novel Rearrangement of Alkoxy Radicals of Structure RC(O)OCH(O.)R'“, J. Phys. Chem A 102, 2316-2321.

Zafonte, L., P. L. Rieger, and J. R. Holmes (1977): "Nitrogen Dioxide Photolysis in the Los Angeles Atmosphere," Environ. Sci. Technol. 11, 483-487.

APPENDIX A.
MECHANISM LISTING AND TABULATIONS

This Appendix gives a complete listing of the mechanisms used in the SAPRC-99 model simulations of the environmental chamber experiments and the mineral spirits atmospheric reactivity simulations in this report. Table A-1 contains a list of all the model species used, and Table A-2 lists all the reactions and rate parameters used in the simulations in this work, Table A-3 lists the absorption cross sections and photolysis reactions used in the mechanism. In addition, Table A-4 gives the chamber-dependent parameters used in the model simulations of the chamber experiments.

Table A-1. Listing of the model species in the mechanism used in the model simulations discussed in this report.

Type and Name	Description
	Species used in Base Mechanism
Constant Species.	
O2	Oxygen
M	Air
H2O	Water
H2	Hydrogen Molecules
HV	Light
Active Inorganic Species.	
O3	Ozone
NO	Nitric Oxide
NO2	Nitrogen Dioxide
NO3	Nitrate Radical
N2O5	Nitrogen Pentoxide
HONO	Nitrous Acid
HNO3	Nitric Acid
HNO4	Peroxynitric Acid
HO2H	Hydrogen Peroxide
CO	Carbon Monoxide
SO2	Sulfur Dioxide
Active Radical Species and Operators.	
HO.	Hydroxyl Radicals
HO2.	Hydroperoxide Radicals
C-O2.	Methyl Peroxy Radicals
RO2-R.	Peroxy Radical Operator representing NO to NO2 conversion with HO2 formation.
R2O2.	Peroxy Radical Operator representing NO to NO2 conversion without HO2 formation.
RO2-N.	Peroxy Radical Operator representing NO consumption with organic nitrate formation.
CCO-O2.	Acetyl Peroxy Radicals
RCO-O2.	Peroxy Propionyl and higher peroxy acyl Radicals
BZCO-O2.	Peroxyacyl radical formed from Aromatic Aldehydes
MA-RCO3.	Peroxyacyl radicals formed from methacrolein and other acroleins.
Steady State Radical Species	
O3P	Ground State Oxygen Atoms
O*1D2	Excited Oxygen Atoms
TBU-O.	t-Butoxy Radicals
BZ-O.	Phenoxy Radicals
BZ(NO2)-O.	Nitro-substituted Phenoxy Radical
HOCOO.	Radical formed when Formaldehyde reacts with HO2
PAN and PAN Analogues	
PAN	Peroxy Acetyl Nitrate
PAN2	PPN and other higher alkyl PAN analogues
PBZN	PAN analogues formed from Aromatic Aldehydes
MA-PAN	PAN analogue formed from Methacrolein
Explicit and Lumped Molecule Reactive Organic Product Species	

Table A-1 (continued)

Type and Name	Description
HCHO	Formaldehyde
CCHO	Acetaldehyde
RCHO	Lumped C3+ Aldehydes
ACET	Acetone
MEK	Ketones and other non-aldehyde oxygenated products that react with OH radicals slower than 5 x 10^{-12} cm^3 $molec^{-2}$ sec^{-1}.
MEOH	Methanol
COOH	Methyl Hydroperoxide
ROOH	Lumped higher organic hydroperoxides
GLY	Glyoxal
MGLY	Methyl Glyoxal
BACL	Biacetyl
PHEN	Phenol
CRES	Cresols
NPHE	Nitrophenols
BALD	Aromatic aldehydes (e.g., benzaldehyde)
METHACRO	Methacrolein
MVK	Methyl Vinyl Ketone
ISO-PROD	Lumped isoprene product species
Lumped Parameter Products	
PROD2	Ketones and other non-aldehyde oxygenated products that react with OH radicals faster than 5 x 10^{-12} cm^3 $molec^{-2}$ sec^{-1}.
RNO3	Lumped Organic Nitrates
Uncharacterized Reactive Aromatic Ring Fragmentation Products	
DCB1	Reactive Aromatic Fragmentation Products that do not undergo significant photodecomposition to radicals.
DCB2	Reactive Aromatic Fragmentation Products which photolyze with alpha-dicarbonyl-like action spectrum.
DCB3	Reactive Aromatic Fragmentation Products which photolyze with acrolein action spectrum.
Non-Reacting Species	
CO2	Carbon Dioxide
XC	Lost Carbon
XN	Lost Nitrogen
SULF	Sulfates (SO_3 or H_2SO_4)
Low Reactivity Compounds or Unknown Products Represented as Unreactive	
H2	Hydrogen
HCOOH	Formic Acid
CCO-OH	Acetic Acid
RCO-OH	Higher organic acids
CCO-OOH	Peroxy Acetic Acid
RCO-OOH	Higher organic peroxy acids
NROG	Unspecified Unreactive Carbon

Table A-1 (continued)

Type and Name	Description
	Base ROG VOC Species used in the Chamber Simulations
N-C4	n-Butane
N-C6	n-Hexane
N-C8	n-Octane
ETHENE	Ethene
PROPENE	Propene
T-2-BUTE	*Trans*-2-Butene
TOLUENE	Toluene
M-XYLENE	m-Xylene
135-TMB	1,3,5-Trimethyl Benzene
	Normal Alkane Mineral Spirit Constituents
N-C8	n-Octane
N-C9	n-Nonane
N-C10	n-Decane
N-C11	n-Undecane
N-C12	n-Dodecane
N-C13	n-Tridecane
N-C14	n-Tetradecane
N-C15	n-Pentadecane
	Lumped Model Species used to Represent Hydrocarbon Fluid Constituents studied for this project[a]
D95	Exxal® D95 Fluid
ISOPAR-M	Isopar®-M Fluid (Standard Representation)
ISOPARMB	Isopar®-M Fluid (High Branching Representation) [c]
	Lumped Model Species used to Represent the Mineral Spirits Studied for Safety-Kleen [d]
MS-A-ALK	Alkanes in mineral spirits sample “A” (91.7% of total, by weight)
MS-A-ARO	Aromatics in mineral spirits sample “A” (6.1% of total, by weight)
MS-A-OLE	Olefins in mineral spirits sample “A” (2.2% of total, by weight)
MS-B	Mineral spirits sample “B” (all alkanes)
MS-C	Mineral spirits sample “B” (all alkanes)
MS-D	Mineral spirits sample “B” (all alkanes)
	Lumped Model Species used to Represent the Mineral Spirits Studied for Safety-Kleen [e]
OC6-ACET	Exxate® 600 Fluid
OC7-ACET	Exxate® 700 Fluid
OC8-ACET	Exxate® 800 Fluid
OC9-ACET	Exxate® 900 Fluid
OC10ACET	Exxate® 1000 Fluid
OC12ACET	Exxate® 1200 Fluid
OC13ACET	Exxate® 1300 Fluid
	Explicit and Lumped VOC Species used in the Ambient Simulations
Primary Organics Represented explicitly	
CH4	Methane
ETHENE	Ethene
ISOPRENE	Isoprene

Table A-1 (continued)

Type and Name	Description
Example Test VOCs not in the Base Mechanism	
ETHANE	Ethane
Lumped Parameter Species	
ALK1	Alkanes and other non-aromatic compounds that react only with OH, and have kOH < 5 x 10^2 ppm-1 min-1. (Primarily ethane)
ALK2	Alkanes and other non-aromatic compounds that react only with OH, and have kOH between 5 x 10^2 and 2.5 x 10^3 ppm-1 min-1. (Primarily propane and acetylene)
ALK3	Alkanes and other non-aromatic compounds that react only with OH, and have kOH between 2.5 x 10^3 and 5 x 10^3 ppm-1 min-1.
ALK4	Alkanes and other non-aromatic compounds that react only with OH, and have kOH between 5 x 10^3 and 1 x 10^4 ppm-1 min-1.
ALK5	Alkanes and other non-aromatic compounds that react only with OH, and have kOH greater than 1 x 10^4 ppm-1 min-1.
ARO1	Aromatics with kOH < 2x10^4 ppm-1 min-1.
ARO2	Aromatics with kOH > 2x10^4 ppm-1 min-1.
OLE1	Alkenes (other than ethene) with kOH < 7x10^4 ppm-1 min-1.
OLE2	Alkenes with kOH > 7x10^4 ppm-1 min-1.
TERP	Terpenes

[a] See Table 9 for the mechanisms of the individual fluid constituent compounds.

[b] Assumed compositions in terms of normal, branched, and cyclic alkane constituents are given in Table 3. Compounds used to represent cyclic alkane constituents are given in Table 5. Unless indicated otherwise, the compounds used to represent the branched alkane constituents are given in the "standard representation" columns of Table 4.

[c] Compounds used to represent the branched alkane constituents are given in the "highly branched representation" columns of Table 5

[d] Compositions and mechanisms given by Carter et al (2000?). The representation and mechanisms for the alkane constituents are consistent with those used for D95 and the "standard representation" of Isopar-M.

[e] Assumed compositions are given in Table 6.

.

Table A-2. Listing of the reactions in the mechanism used in the model simulations discussed in this report. See Carter (2000) for documentation.

Label	Rate Parameters [a]				Reaction and Products [b]
	k(298)	A	Ea	B	
Inorganic Reactions					
1		Phot Set= NO2			NO2 + HV = NO + O3P
2	5.79e-34	5.68e-34	0.00	-2.8	O3P + O2 + M = O3 + M
3	7.96e-15	8.00e-12	4.09		O3P + O3 = #2 O2
4	1.01e-31	1.00e-31	0.00	-1.6	O3P + NO + M = NO2 + M
5	9.72e-12	6.50e-12	-0.24		O3P + NO2 = NO + O2
6	1.82e-12	Falloff, F=0.80			O3P + NO2 = NO3 + M
	0:	9.00e-32	0.00	-2.0	
	inf:	2.20e-11	0.00	0.0	
8	1.81e-14	1.80e-12	2.72		O3 + NO = NO2 + O2
9	3.52e-17	1.40e-13	4.91		O3 + NO2 = O2 + NO3
10	2.60e-11	1.80e-11	-0.22		NO + NO3 = #2 NO2
11	1.95e-38	3.30e-39	-1.05		NO + NO + O2 = #2 NO2
12	1.54e-12	Falloff, F=0.45			NO2 + NO3 = N2O5
	0:	2.80e-30	0.00	-3.5	
	inf:	2.00e-12	0.00	0.2	
13	5.28e-2	Falloff, F=0.45			N2O5 = NO2 + NO3
	0:	1.00e-3	21.86	-3.5	
	inf:	9.70e+14	22.02	0.1	
14	2.60e-22	2.60e-22			N2O5 + H2O = #2 HNO3
15		(Slow)			N2O5 + HV = NO3 + NO + O3P
16		(Slow)			N2O5 + HV = NO3 + NO2
17	6.56e-16	4.50e-14	2.50		NO2 + NO3 = NO + NO2 + O2
18		Phot Set= NO3NO			NO3 + HV = NO + O2
19		Phot Set= NO3NO2			NO3 + HV = NO2 + O3P
20		Phot Set= O3O3P			O3 + HV = O3P + O2
21		Phot Set= O3O1D			O3 + HV = O*1D2 + O2
22	2.20e-10	2.20e-10			O*1D2 + H2O = #2 HO.
23	2.87e-11	2.09e-11	-0.19		O*1D2 + M = O3P + M
24	7.41e-12	Falloff, F=0.60			HO. + NO = HONO
	0:	7.00e-31	0.00	-2.6	
	inf:	3.60e-11	0.00	-0.1	
25		Phot Set= HONO-NO			HONO + HV = HO. + NO
26		Phot Set= HONO-NO2			HONO + HV = HO2. + NO2
27	6.46e-12	2.70e-12	-0.52		HO. + HONO = H2O + NO2
28	8.98e-12	Falloff, F=0.60			HO. + NO2 = HNO3
	0:	2.43e-30	0.00	-3.1	
	inf:	1.67e-11	0.00	-2.1	
29	2.00e-11	2.00e-11			HO. + NO3 = HO2. + NO2
30	1.47e-13	k = k0+k3M/(1+k3M/k2)			HO. + HNO3 = H2O + NO3
	k0:	7.20e-15	-1.56	0.0	
	k2:	4.10e-16	-2.86	0.0	
	k3:	1.90e-33	-1.44	0.0	
31		Phot Set= HNO3			HNO3 + HV = HO. + NO2
32	2.09e-13	k = k1 + k2 [M]			HO. + CO = HO2. + CO2
	k1:	1.30e-13	0.00	0.0	
	k2:	3.19e-33	0.00	0.0	
33	6.63e-14	1.90e-12	1.99		HO. + O3 = HO2. + O2

Table A-2 (continued)

Label	Rate Parameters [a] k(298)	A	Ea	B	Reaction and Products [b]
34	8.41e-12	3.40e-12	-0.54		HO2. + NO = HO. + NO2
35	1.38e-12	Falloff, F=0.60			HO2. + NO2 = HNO4
	0:	1.80e-31	0.00	-3.2	
	inf:	4.70e-12	0.00	0.0	
36	7.55e-2	Falloff, F=0.50			HNO4 = HO2. + NO2
	0:	4.10e-5	21.16	0.0	
	inf:	5.70e+15	22.20	0.0	
37	Phot Set= HO2NO2				HNO4 + HV = #.61 {HO2. + NO2} + #.39 {HO. + NO3}
38	5.02e-12	1.50e-12	-0.72		HNO4 + HO. = H2O + NO2 + O2
39	1.87e-15	1.40e-14	1.19		HO2. + O3 = HO. + #2 O2
40A	2.87e-12	k = k1 + k2 [M]			HO2. + HO2. = HO2H + O2
	k1:	2.20e-13	-1.19	0.0	
	k2:	1.85e-33	-1.95	0.0	
40B	6.46e-30	k = k1 + k2 [M]			HO2. + HO2. + H2O = HO2H + O2 + H2O
	k1:	3.08e-34	-5.56	0.0	
	k2:	2.59e-54	-6.32	0.0	
41	4.00e-12	4.00e-12			NO3 + HO2. = #.8 {HO. + NO2 + O2} + #.2 {HNO3 + O2}
42	2.28e-16	8.50e-13	4.87		NO3 + NO3 = #2 NO2 + O2
43	Phot Set= H2O2				HO2H + HV = #2 HO.
44	1.70e-12	2.90e-12	0.32		HO2H + HO. = HO2. + H2O
45	1.11e-10	4.80e-11	-0.50		HO. + HO2. = H2O + O2
S2OH	9.77e-13	Falloff, F=0.45			HO. + SO2 = HO2. + SULF
	0:	4.00e-31	0.00	-3.3	
	inf:	2.00e-12	0.00	0.0	
H2OH	6.70e-15	7.70e-12	4.17		HO. + H2 = HO2. + H2O
Methyl peroxy and methoxy reactions					
MER1	7.29e-12	2.80e-12	-0.57		C-O2. + NO = NO2 + HCHO + HO2.
MER4	5.21e-12	3.80e-13	-1.55		C-O2. + HO2. = COOH + O2
MEN3	1.30e-12	1.30e-12			C-O2. + NO3 = HCHO + HO2. + NO2
MER5	2.65e-13	2.45e-14	-1.41		C-O2. + C-O2. = MEOH + HCHO + O2
MER6	1.07e-13	5.90e-13	1.01		C-O2. + C-O2. = #2 {HCHO + HO2.}
Peroxy Racical Operators					
RRNO	9.04e-12	2.70e-12	-0.72		RO2-R. + NO = NO2 + HO2.
RRH2	1.49e-11	1.90e-13	-2.58		RO2-R. + HO2. = ROOH + O2 + #-3 XC
RRN3	2.30e-12	2.30e-12			RO2-R. + NO3 = NO2 + O2 + HO2.
RRME	2.00e-13	2.00e-13			RO2-R. + C-O2. = HO2. + #.75 HCHO + #.25 MEOH
RRR2	3.50e-14	3.50e-14			RO2-R. + RO2-R. = HO2.
R2NO	Same k as rxn RRNO				R2O2. + NO = NO2
R2H2	Same k as rxn RRH2				R2O2. + HO2. = HO2.
R2N3	Same k as rxn RRN3				R2O2. + NO3 = NO2
R2ME	Same k as rxn RRME				R2O2. + C-O2. = C-O2.
R2RR	Same k as rxn RRR2				R2O2. + RO2-R. = RO2-R.
R2R3	Same k as rxn RRR2				R2O2. + R2O2. =
RNNO	Same k as rxn RRNO				RO2-N. + NO = RNO3
RNH2	Same k as rxn RRH2				RO2-N. + HO2. = ROOH + #3 XC
RNME	Same k as rxn RRME				RO2-N. + C-O2. = HO2. + #.25 MEOH + #.5 {MEK + PROD2} + #.75 HCHO + XC
RNN3	Same k as rxn RRN3				RO2-N. + NO3 = NO2 + O2 + HO2. + MEK + #2 XC
RNRR	Same k as rxn RRR2				RO2-N. + RO2-R. = HO2. + #.5 {MEK + PROD2} + O2 + XC

Table A-2 (continued)

Label	Rate Parameters [a] k(298)	A	Ea	B	Reaction and Products [b]
RNR2	Same k as rxn RRR2				RO2-N. + R2O2. = RO2-N.
RNRN	Same k as rxn RRR2				RO2-N. + RO2-N. = MEK + HO2. + PROD2 + O2 + #2 XC
APN2	1.05e-11	Falloff, F=0.30			CCO-O2. + NO2 = PAN
	0:	2.70e-28	0.00	-7.1	
	inf:	1.20e-11	0.00	-0.9	
DPAN	5.21e-4	Falloff, F=0.30			PAN = CCO-O2. + NO2
	0:	4.90e-3	24.05	0.0	
	inf:	4.00e+16	27.03	0.0	
APNO	2.13e-11	7.80e-12	-0.60		CCO-O2. + NO = C-O2. + CO2 + NO2
APH2	1.41e-11	4.30e-13	-2.07		CCO-O2. + HO2. = #.75 {CCO-OOH +O2} + #.25 {CCO-OH + O3}
APN3	4.00e-12	4.00e-12			CCO-O2. + NO3 = C-O2. + CO2 + NO2 + O2
APME	9.64e-12	1.80e-12	-0.99		CCO-O2. + C-O2. = CCO-OH + HCHO + O2
APRR	7.50e-12	7.50e-12			CCO-O2. + RO2-R. = CCO-OH
APR2	Same k as rxn APRR				CCO-O2. + R2O2. = CCO-O2.
APRN	Same k as rxn APRR				CCO-O2. + RO2-N. = CCO-OH + PROD2
APAP	1.55e-11	2.90e-12	-0.99		CCO-O2. + CCO-O2. = #2 {C-O2. + CO2} + O2
PPN2	1.21e-11	1.20e-11	0.00	-0.9	RCO-O2. + NO2 = PAN2
PAN2	4.43e-4	2.00e+15	25.44		PAN2 = RCO-O2. + NO2
PPNO	2.80e-11	1.25e-11	-0.48		RCO-O2. + NO = NO2 + CCHO + RO2-R. + CO2
PPH2	Same k as rxn APH2				RCO-O2. + HO2. = #.75 {RCO-OOH + O2} + #.25 {RCO-OH + O3}
PPN3	Same k as rxn APN3				RCO-O2. + NO3 = NO2 + CCHO + RO2-R. + CO2 + O2
PPME	Same k as rxn APME				RCO-O2. + C-O2. = RCO-OH + HCHO + O2
PPRR	Same k as rxn APRR				RCO-O2. + RO2-R. = RCO-OH + O2
PPR2	Same k as rxn APRR				RCO-O2. + R2O2. = RCO-O2.
PPRN	Same k as rxn APRR				RCO-O2. + RO2-N. = RCO-OH + PROD2 + O2
PPAP	Same k as rxn APAP				RCO-O2. + CCO-O2. = #2 CO2 + C-O2. + CCHO + RO2-R. + O2
PPPP	Same k as rxn APAP				RCO-O2. + RCO-O2. = #2 {CCHO + RO2-R. + CO2}
BPN2	1.37e-11	1.37e-11			BZCO-O2. + NO2 = PBZN
BPAN	3.12e-4	7.90e+16	27.82		PBZN = BZCO-O2. + NO2
BPNO	Same k as rxn PPNO				BZCO-O2. + NO = NO2 + CO2 + BZ-O. + R2O2.
BPH2	Same k as rxn APH2				BZCO-O2. + HO2. = #.75 {RCO-OOH + O2} + #.25 {RCO-OH + O3} + #4 XC
BPN3	Same k as rxn APN3				BZCO-O2. + NO3 = NO2 + CO2 + BZ-O. + R2O2. + O2
BPME	Same k as rxn APME				BZCO-O2. + C-O2. = RCO-OH + HCHO + O2 + #4 XC
BPRR	Same k as rxn APRR				BZCO-O2. + RO2-R. = RCO-OH + O2 + #4 XC
BPR2	Same k as rxn APRR				BZCO-O2. + R2O2. = BZCO-O2.
BPRN	Same k as rxn APRR				BZCO-O2. + RO2-N. = RCO-OH + PROD2 + O2 + #4 XC
BPAP	Same k as rxn APAP				BZCO-O2. + CCO-O2. = #2 CO2 + C-O2. + BZ-O. + R2O2.
BPPP	Same k as rxn APAP				BZCO-O2. + RCO-O2. = #2 CO2 + CCHO + RO2-R. + BZ-O. + R2O2.
BPBP	Same k as rxn APAP				BZCO-O2. + BZCO-O2. = #2 {BZ-O. + R2O2. + CO2}
MPN2	Same k as rxn PPN2				MA-RCO3. + NO2 = MA-PAN
MPPN	3.55e-4	1.60e+16	26.80		MA-PAN = MA-RCO3. + NO2
MPNO	Same k as rxn PPNO				MA-RCO3. + NO = NO2 + CO2 + HCHO + CCO-O2.
MPH2	Same k as rxn APH2				MA-RCO3. + HO2. = #.75 {RCO-OOH + O2} + #.25 {RCO-OH + O3} + XC
MPN3	Same k as rxn APN3				MA-RCO3. + NO3 = NO2 + CO2 + HCHO + CCO-O2. + O2

Table A-2 (continued)

Label	Rate Parameters [a] k(298)	A	Ea	B	Reaction and Products [b]
MPME	Same k as rxn APME				MA-RCO3. + C-O2. = RCO-OH + HCHO + XC + O2
MPRR	Same k as rxn APRR				MA-RCO3. + RO2-R. = RCO-OH + XC
MPR2	Same k as rxn APRR				MA-RCO3. + R2O2. = MA-RCO3.
MPRN	Same k as rxn APRR				MA-RCO3. + RO2-N. = #2 RCO-OH + O2 + #4 XC
MPAP	Same k as rxn APAP				MA-RCO3. + CCO-O2. = #2 CO2 + C-O2. + HCHO + CCO-O2. + O2
MPPP	Same k as rxn APAP				MA-RCO3. + RCO-O2. = HCHO + CCO-O2. + CCHO + RO2-R. + #2 CO2
MPBP	Same k as rxn APAP				MA-RCO3. + BZCO-O2. = HCHO + CCO-O2. + BZ-O. + R2O2. + #2 CO2
MPMP	Same k as rxn APAP				MA-RCO3. + MA-RCO3. = #2 {HCHO + CCO-O2. + CO2}
Other Organic Radical Species					
TBON	2.40e-11	2.40e-11			TBU-O. + NO2 = RNO3 + #-2 XC
TBOD	9.87e+2	7.50e+14	16.20		TBU-O. = ACET + C-O2.
BRN2	3.80e-11	2.30e-11	-0.30		BZ-O. + NO2 = NPHE
BRH2	Same k as rxn RRH2				BZ-O. + HO2. = PHEN
BRXX	1.00e-3	1.00e-3			BZ-O. = PHEN
BNN2	Same k as rxn BRN2				BZ(NO2)-O. + NO2 = #2 XN + #6 XC
BNH2	Same k as rxn RRH2				BZ(NO2)-O. + HO2. = NPHE
BNXX	Same k as rxn BRXX				BZ(NO2)-O. = NPHE
Explicit and Lumped Molecule Organic Products					
FAHV	Phot Set= HCHO_R				HCHO + HV = #2 HO2. + CO
FAVS	Phot Set= HCHO_M				HCHO + HV = H2 + CO
FAOH	9.20e-12	8.60e-12	-0.04		HCHO + HO. = HO2. + CO + H2O
FAH2	7.90e-14	9.70e-15	-1.24		HCHO + HO2. = HOCOO.
FAHR	1.51e+2	2.40e+12	13.91		HOCOO. = HO2. + HCHO
FAHN	Same k as rxn MER1				HOCOO. + NO = HCOOH + NO2 + HO2.
FAN3	5.74e-16	2.00e-12	4.83		HCHO + NO3 = HNO3 + HO2. + CO
AAOH	1.58e-11	5.60e-12	-0.62		CCHO + HO. = CCO-O2. + H2O
AAHV	Phot Set= CCHO_R				CCHO + HV = CO + HO2. + C-O2.
AAN3	2.73e-15	1.40e-12	3.70		CCHO + NO3 = HNO3 + CCO-O2.
PAOH	2.00e-11	2.00e-11			RCHO + HO. = #.034 RO2-R. + #.001 RO2-N. + #.965 RCO-O2. + #.034 CO + #.034 CCHO + #-0.003 XC
PAHV	Phot Set= C2CHO				RCHO + HV = CCHO + RO2-R. + CO + HO2.
PAN3	3.67e-15	1.40e-12	3.52		RCHO + NO3 = HNO3 + RCO-O2.
K3OH	1.92e-13	1.10e-12	1.03		ACET + HO. = HCHO + CCO-O2. + R2O2.
K3HV	Phot Set= ACETONE				ACET + HV = CCO-O2. + C-O2.
K4OH	1.18e-12	1.30e-12	0.05	2.0	MEK + HO. = #.37 RO2-R. + #.042 RO2-N. + #.616 R2O2. + #.492 CCO-O2. + #.096 RCO-O2. + #.115 HCHO + #.482 CCHO + #.37 RCHO + #.287 XC
K4HV	Phot Set= KETONE, qy= 1.5e-1				MEK + HV = CCO-O2. + CCHO + RO2-R.
MeOH	9.14e-13	3.10e-12	0.72	2.0	MEOH + HO. = HCHO + HO2.
MER9	5.49e-12	2.90e-12	-0.38		COOH + HO. = H2O + #.35 {HCHO + HO.} + #.65 C-O2.
MERA	Phot Set= COOH				COOH + HV = HCHO + HO2. + HO.
LPR9	1.10e-11	1.10e-11			ROOH + HO. = H2O + RCHO + #.34 RO2-R. + #.66 HO.
LPRA	Phot Set= COOH				ROOH + HV = RCHO + HO2. + HO.

Table A-2 (continued)

Label	Rate Parameters [a] k(298)	A	Ea	B	Reaction and Products [b]
GLHV	Phot Set= GLY_R				GLY + HV = #2 {CO + HO2.}
GLVM	Phot Set= GLY_ABS, qy= 6.0e-3				GLY + HV = HCHO + CO
GLOH	1.10e-11	1.10e-11			GLY + HO. = #.63 HO2. + #1.26 CO + #.37 RCO-O2. + #-.37 XC
GLN3	9.63e-16	2.80e-12	4.72		GLY + NO3 = HNO3 + #.63 HO2. + #1.26 CO + #.37 RCO-O2. + #-.37 XC
MGHV	Phot Set= MGLY_ADJ				MGLY + HV = HO2. + CO + CCO-O2.
MGOH	1.50e-11	1.50e-11			MGLY + HO. = CO + CCO-O2.
MGN3	2.43e-15	1.40e-12	3.77		MGLY + NO3 = HNO3 + CO + CCO-O2.
BAHV	Phot Set= BACL_ADJ				BACL + HV = #2 CCO-O2.
PHOH	2.63e-11	2.63e-11			PHEN + HO. = #.24 BZ-O. + #.76 RO2-R. + #.23 GLY + #4.1 XC
PHN3	3.78e-12	3.78e-12			PHEN + NO3 = HNO3 + BZ-O.
CROH	4.20e-11	4.20e-11			CRES + HO. = #.24 BZ-O. + #.76 RO2-R. + #.23 MGLY + #4.87 XC
CRN3	1.37e-11	1.37e-11			CRES + NO3 = HNO3 + BZ-O. + XC
NPN3	Same k as rxn PHN3				NPHE + NO3 = HNO3 + BZ(NO2)-O.
BZOH	1.29e-11	1.29e-11			BALD + HO. = BZCO-O2.
BZHV	Phot Set= BZCHO, qy= 5.0e-2				BALD + HV = #7 XC
BZNT	2.62e-15	1.40e-12	3.72		BALD + NO3 = HNO3 + BZCO-O2.
MAOH	3.36e-11	1.86e-11	-0.35		METHACRO + HO. = #.5 RO2-R. + #.416 CO + #.084 HCHO + #.416 MEK + #.084 MGLY + #.5 MA-RCO3. + #-0.416 XC
MAO3	1.13e-18	1.36e-15	4.20		METHACRO + O3 = #.008 HO2. + #.1 RO2-R. + #.208 HO. + #.1 RCO-O2. + #.45 CO + #.117 CO2 + #.2 HCHO + #.9 MGLY + #.333 HCOOH + #-0.1 XC
MAN3	4.58e-15	1.50e-12	3.43		METHACRO + NO3 = #.5 {HNO3 + RO2-R. + CO +MA-RCO3.} + #1.5 XC + #.5 XN
MAOP	6.34e-12	6.34e-12			METHACRO + O3P = RCHO + XC
MAHV	Phot Set= ACROLEIN, qy= 4.1e-3				METHACRO + HV = #.34 HO2. + #.33 RO2-R. + #.33 HO. + #.67 CCO-O2. + #.67 CO + #.67 HCHO + #.33 MA-RCO3. + #-0 XC
MVOH	1.89e-11	4.14e-12	-0.90		MVK + HO. = #.3 RO2-R. + #.025 RO2-N. + #.675 R2O2. + #.675 CCO-O2. + #.3 HCHO + #.675 RCHO + #.3 MGLY + #-0.725 XC
MVO3	4.58e-18	7.51e-16	3.02		MVK + O3 = #.064 HO2. + #.05 RO2-R. + #.164 HO. + #.05 RCO-O2. + #.475 CO + #.124 CO2 + #.1 HCHO + #.95 MGLY + #.351 HCOOH + #-0.05 XC
MVN3	(Slow)				MVK + NO3 = #4 XC + XN
MVOP	4.32e-12	4.32e-12			MVK + O3P = #.45 RCHO + #.55 MEK + #.45 XC
MVHV	Phot Set= ACROLEIN, qy= 2.1e-3				MVK + HV = #.3 C-O2. + #.7 CO + #.7 PROD2 + #.3 MA-RCO3. + #-2.4 XC
IPOH	6.19e-11	6.19e-11			ISO-PROD + HO. = #.67 RO2-R. + #.041 RO2-N. + #.289 MA-RCO3. + #.336 CO + #.055 HCHO + #.129 CCHO + #.013 RCHO + #.15 MEK + #.332 PROD2 + #.15 GLY + #.174 MGLY + #-0.504 XC
IPO3	4.18e-18	4.18e-18			ISO-PROD + O3 = #.4 HO2. + #.048 RO2-R. + #.048 RCO-O2. + #.285 HO. + #.498 CO + #.14 CO2 + #.125 HCHO + #.047 CCHO + #.21 MEK + #.023 GLY + #.742 MGLY + #.1 HCOOH + #.372 RCO-OH + #-.33 XC

Table A-2 (continued)

Label	Rate Parameters [a] k(298)	A	Ea	B	Reaction and Products [b]
IPN3	1.00e-13	1.00e-13			ISO-PROD + NO3 = #.799 RO2-R. + #.051 RO2-N. + #.15 MA-RCO3. + #.572 CO + #.15 HNO3 + #.227 HCHO + #.218 RCHO + #.008 MGLY + #.572 RNO3 + #.28 XN + #-.815 XC
IPHV	Phot Set= ACROLEIN, qy= 4.1e-3				ISO-PROD + HV = #1.233 HO2. + #.467 CCO-O2. + #.3 RCO-O2. + #1.233 CO + #.3 HCHO + #.467 CCHO + #.233 MEK + #-.233 XC
Lumped Parameter Organic Products					
K6OH	1.50e-11	1.50e-11			PROD2 + HO. = #.379 HO2. + #.473 RO2-R. + #.07 RO2-N. + #.029 CCO-O2. + #.049 RCO-O2. + #.213 HCHO + #.084 CCHO + #.558 RCHO + #.115 MEK + #.329 PROD2 + #.886 XC
K6HV	Phot Set= KETONE, qy= 2.0e-2				PROD2 + HV = #.96 RO2-R. + #.04 RO2-N. + #.515 R2O2. + #.667 CCO-O2. + #.333 RCO-O2. + #.506 HCHO + #.246 CCHO + #.71 RCHO + #.299 XC
RNOH	7.80e-12	7.80e-12			RNO3 + HO. = #.338 NO2 + #.113 HO2. + #.376 RO2-R. + #.173 RO2-N. + #.596 R2O2. + #.01 HCHO + #.439 CCHO + #.213 RCHO + #.006 ACET + #.177 MEK + #.048 PROD2 + #.31 RNO3 + #.351 XN + #.56 XC
RNHV	Phot Set= IC3ONO2				RNO3 + HV = NO2 + #.341 HO2. + #.564 RO2-R. + #.095 RO2-N. + #.152 R2O2. + #.134 HCHO + #.431 CCHO + #.147 RCHO + #.02 ACET + #.243 MEK + #.435 PROD2 + #.35 XC
Uncharacterized Reactive Aromatic Ring Fragmentation Products					
D1OH	5.00e-11	5.00e-11			DCB1 + HO. = RCHO + RO2-R. + CO
D1HV		(Slow)			DCB1 + HV = HO2. + #2 CO + RO2-R. + GLY + R2O2.
D1O3	2.00e-18	2.00e-18			DCB1 + O3 = #1.5 HO2. + #.5 HO. + #1.5 CO + #.5 CO2 + GLY
D2OH	5.00e-11	5.00e-11			DCB2 + HO. = R2O2. + RCHO + CCO-O2.
D2HV	Phot Set= MGLY_ABS, qy= 3.7e-1				DCB2 + HV = RO2-R. + #.5 {CCO-O2. + HO2.} + CO + R2O2. + #.5 {GLY + MGLY + XC}
D3OH	5.00e-11	5.00e-11			DCB3 + HO. = R2O2. + RCHO + CCO-O2.
D3HV	Phot Set= ACROLEIN, qy= 7.3e+0				DCB3 + HV = RO2-R. + #.5 {CCO-O2. + HO2.} + CO + R2O2. + #.5 {GLY + MGLY + XC}
Base ROG VOCs Used in the Chamber Simulations and Explicit VOCs in the Ambient Simulations					
c1OH	6.37e-15	2.15e-12	3.45		CH4 + HO. = H2O + C-O2.
c2OH	2.54e-13	1.37e-12	0.99	2.0	ETHANE + HO. = RO2-R. + CCHO
c4OH	2.44e-12	1.52e-12	-0.29	2.0	N-C4 + HO. = #.921 RO2-R. + #.079 RO2-N. + #.413 R2O2. + #.632 CCHO + #.12 RCHO + #.485 MEK + #-0.038 XC
c6OH	5.47e-12	1.38e-12	-0.82	2.0	N-C6 + HO. = #.775 RO2-R. + #.225 RO2-N. + #.787 R2O2. + #.011 CCHO + #.113 RCHO + #.688 PROD2 + #.162 XC
c8OH	8.70e-12	2.48e-12	-0.75	2.0	N-C8 + HO. = #.646 RO2-R. + #.354 RO2-N. + #.786 R2O2. + #.024 RCHO + #.622 PROD2 + #2.073 XC
etOH	8.52e-12	1.96e-12	-0.87		ETHENE + HO. = RO2-R. + #1.61 HCHO + #.195 CCHO
etO3	1.59e-18	9.14e-15	5.13		ETHENE + O3 = #.12 HO. + #.12 HO2. + #.5 CO + #.13 CO2 + HCHO + #.37 HCOOH
etN3	2.05e-16	4.39e-13	4.53	2.0	ETHENE + NO3 = RO2-R. + RCHO + #-1 XC + XN
etOA	7.29e-13	1.04e-11	1.57		ETHENE + O3P = #.5 HO2. + #.2 RO2-R. + #.3 C-O2. + #.491 CO + #.191 HCHO + #.25 CCHO + #.009 GLY + #.5 XC
prOH	2.63e-11	4.85e-12	-1.00		PROPENE + HO. = #.984 RO2-R. + #.016 RO2-N. + #.984 HCHO + #.984 CCHO + #-0.048 XC

Table A-2 (continued)

Label	Rate Parameters [a] k(298)	A	Ea	B	Reaction and Products [b]
prO3	1.01e-17	5.51e-15	3.73		PROPENE + O3 = #.32 HO. + #.06 HO2. + #.26 C-O2. + #.51 CO + #.135 CO2 + #.5 HCHO + #.5 CCHO + #.185 HCOOH + #.17 CCO-OH + #.07 INERT + #.07 XC
prN3	9.49e-15	4.59e-13	2.30		PROPENE + NO3 = #.949 RO2-R. + #.051 RO2-N. + #2.693 XC + XN
prOP	3.98e-12	1.18e-11	0.64		PROPENE + O3P = #.45 RCHO + #.55 MEK + #-0.55 XC
t2OH	6.40e-11	1.01e-11	-1.09		T-2-BUTE + HO. = #.965 RO2-R. + #.035 RO2-N. + #1.93 CCHO + #-0.07 XC
t2O3	1.90e-16	6.64e-15	2.10		T-2-BUTE + O3 = #.52 HO. + #.52 C-O2. + #.52 CO + #.14 CO2 + CCHO + #.34 CCO-OH + #.14 INERT + #.14 XC
t2N3	3.91e-13	1.10e-13	-0.76	2.0	T-2-BUTE + NO3 = #.705 NO2 + #.215 RO2-R. + #.08 RO2-N. + #.705 R2O2. + #1.41 CCHO + #.215 RNO3 + #-0.59 XC + #.08 XN
t2OP	2.18e-11	2.18e-11			T-2-BUTE + O3P = MEK
isOH	9.82e-11	2.50e-11	-0.81		ISOPRENE + HO. = #.907 RO2-R. + #.093 RO2-N. + #.079 R2O2. + #.624 HCHO + #.23 METHACRO + #.32 MVK + #.357 ISO-PROD + #-0.167 XC
isO3	1.28e-17	7.86e-15	3.80		ISOPRENE + O3 = #.266 HO. + #.066 RO2-R. + #.008 RO2-N. + #.126 R2O2. + #.192 MA-RCO3. + #.275 CO + #.122 CO2 + #.592 HCHO + #.1 PROD2 + #.39 METHACRO + #.16 MVK + #.204 HCOOH + #.15 RCO-OH + #-0.259 XC
isN3	6.74e-13	3.03e-12	0.89		ISOPRENE + NO3 = #.187 NO2 + #.749 RO2-R. + #.064 RO2-N. + #.187 R2O2. + #.936 ISO-PROD + #-0.064 XC + #.813 XN
isOP	3.60e-11	3.60e-11			ISOPRENE + O3P = #.01 RO2-N. + #.24 R2O2. + #.25 C-O2. + #.24 MA-RCO3. + #.24 HCHO + #.75 PROD2 + #-1.01 XC
tlOH	5.95e-12	1.81e-12	-0.71	0.0	TOLUENE + HO. = #.234 HO2. + #.758 RO2-R. + #.008 RO2-N. + #.116 GLY + #.135 MGLY + #.234 CRES + #.085 BALD + #.46 DCB1 + #.156 DCB2 + #.057 DCB3 + #1.178 XC
mxOH	2.36e-11	2.36e-11	0.00	0.0	M-XYLENE + HO. = #.21 HO2. + #.782 RO2-R. + #.008 RO2-N. + #.107 GLY + #.335 MGLY + #.21 CRES + #.037 BALD + #.347 DCB1 + #.29 DCB2 + #.108 DCB3 + #1.628 XC
<u>Lumped Organic Species used in the Ambient Reactivity Simulations</u>					
t1OH	8.27e-11	1.83e-11	-0.89		TERP + HO. = #.75 RO2-R. + #.25 RO2-N. + #.5 R2O2. + #.276 HCHO + #.474 RCHO + #.276 PROD2 + #5.146 XC
t1O3	6.88e-17	1.08e-15	1.63		TERP + O3 = #.567 HO. + #.033 HO2. + #.031 RO2-R. + #.18 RO2-N. + #.729 R2O2. + #.123 CCO-O2. + #.201 RCO-O2. + #.157 CO + #.037 CO2 + #.235 HCHO + #.205 RCHO + #.13 ACET + #.276 PROD2 + #.001 GLY + #.031 BACL + #.103 HCOOH + #.189 RCO-OH + #4.183 XC
t1N3	6.57e-12	3.66e-12	-0.35		TERP + NO3 = #.474 NO2 + #.276 RO2-R. + #.25 RO2-N. + #.75 R2O2. + #.474 RCHO + #.276 RNO3 + #5.421 XC + #.25 XN
t1OP	3.27e-11	3.27e-11			TERP + O3P = #.147 RCHO + #.853 PROD2 + #4.441 XC
a1OH	2.54e-13	1.37e-12	0.99	2.0	ALK1 + HO. = RO2-R. + CCHO
a2OH	1.04e-12	9.87e-12	1.33		ALK2 + HO. = #.246 HO. + #.121 HO2. + #.612 RO2-R. + #.021 RO2-N. + #.16 CO + #.039 HCHO + #.155 RCHO + #.417 ACET + #.248 GLY + #.121 HCOOH + #0.338 XC
a3OH	2.38e-12	1.02e-11	0.86		ALK3 + HO. = #.695 RO2-R. + #.07 RO2-N. + #.559 R2O2. + #.236 TBU-O. + #.026 HCHO + #.445 CCHO + #.122 RCHO + #.024 ACET + #.332 MEK + #-0.05 XC

Table A-2 (continued)

Label	Rate Parameters [a] k(298)	A	Ea	B	Reaction and Products [b]
a4OH	4.39e-12	5.95e-12	0.18		ALK4 + HO. = #.835 RO2-R. + #.143 RO2-N. + #.936 R2O2. + #.011 C-O2. + #.011 CCO-O2. + #.002 CO + #.024 HCHO + #.455 CCHO + #.244 RCHO + #.452 ACET + #.11 MEK + #.125 PROD2 + #-0.105 XC
a5OH	9.34e-12	1.11e-11	0.10		ALK5 + HO. = #.653 RO2-R. + #.347 RO2-N. + #.948 R2O2. + #.026 HCHO + #.099 CCHO + #.204 RCHO + #.072 ACET + #.089 MEK + #.417 PROD2 + #2.008 XC
b1OH	5.95e-12	1.81e-12	-0.71		ARO1 + HO. = #.224 HO2. + #.765 RO2-R. + #.011 RO2-N. + #.055 PROD2 + #.118 GLY + #.119 MGLY + #.017 PHEN + #.207 CRES + #.059 BALD + #.491 DCB1 + #.108 DCB2 + #.051 DCB3 + #1.288 XC
b2OH	2.64e-11	2.64e-11	0.00		ARO2 + HO. = #.187 HO2. + #.804 RO2-R. + #.009 RO2-N. + #.097 GLY + #.287 MGLY + #.087 BACL + #.187 CRES + #.05 BALD + #.561 DCB1 + #.099 DCB2 + #.093 DCB3 + #1.68 XC
o1OH	3.23e-11	7.10e-12	-0.90		OLE1 + HO. = #.91 RO2-R. + #.09 RO2-N. + #.205 R2O2. + #.732 HCHO + #.294 CCHO + #.497 RCHO + #.005 ACET + #.119 PROD2 + #.92 XC
o1O3	1.06e-17	2.62e-15	3.26		OLE1 + O3 = #.155 HO. + #.056 HO2. + #.022 RO2-R. + #.001 RO2-N. + #.076 C-O2. + #.345 CO + #.086 CO2 + #.5 HCHO + #.154 CCHO + #.363 RCHO + #.001 ACET + #.215 PROD2 + #.185 HCOOH + #.05 CCO-OH + #.119 RCO-OH + #.654 XC
o1N3	1.26e-14	4.45e-14	0.75		OLE1 + NO3 = #.824 RO2-R. + #.176 RO2-N. + #.488 R2O2. + #.009 CCHO + #.037 RCHO + #.024 ACET + #.511 RNO3 + #.677 XC + #.489 XN
o1OP	4.90e-12	1.07e-11	0.47		OLE1 + O3P = #.45 RCHO + #.437 MEK + #.113 PROD2 + #1.224 XC
o2OH	6.33e-11	1.74e-11	-0.76		OLE2 + HO. = #.918 RO2-R. + #.082 RO2-N. + #.001 R2O2. + #.244 HCHO + #.732 CCHO + #.511 RCHO + #.127 ACET + #.072 MEK + #.061 BALD + #.025 METHACRO + #.025 ISO-PROD + #-.054 XC
o2O3	1.07e-16	5.02e-16	0.92		OLE2 + O3 = #.378 HO. + #.003 HO2. + #.033 RO2-R. + #.002 RO2-N. + #.137 R2O2. + #.197 C-O2. + #.137 CCO-O2. + #.006 RCO-O2. + #.265 CO + #.07 CO2 + #.269 HCHO + #.456 CCHO + #.305 RCHO + #.045 ACET + #.026 MEK + #.006 PROD2 + #.042 BALD + #.026 METHACRO + #.073 HCOOH + #.129 CCO-OH + #.303 RCO-OH + #.155 XC
o2N3	7.27e-13	7.27e-13	0.00		OLE2 + NO3 = #.391 NO2 + #.442 RO2-R. + #.136 RO2-N. + #.711 R2O2. + #.03 C-O2. + #.079 HCHO + #.507 CCHO + #.151 RCHO + #.102 ACET + #.001 MEK + #.015 BALD + #.048 MVK + #.321 RNO3 + #.075 XC + #.288 XN
o2OP	2.09e-11	2.09e-11			OLE2 + O3P = #.013 HO2. + #.012 RO2-R. + #.001 RO2-N. + #.012 CO + #.069 RCHO + #.659 MEK + #.259 PROD2 + #.012 METHACRO + #.537 XC
<u>Lumped Species Representing Hydrocarbon Mixtures Studied for Safety-Kleen [c,d]</u>					
	1.44e-11	1.44e-11			MS-A-ALK + HO. = 0.528 RO2-R. + 0.471 RO2-N. + 0.985 R2O2. + 0.001 RCO-O2. + 0.001 CO + 0.005 HCHO + 0.046 CCHO + 0.156 RCHO + 0.027 ACET + 0.009 MEK + 0.406 PROD2

Table A-2 (continued)

Label	Rate Parameters [a] k(298)	A	Ea	B	Reaction and Products [b]
	3.10e-11	3.10e-11			MS-A-ARO + HO. = 0.189 HO2. + 0.783 RO2-R. + 0.012 RO2-N. + 0.016 RCO-O2. + 0.011 PROD2 + 0.072 GLY + 0.308 MGLY + 0.107 BACL + 0.008 PHEN + 0.181 CRES + 0.042 BALD + 0.565 DCB1 + 0.074 DCB2 + 0.09 DCB3 + 2.318 XC
	3.80e-11	3.80e-11			MS-A-OLE + HO. = 0.681 RO2-R. + 0.319 RO2-N. + 0.324 R2O2. + 0.309 HCHO + 0.656 RCHO + 0.174 PROD2
	3.10e-17	3.10e-17			MS-A-OLE + O3 = 0.054 HO. + 0.048 HO2. + 0.006 RO2-R. + 0.003 R2O2. + 0.206 CO + 0.052 CO2 + 0.4 HCHO + 0.606 RCHO + 0.563 PROD2 + 0.148 HCOOH + 0.031 RCO-OH
	8.49e-14	8.49e-14			MS-A-OLE + NO3 = 0.556 RO2-R. + 0.443 RO2-N. + 0.777 R2O2. + 0.001 RCHO + 0.556 RNO3 + 0.443 XN
	8.58e-12	8.58e-12			MS-A-OLE + O3P = 0.36 RCHO + 0.64 PROD2
	1.7e0-11	1.70e-11			MS-B + HO. = 0.493 RO2-R. + 0.506 RO2-N. + 1.016 R2O2. + 0.001 RCO-O2. + 0.001 CO + 0.003 HCHO + 0.051 CCHO + 0.147 RCHO + 0.007 ACET + 0.011 MEK + 0.388 PROD2
	1.61e-11				MS-C + HO. = 0.502 RO2-R. + 0.497 RO2-N. + 0.979 R2O2. + 0.001 RCO-O2. + 0.001 CO + 0.003 HCHO + 0.047 CCHO + 0.129 RCHO + 0.002 ACET + 0.007 MEK + 0.403 PROD2
	1.58e-11				MS-D + HO. = 0.504 RO2-R. + 0.495 RO2-N. + 0.978 R2O2. + 0.001 RCO-O2. + 0.001 CO + 0.003 HCHO + 0.047 CCHO + 0.125 RCHO + 0.002 ACET + 0.009 MEK + 0.411 PROD2
<u>Lumped Species Representing Hydrocarbon Mixtures Studied for This Project [d,e]</u>					
	1.85e-11	1.85e-11			D95 + HO. = #.496 RO2-R. + #.504 RO2-N. + #.938 R2O2. + #.002 HCHO + #.026 CCHO + #.106 RCHO + #.007 MEK + #.429 PROD2
	1.76e-11	1.76e-11			ISOPAR-M + HO. = #.497 RO2-R. + #.503 RO2-N. + #.949 R2O2. + #.001 HCHO + #.035 CCHO + #.089 RCHO + #.017 MEK + #.45 PROD2
	1.80e-11	1.80e-11			ISOPARMB + HO. = #.456 RO2-R. + #.544 RO2-N. + #1.314 R2O2. + #.013 HCHO + #.07 CCHO + #.211 RCHO + #.291 ACET + #.022 MEK + #.449 PROD2
<u>Lumped Species Representing Exxate Mixtures [e]</u>					
	7.62e-12	7.62e-12			OC6-ACET + HO. = #.664 RO2-R. + #.291 RO2-N. + #.888 R2O2. + #.045 RCO-O2. + #.003 CO + #.002 HCHO + #.049 CCHO + #.231 RCHO + #.036 ACET + #.155 MEK + #.398 PROD2 + #.048 CCO-OH + #.022 INERT
	9.16e-12	9.16e-12			OC7-ACET + HO. = #.59 RO2-R. + #.355 RO2-N. + #.985 R2O2. + #.054 RCO-O2. + #.002 CO + #.025 HCHO + #.084 CCHO + #.182 RCHO + #.008 ACET + #.165 MEK + #.38 PROD2 + #.056 CCO-OH + #.048 INERT
	1.07e-11	1.07e-11			OC8-ACET + HO. = #.558 RO2-R. + #.403 RO2-N. + #1.024 R2O2. + #.039 RCO-O2. + #.001 CO + #.02 HCHO + #.114 CCHO + #.17 RCHO + #.039 ACET + #.098 MEK + #.451 PROD2 + #.039 CCO-OH + #.024 INERT

Table A-2 (continued)

Label	Rate Parameters [a] k(298)	A	Ea	B	Reaction and Products [b]
	1.24e-11	1.24e-11			OC9-ACET + HO. = #.51 RO2-R. + #.462 RO2-N. + #1.083 R2O2. + #.027 RCO-O2. + #.002 CO + #.007 HCHO + #.102 CCHO + #.155 RCHO + #.028 ACET + #.062 MEK + #.472 PROD2 + #.029 CCO-OH + #.018 INERT
	1.36e-11	1.36e-11			OC10ACET + HO. = #.5 RO2-R. + #.473 RO2-N. + #1.084 R2O2. + #.027 RCO-O2. + #.002 HCHO + #.094 CCHO + #.172 RCHO + #.074 ACET + #.036 MEK + #.468 PROD2 + #.027 CCO-OH + #.002 INERT
	1.68e-11	1.68e-11			OC12ACET + HO. = #.457 RO2-R. + #.527 RO2-N. + #1.176 R2O2. + #.016 RCO-O2. + #.001 CO + #.015 HCHO + #.055 CCHO + #.198 RCHO + #.014 ACET + #.088 MEK + #.421 PROD2 + #.017 CCO-OH + #.021 INERT
	1.79e-11	1.79e-11			OC13ACET + HO. = #.445 RO2-R. + #.53 RO2-N. + #1.175 R2O2. + #.025 RCO-O2. + #.001 CO + #.013 HCHO + #.06 CCHO + #.163 RCHO + #.014 ACET + #.09 MEK + #.417 PROD2 + #.026 CCO-OH + #.024 INERT

[a] Except as indicated, the rate constants are given by $k(T) = A \cdot (T/300)^B \cdot e^{-Ea/RT}$, where the units of k and A are cm^3 $molec^{-1}$ s^{-1}, Ea are kcal mol^{-1}, T is ^oK, and R=0.0019872 kcal mol^{-1} deg^{-1}. The following special rate constant expressions are used: Phot Set = *name*: The absorption cross sections and quantum yields for the photolysis reaction are given in Table A-3, where "*name*" indicates the photolysis set used. If a "qy=*number*" notation is given, the number given is the overall quantum yield, which is assumed to be wavelength independent. Falloff: The rate constant as a function of temperature and pressure is calculated using $k(T,M) = \{k0(T)\cdot[M]/[1 + k0(T)\cdot[M]/kinf(T)]\}\cdot F^Z$, where $Z = \{1 + [\log_{10}\{k0(T)\cdot[M])/kinf(T)\}]^2\}^{-1}$, [M] is the total pressure in molecules cm^{-3}, F is as indicated on the table, and the temperature dependences of k0 and kinf are as indicated on the table. (Slow): The reaction is assumed to be negligible and is not included in the mechanism. It is shown on the listing for documentation purposes only. k = k0+k3M(1+k3M/k2): The rate constant as a function of temperature and pressure is calculated using $k(T,M) = k0(T) + k3(T)\cdot[M] \cdot(1 + k3(T)\cdot[M]/k2(T))$, where [M] is the total bath gas (air) concentration in molecules cm^{-3}, and the temperature dependences for k0, k2 and k3 are as indicated on the table. k = k1 + k2 [M]: The rate constant as a function of temperature and pressure is calculated using $k(T,M) = k1(T) + k2(T)\cdot[M]$, where [M] is the total bath gas (air) concentration in molecules cm^{-3}, and the temperature dependences for k1, and k2 are as indicated on the table. Same k as Rxn *label*: The rate constant is the same as the reaction with the indicated label.

[b] Format of reaction listing: "=" separates reactants from products; "*#number*" indicates stoichiometric coefficient, "*#coefficient* { *product list* }" means that the stoichiometric coefficient is applied to all the products listed. See Table A-1 for a listing of the model species used.

[c] Mechanisms the same as used by Carter et al (2000a).

[d] The model species shown are those used in the chamber simulations in this work and by Carter et al (2000a). To be consistent with the approach used by Carter (2000), in the atmospheric reactivity simulations the alkanes and (where applicable) aromatics were lumped according to their OH radical rate constants, with compounds with OH rate constants in the ranges 1.7 - 3.4 x 10^{-12}, 3.4 - 6.8 x 10^{-12}, 0.68 - 1.4 x 10^{-11}, and ≥1.4 x 10^{-11} cm^3 $molec^{-1}$ s^{-1} being represented by separate model species. This gives a different representation of the alkanes and aromatics in mineral spirits sample "A", and gives two rather than a single model species being used to represent the alkanes in mineral spirits samples "C" and "D" and the two Isopar-M representations. The effects of this difference in lumping procedure were found to be insignificant.

[e] See text for derivation of the mechanisms of the lumped species used to represent the reactions of the constituents of these fluids.

Table A-3. Listing of the absorption cross sections and quantum yields for the photolysis reactions.

WL (nm)	Abs (cm^2)	QY	WL (nm)	Abs (cm^2)	QY	WL (nm)	Abs (cm^2)	QY	WL (nm)	Abs (cm^2)	QY	WL (nm)	Abs (cm^2)	QY
							NO2							
205.0	4.31e-19	1.000	210.0	4.72e-19	1.000	215.0	4.95e-19	1.000	220.0	4.56e-19	1.000	225.0	3.79e-19	1.000
230.0	2.74e-19	1.000	235.0	1.67e-19	1.000	240.0	9.31e-20	1.000	245.0	4.74e-20	1.000	250.0	2.48e-20	1.000
255.0	1.95e-20	1.000	260.0	2.24e-20	1.000	265.0	2.73e-20	1.000	270.0	4.11e-20	1.000	275.0	4.90e-20	1.000
280.0	5.92e-20	1.000	285.0	7.39e-20	1.000	290.0	9.00e-20	1.000	295.0	1.09e-19	1.000	300.0	1.31e-19	1.000
305.0	1.57e-19	1.000	310.0	1.86e-19	1.000	315.0	2.15e-19	0.990	320.0	2.48e-19	0.990	325.0	2.81e-19	0.990
330.0	3.13e-19	0.990	335.0	3.43e-19	0.990	340.0	3.80e-19	0.990	345.0	4.07e-19	0.990	350.0	4.31e-19	0.990
355.0	4.72e-19	0.990	360.0	4.83e-19	0.980	365.0	5.17e-19	0.980	370.0	5.32e-19	0.980	375.0	5.51e-19	0.980
380.0	5.64e-19	0.970	385.0	5.76e-19	0.970	390.0	5.93e-19	0.960	395.0	5.85e-19	0.935	400.0	6.02e-19	0.820
405.0	5.78e-19	0.355	410.0	6.00e-19	0.130	411.0	5.93e-19	0.110	412.0	5.86e-19	0.094	413.0	5.79e-19	0.083
414.0	5.72e-19	0.070	415.0	5.65e-19	0.059	416.0	5.68e-19	0.048	417.0	5.71e-19	0.039	418.0	5.75e-19	0.030
419.0	5.78e-19	0.023	420.0	5.81e-19	0.018	421.0	5.72e-19	0.012	422.0	5.64e-19	0.008	423.0	5.55e-19	0.004
424.0	5.47e-19	0.000												
							NO3NO							
585.0	2.89e-18	0.000	586.0	3.32e-18	0.050	587.0	4.16e-18	0.100	588.0	5.04e-18	0.150	589.0	6.13e-18	0.200
590.0	5.96e-18	0.250	591.0	5.44e-18	0.280	592.0	5.11e-18	0.310	593.0	4.58e-18	0.340	594.0	4.19e-18	0.370
595.0	4.29e-18	0.400	596.0	4.62e-18	0.370	597.0	4.36e-18	0.340	598.0	3.67e-18	0.310	599.0	3.10e-18	0.280
600.0	2.76e-18	0.250	601.0	2.86e-18	0.240	602.0	3.32e-18	0.230	603.0	3.80e-18	0.220	604.0	4.37e-18	0.210
605.0	4.36e-18	0.200	606.0	3.32e-18	0.200	607.0	2.40e-18	0.200	608.0	1.85e-18	0.200	609.0	1.71e-18	0.200
610.0	1.77e-18	0.200	611.0	1.91e-18	0.180	612.0	2.23e-18	0.160	613.0	2.63e-18	0.140	614.0	2.55e-18	0.120
615.0	2.26e-18	0.100	616.0	2.09e-18	0.100	617.0	2.11e-18	0.100	618.0	2.39e-18	0.100	619.0	2.56e-18	0.100
620.0	3.27e-18	0.100	621.0	5.24e-18	0.090	622.0	1.02e-17	0.080	623.0	1.47e-17	0.070	624.0	1.21e-17	0.060
625.0	8.38e-18	0.050	626.0	7.30e-18	0.050	627.0	7.53e-18	0.050	628.0	7.37e-18	0.050	629.0	6.98e-18	0.050
630.0	6.76e-18	0.050	631.0	4.84e-18	0.046	632.0	3.27e-18	0.042	633.0	2.17e-18	0.038	634.0	1.64e-18	0.034
635.0	1.44e-18	0.030	636.0	1.69e-18	0.024	637.0	2.07e-18	0.018	638.0	2.03e-18	0.012	639.0	1.58e-18	0.006
640.0	1.23e-18	0.000												
							NO3NO2							
400.0	0.00e+00	1.000	401.0	0.00e+00	1.000	402.0	0.00e+00	1.000	403.0	2.00e-20	1.000	404.0	0.00e+00	1.000
405.0	3.00e-20	1.000	406.0	2.00e-20	1.000	407.0	1.00e-20	1.000	408.0	3.00e-20	1.000	409.0	0.00e+00	1.000
410.0	1.00e-20	1.000	411.0	2.00e-20	1.000	412.0	5.00e-20	1.000	413.0	5.00e-20	1.000	414.0	2.00e-20	1.000
415.0	6.00e-20	1.000	416.0	6.00e-20	1.000	417.0	7.00e-20	1.000	418.0	5.00e-20	1.000	419.0	8.00e-20	1.000
420.0	8.00e-20	1.000	421.0	8.00e-20	1.000	422.0	9.00e-20	1.000	423.0	1.10e-19	1.000	424.0	9.00e-20	1.000
425.0	7.00e-20	1.000	426.0	1.40e-19	1.000	427.0	1.40e-19	1.000	428.0	1.20e-19	1.000	429.0	1.10e-19	1.000
430.0	1.70e-19	1.000	431.0	1.30e-19	1.000	432.0	1.50e-19	1.000	433.0	1.80e-19	1.000	434.0	1.80e-19	1.000
435.0	1.60e-19	1.000	436.0	1.50e-19	1.000	437.0	1.80e-19	1.000	438.0	2.10e-19	1.000	439.0	2.00e-19	1.000
440.0	1.90e-19	1.000	441.0	1.80e-19	1.000	442.0	2.10e-19	1.000	443.0	1.80e-19	1.000	444.0	1.90e-19	1.000
445.0	2.00e-19	1.000	446.0	2.40e-19	1.000	447.0	2.90e-19	1.000	448.0	2.40e-19	1.000	449.0	2.80e-19	1.000
450.0	2.90e-19	1.000	451.0	3.00e-19	1.000	452.0	3.30e-19	1.000	453.0	3.10e-19	1.000	454.0	3.60e-19	1.000
455.0	3.60e-19	1.000	456.0	3.60e-19	1.000	457.0	4.00e-19	1.000	458.0	3.70e-19	1.000	459.0	4.20e-19	1.000
460.0	4.00e-19	1.000	461.0	3.90e-19	1.000	462.0	4.00e-19	1.000	463.0	4.10e-19	1.000	464.0	4.80e-19	1.000
465.0	5.10e-19	1.000	466.0	5.40e-19	1.000	467.0	5.70e-19	1.000	468.0	5.60e-19	1.000	469.0	5.80e-19	1.000
470.0	5.90e-19	1.000	471.0	6.20e-19	1.000	472.0	6.40e-19	1.000	473.0	6.20e-19	1.000	474.0	6.20e-19	1.000
475.0	6.80e-19	1.000	476.0	7.80e-19	1.000	477.0	7.70e-19	1.000	478.0	7.30e-19	1.000	479.0	7.30e-19	1.000
480.0	7.00e-19	1.000	481.0	7.10e-19	1.000	482.0	7.10e-19	1.000	483.0	7.20e-19	1.000	484.0	7.70e-19	1.000
485.0	8.20e-19	1.000	486.0	9.10e-19	1.000	487.0	9.20e-19	1.000	488.0	9.50e-19	1.000	489.0	9.60e-19	1.000
490.0	1.03e-18	1.000	491.0	9.90e-19	1.000	492.0	9.90e-19	1.000	493.0	1.01e-18	1.000	494.0	1.01e-18	1.000
495.0	1.06e-18	1.000	496.0	1.21e-18	1.000	497.0	1.22e-18	1.000	498.0	1.20e-18	1.000	499.0	1.17e-18	1.000
500.0	1.13e-18	1.000	501.0	1.11e-18	1.000	502.0	1.11e-18	1.000	503.0	1.11e-18	1.000	504.0	1.26e-18	1.000
505.0	1.28e-18	1.000	506.0	1.34e-18	1.000	507.0	1.28e-18	1.000	508.0	1.27e-18	1.000	509.0	1.35e-18	1.000
510.0	1.51e-18	1.000	511.0	1.73e-18	1.000	512.0	1.77e-18	1.000	513.0	1.60e-18	1.000	514.0	1.58e-18	1.000
515.0	1.58e-18	1.000	516.0	1.56e-18	1.000	517.0	1.49e-18	1.000	518.0	1.44e-18	1.000	519.0	1.54e-18	1.000
520.0	1.68e-18	1.000	521.0	1.83e-18	1.000	522.0	1.93e-18	1.000	523.0	1.77e-18	1.000	524.0	1.64e-18	1.000
525.0	1.58e-18	1.000	526.0	1.63e-18	1.000	527.0	1.81e-18	1.000	528.0	2.10e-18	1.000	529.0	2.39e-18	1.000
530.0	2.23e-18	1.000	531.0	2.09e-18	1.000	532.0	2.02e-18	1.000	533.0	1.95e-18	1.000	534.0	2.04e-18	1.000
535.0	2.30e-18	1.000	536.0	2.57e-18	1.000	537.0	2.58e-18	1.000	538.0	2.34e-18	1.000	539.0	2.04e-18	1.000
540.0	2.10e-18	1.000	541.0	2.04e-18	1.000	542.0	1.88e-18	1.000	543.0	1.68e-18	1.000	544.0	1.70e-18	1.000
545.0	1.96e-18	1.000	546.0	2.42e-18	1.000	547.0	2.91e-18	1.000	548.0	2.98e-18	1.000	549.0	2.71e-18	1.000
550.0	2.48e-18	1.000	551.0	2.43e-18	1.000	552.0	2.47e-18	1.000	553.0	2.53e-18	1.000	554.0	2.78e-18	1.000
555.0	3.11e-18	1.000	556.0	3.26e-18	1.000	557.0	3.29e-18	1.000	558.0	3.51e-18	1.000	559.0	3.72e-18	1.000
560.0	3.32e-18	1.000	561.0	2.98e-18	1.000	562.0	2.90e-18	1.000	563.0	2.80e-18	1.000	564.0	2.72e-18	1.000
565.0	2.73e-18	1.000	566.0	2.85e-18	1.000	567.0	2.81e-18	1.000	568.0	2.85e-18	1.000	569.0	2.89e-18	1.000
570.0	2.79e-18	1.000	571.0	2.76e-18	1.000	572.0	2.74e-18	1.000	573.0	2.78e-18	1.000	574.0	2.86e-18	1.000
575.0	3.08e-18	1.000	576.0	3.27e-18	1.000	577.0	3.38e-18	1.000	578.0	3.31e-18	1.000	579.0	3.24e-18	1.000
580.0	3.34e-18	1.000	581.0	3.55e-18	1.000	582.0	3.28e-18	1.000	583.0	2.93e-18	1.000	584.0	2.82e-18	1.000
585.0	2.89e-18	1.000	586.0	3.32e-18	0.950	587.0	4.16e-18	0.900	588.0	5.04e-18	0.850	589.0	6.13e-18	0.800
590.0	5.96e-18	0.750	591.0	5.44e-18	0.720	592.0	5.11e-18	0.690	593.0	4.58e-18	0.660	594.0	4.19e-18	0.630
595.0	4.29e-18	0.600	596.0	4.62e-18	0.590	597.0	4.36e-18	0.580	598.0	3.67e-18	0.570	599.0	3.10e-18	0.560
600.0	2.76e-18	0.550	601.0	2.86e-18	0.540	602.0	3.32e-18	0.530	603.0	3.80e-18	0.520	604.0	4.37e-18	0.510
605.0	4.36e-18	0.400	606.0	3.32e-18	0.380	607.0	2.40e-18	0.360	608.0	1.85e-18	0.340	609.0	1.71e-18	0.320

Table A-3 (continued)

WL (nm)	Abs (cm^2)	QY	WL (nm)	Abs (cm^2)	QY	WL (nm)	Abs (cm^2)	QY	WL (nm)	Abs (cm^2)	QY	WL (nm)	Abs (cm^2)	QY
610.0	1.77e-18	0.300	611.0	1.91e-18	0.290	612.0	2.23e-18	0.280	613.0	2.63e-18	0.270	614.0	2.55e-18	0.260
615.0	2.26e-18	0.250	616.0	2.09e-18	0.240	617.0	2.11e-18	0.230	618.0	2.39e-18	0.220	619.0	2.56e-18	0.210
620.0	3.27e-18	0.200	621.0	5.24e-18	0.190	622.0	1.02e-17	0.180	623.0	1.47e-17	0.170	624.0	1.21e-17	0.160
625.0	8.38e-18	0.150	626.0	7.30e-18	0.130	627.0	7.53e-18	0.110	628.0	7.37e-18	0.090	629.0	6.98e-18	0.070
630.0	6.76e-18	0.050	631.0	4.84e-18	0.040	632.0	3.27e-18	0.030	633.0	2.17e-18	0.020	634.0	1.64e-18	0.010
635.0	1.44e-18	0.000												
							O3O3P							
280.0	3.94e-18	0.095	281.0	3.62e-18	0.093	282.0	3.31e-18	0.090	283.0	2.99e-18	0.088	284.0	2.70e-18	0.086
285.0	2.46e-18	0.084	286.0	2.22e-18	0.082	287.0	1.98e-18	0.079	288.0	1.75e-18	0.077	289.0	1.59e-18	0.075
290.0	1.42e-18	0.073	291.0	1.25e-18	0.070	292.0	1.09e-18	0.068	293.0	9.81e-19	0.066	294.0	8.73e-19	0.064
295.0	7.65e-19	0.061	296.0	6.58e-19	0.059	297.0	5.81e-19	0.057	298.0	5.18e-19	0.055	299.0	4.55e-19	0.052
300.0	3.92e-19	0.050	301.0	3.35e-19	0.035	302.0	3.01e-19	0.025	303.0	2.66e-19	0.015	304.0	2.32e-19	0.010
305.0	1.97e-19	0.020	306.0	1.73e-19	0.050	307.0	1.55e-19	0.123	308.0	1.37e-19	0.227	309.0	1.18e-19	0.333
310.0	9.98e-20	0.400	311.0	8.92e-20	0.612	312.0	7.94e-20	0.697	313.0	6.96e-20	0.738	314.0	5.99e-20	0.762
315.0	5.01e-20	0.765	316.0	4.51e-20	0.779	317.0	4.00e-20	0.791	318.0	3.50e-20	0.806	319.0	2.99e-20	0.822
320.0	2.49e-20	0.852	321.0	2.23e-20	0.879	322.0	1.97e-20	0.903	323.0	1.72e-20	0.908	324.0	1.46e-20	0.920
325.0	1.20e-20	0.930	326.0	1.08e-20	0.934	327.0	9.67e-21	0.938	328.0	8.50e-21	0.942	329.0	7.34e-21	0.946
330.0	6.17e-21	0.950	331.0	5.48e-21	0.950	332.0	4.80e-21	0.950	333.0	4.11e-21	0.950	334.0	3.43e-21	0.950
335.0	2.74e-21	0.950	336.0	2.43e-21	0.960	337.0	2.11e-21	0.970	338.0	1.80e-21	0.980	339.0	1.48e-21	0.990
340.0	1.17e-21	1.000	350.0	0.00e+00	1.000	400.0	0.00e+00	1.000	410.0	1.20e-23	1.000	420.0	2.20e-23	1.000
440.0	1.12e-22	1.000	460.0	3.28e-22	1.000	480.0	6.84e-22	1.000	500.0	1.22e-21	1.000	520.0	1.82e-21	1.000
540.0	2.91e-21	1.000	560.0	3.94e-21	1.000	580.0	4.59e-21	1.000	600.0	5.11e-21	1.000	620.0	4.00e-21	1.000
640.0	2.96e-21	1.000	660.0	2.09e-21	1.000	680.0	1.36e-21	1.000	700.0	9.10e-22	1.000	750.0	3.20e-22	1.000
800.0	1.60e-22	1.000	900.0	0.00e+00	1.000									
							O3O1D							
280.0	3.94e-18	0.905	281.0	3.62e-18	0.907	282.0	3.31e-18	0.910	283.0	2.99e-18	0.912	284.0	2.70e-18	0.914
285.0	2.46e-18	0.916	286.0	2.22e-18	0.918	287.0	1.98e-18	0.921	288.0	1.75e-18	0.923	289.0	1.59e-18	0.925
290.0	1.42e-18	0.927	291.0	1.25e-18	0.930	292.0	1.09e-18	0.932	293.0	9.81e-19	0.934	294.0	8.73e-19	0.936
295.0	7.65e-19	0.939	296.0	6.58e-19	0.941	297.0	5.81e-19	0.943	298.0	5.18e-19	0.945	299.0	4.55e-19	0.948
300.0	3.92e-19	0.950	301.0	3.35e-19	0.965	302.0	3.01e-19	0.975	303.0	2.66e-19	0.985	304.0	2.32e-19	0.990
305.0	1.97e-19	0.980	306.0	1.73e-19	0.950	307.0	1.55e-19	0.877	308.0	1.37e-19	0.773	309.0	1.18e-19	0.667
310.0	9.98e-20	0.600	311.0	8.92e-20	0.388	312.0	7.94e-20	0.303	313.0	6.96e-20	0.262	314.0	5.99e-20	0.238
315.0	5.01e-20	0.235	316.0	4.51e-20	0.221	317.0	4.00e-20	0.209	318.0	3.50e-20	0.194	319.0	2.99e-20	0.178
320.0	2.49e-20	0.148	321.0	2.23e-20	0.121	322.0	1.97e-20	0.097	323.0	1.72e-20	0.092	324.0	1.46e-20	0.080
325.0	1.20e-20	0.070	326.0	1.08e-20	0.066	327.0	9.67e-21	0.062	328.0	8.50e-21	0.058	329.0	7.34e-21	0.054
330.0	6.17e-21	0.050	331.0	5.48e-21	0.050	332.0	4.80e-21	0.050	333.0	4.11e-21	0.050	334.0	3.43e-21	0.050
335.0	2.74e-21	0.050	336.0	2.43e-21	0.040	337.0	2.11e-21	0.030	338.0	1.80e-21	0.020	339.0	1.48e-21	0.010
340.0	1.17e-21	0.000												
							HONO-NO							
309.0	0.00e+00	0.410	310.0	1.30e-20	0.410	311.0	1.90e-20	0.411	312.0	2.80e-20	0.421	313.0	2.20e-20	0.432
314.0	3.60e-20	0.443	315.0	3.00e-20	0.454	316.0	1.40e-20	0.464	317.0	3.10e-20	0.475	318.0	5.60e-20	0.486
319.0	3.60e-20	0.496	320.0	4.90e-20	0.507	321.0	7.80e-20	0.518	322.0	4.90e-20	0.529	323.0	5.10e-20	0.539
324.0	7.10e-20	0.550	325.0	5.00e-20	0.561	326.0	2.90e-20	0.571	327.0	6.60e-20	0.582	328.0	1.17e-19	0.593
329.0	6.10e-20	0.604	330.0	1.11e-19	0.614	331.0	1.79e-19	0.625	332.0	8.70e-20	0.636	333.0	7.60e-20	0.646
334.0	9.60e-20	0.657	335.0	9.60e-20	0.668	336.0	7.20e-20	0.679	337.0	5.30e-20	0.689	338.0	1.00e-19	0.700
339.0	1.88e-19	0.711	340.0	1.00e-19	0.721	341.0	1.70e-19	0.732	342.0	3.86e-19	0.743	343.0	1.49e-19	0.754
344.0	9.70e-20	0.764	345.0	1.09e-19	0.775	346.0	1.23e-19	0.786	347.0	1.04e-19	0.796	348.0	9.10e-20	0.807
349.0	7.90e-20	0.818	350.0	1.12e-19	0.829	351.0	2.12e-19	0.839	352.0	1.55e-19	0.850	353.0	1.91e-19	0.861
354.0	5.81e-19	0.871	355.0	3.64e-19	0.882	356.0	1.41e-19	0.893	357.0	1.17e-19	0.904	358.0	1.20e-19	0.914
359.0	1.04e-19	0.925	360.0	9.00e-20	0.936	361.0	8.30e-20	0.946	362.0	8.00e-20	0.957	363.0	9.60e-20	0.968
364.0	1.46e-19	0.979	365.0	1.68e-19	0.989	366.0	1.83e-19	1.000	367.0	3.02e-19	1.000	368.0	5.20e-19	1.000
369.0	3.88e-19	1.000	370.0	1.78e-19	1.000	371.0	1.13e-19	1.000	372.0	1.00e-19	1.000	373.0	7.70e-20	1.000
374.0	6.20e-20	1.000	375.0	5.30e-20	1.000	376.0	5.30e-20	1.000	377.0	5.00e-20	1.000	378.0	5.80e-20	1.000
379.0	8.00e-20	1.000	380.0	9.60e-20	1.000	381.0	1.13e-19	1.000	382.0	1.59e-19	1.000	383.0	2.10e-19	1.000
384.0	2.41e-19	1.000	385.0	2.03e-19	1.000	386.0	1.34e-19	1.000	387.0	9.00e-20	1.000	388.0	5.60e-20	1.000
389.0	3.40e-20	1.000	390.0	2.70e-20	1.000	391.0	2.00e-20	1.000	392.0	1.50e-20	1.000	393.0	1.10e-20	1.000
394.0	6.00e-21	1.000	395.0	1.00e-20	1.000	396.0	4.00e-21	1.000	400.0	0.00e+00	1.000			
							HONO-NO2							
309.0	0.00e+00	0.590	310.0	1.30e-20	0.590	311.0	1.90e-20	0.589	312.0	2.80e-20	0.579	313.0	2.20e-20	0.568
314.0	3.60e-20	0.557	315.0	3.00e-20	0.546	316.0	1.40e-20	0.536	317.0	3.10e-20	0.525	318.0	5.60e-20	0.514
319.0	3.60e-20	0.504	320.0	4.90e-20	0.493	321.0	7.80e-20	0.482	322.0	4.90e-20	0.471	323.0	5.10e-20	0.461
324.0	7.10e-20	0.450	325.0	5.00e-20	0.439	326.0	2.90e-20	0.429	327.0	6.60e-20	0.418	328.0	1.17e-19	0.407
329.0	6.10e-20	0.396	330.0	1.11e-19	0.386	331.0	1.79e-19	0.375	332.0	8.70e-20	0.364	333.0	7.60e-20	0.354
334.0	9.60e-20	0.343	335.0	9.60e-20	0.332	336.0	7.20e-20	0.321	337.0	5.30e-20	0.311	338.0	1.00e-19	0.300
339.0	1.88e-19	0.289	340.0	1.00e-19	0.279	341.0	1.70e-19	0.268	342.0	3.86e-19	0.257	343.0	1.49e-19	0.246
344.0	9.70e-20	0.236	345.0	1.09e-19	0.225	346.0	1.23e-19	0.214	347.0	1.04e-19	0.204	348.0	9.10e-20	0.193
349.0	7.90e-20	0.182	350.0	1.12e-19	0.171	351.0	2.12e-19	0.161	352.0	1.55e-19	0.150	353.0	1.91e-19	0.139
354.0	5.81e-19	0.129	355.0	3.64e-19	0.118	356.0	1.41e-19	0.107	357.0	1.17e-19	0.096	358.0	1.20e-19	0.086
359.0	1.04e-19	0.075	360.0	9.00e-20	0.064	361.0	8.30e-20	0.054	362.0	8.00e-20	0.043	363.0	9.60e-20	0.032

Table A-3 (continued)

WL (nm)	Abs (cm^2)	QY	WL (nm)	Abs (cm^2)	QY	WL (nm)	Abs (cm^2)	QY	WL (nm)	Abs (cm^2)	QY	WL (nm)	Abs (cm^2)	QY
364.0	1.46e-19	0.021	365.0	1.68e-19	0.011	366.0	1.83e-19	0.000						
							HNO3							
190.0	1.36e-17	1.000	195.0	1.02e-17	1.000	200.0	5.88e-18	1.000	205.0	2.80e-18	1.000	210.0	1.04e-18	1.000
215.0	3.65e-19	1.000	220.0	1.49e-19	1.000	225.0	8.81e-20	1.000	230.0	5.75e-20	1.000	235.0	3.75e-20	1.000
240.0	2.58e-20	1.000	245.0	2.11e-20	1.000	250.0	1.97e-20	1.000	255.0	1.95e-20	1.000	260.0	1.91e-20	1.000
265.0	1.80e-20	1.000	270.0	1.62e-20	1.000	275.0	1.38e-20	1.000	280.0	1.12e-20	1.000	285.0	8.58e-21	1.000
290.0	6.15e-21	1.000	295.0	4.12e-21	1.000	300.0	2.63e-21	1.000	305.0	1.50e-21	1.000	310.0	8.10e-22	1.000
315.0	4.10e-22	1.000	320.0	2.00e-22	1.000	325.0	9.50e-23	1.000	330.0	4.30e-23	1.000	335.0	2.20e-23	1.000
340.0	1.00e-23	1.000	345.0	6.00e-24	1.000	350.0	4.00e-24	1.000	355.0	0.00e+00	1.000			
							HO2NO2							
190.0	1.01e-17	1.000	195.0	8.16e-18	1.000	200.0	5.63e-18	1.000	205.0	3.67e-18	1.000	210.0	2.39e-18	1.000
215.0	1.61e-18	1.000	220.0	1.18e-18	1.000	225.0	9.32e-19	1.000	230.0	7.88e-19	1.000	235.0	6.80e-19	1.000
240.0	5.79e-19	1.000	245.0	4.97e-19	1.000	250.0	4.11e-19	1.000	255.0	3.49e-19	1.000	260.0	2.84e-19	1.000
265.0	2.29e-19	1.000	270.0	1.80e-19	1.000	275.0	1.33e-19	1.000	280.0	9.30e-20	1.000	285.0	6.20e-20	1.000
290.0	3.90e-20	1.000	295.0	2.40e-20	1.000	300.0	1.40e-20	1.000	305.0	8.50e-21	1.000	310.0	5.30e-21	1.000
315.0	3.90e-21	1.000	320.0	2.40e-21	1.000	325.0	1.50e-21	1.000	330.0	9.00e-22	1.000	335.0	0.00e+00	1.000
							H2O2							
190.0	6.72e-19	1.000	195.0	5.63e-19	1.000	200.0	4.75e-19	1.000	205.0	4.08e-19	1.000	210.0	3.57e-19	1.000
215.0	3.07e-19	1.000	220.0	2.58e-19	1.000	225.0	2.17e-19	1.000	230.0	1.82e-19	1.000	235.0	1.50e-19	1.000
240.0	1.24e-19	1.000	245.0	1.02e-19	1.000	250.0	8.30e-20	1.000	255.0	6.70e-20	1.000	260.0	5.30e-20	1.000
265.0	4.20e-20	1.000	270.0	3.30e-20	1.000	275.0	2.60e-20	1.000	280.0	2.00e-20	1.000	285.0	1.50e-20	1.000
290.0	1.20e-20	1.000	295.0	9.00e-21	1.000	300.0	6.80e-21	1.000	305.0	5.10e-21	1.000	310.0	3.90e-21	1.000
315.0	2.90e-21	1.000	320.0	2.20e-21	1.000	325.0	1.60e-21	1.000	330.0	1.30e-21	1.000	335.0	1.00e-21	1.000
340.0	7.00e-22	1.000	345.0	5.00e-22	1.000	350.0	4.00e-22	1.000	355.0	0.00e+00	1.000			
							HCHO_R							
240.0	6.40e-22	0.270	241.0	5.60e-22	0.272	242.0	1.05e-21	0.274	243.0	1.15e-21	0.276	244.0	8.20e-22	0.278
245.0	1.03e-21	0.280	246.0	9.80e-22	0.282	247.0	1.35e-21	0.284	248.0	1.91e-21	0.286	249.0	2.82e-21	0.288
250.0	2.05e-21	0.290	251.0	1.70e-21	0.291	252.0	2.88e-21	0.292	253.0	2.55e-21	0.293	254.0	2.55e-21	0.294
255.0	3.60e-21	0.295	256.0	5.09e-21	0.296	257.0	3.39e-21	0.297	258.0	2.26e-21	0.298	259.0	5.04e-21	0.299
260.0	5.05e-21	0.300	261.0	5.49e-21	0.308	262.0	5.20e-21	0.316	263.0	9.33e-21	0.324	264.0	8.23e-21	0.332
265.0	4.30e-21	0.340	266.0	4.95e-21	0.348	267.0	1.24e-20	0.356	268.0	1.11e-20	0.364	269.0	8.78e-21	0.372
270.0	9.36e-21	0.380	271.0	1.79e-20	0.399	272.0	1.23e-20	0.418	273.0	6.45e-21	0.437	274.0	6.56e-21	0.456
275.0	2.23e-20	0.475	276.0	2.42e-20	0.494	277.0	1.40e-20	0.513	278.0	1.05e-20	0.532	279.0	2.55e-20	0.551
280.0	2.08e-20	0.570	281.0	1.48e-20	0.586	282.0	8.81e-21	0.602	283.0	1.07e-20	0.618	284.0	4.49e-20	0.634
285.0	3.59e-20	0.650	286.0	1.96e-20	0.666	287.0	1.30e-20	0.682	288.0	3.36e-20	0.698	289.0	2.84e-20	0.714
290.0	1.30e-20	0.730	291.0	1.75e-20	0.735	292.0	8.32e-21	0.740	293.0	3.73e-20	0.745	294.0	6.54e-20	0.750
295.0	3.95e-20	0.755	296.0	2.33e-20	0.760	297.0	1.51e-20	0.765	298.0	4.04e-20	0.770	299.0	2.87e-20	0.775
300.0	8.71e-21	0.780	301.0	1.72e-20	0.780	302.0	1.06e-20	0.780	303.0	3.20e-20	0.780	304.0	6.90e-20	0.780
305.0	4.91e-20	0.780	306.0	4.63e-20	0.780	307.0	2.10e-20	0.780	308.0	1.49e-20	0.780	309.0	3.41e-20	0.780
310.0	1.95e-20	0.780	311.0	5.21e-21	0.764	312.0	1.12e-20	0.748	313.0	1.12e-20	0.732	314.0	4.75e-20	0.716
315.0	5.25e-20	0.700	316.0	2.90e-20	0.684	317.0	5.37e-20	0.668	318.0	2.98e-20	0.652	319.0	9.18e-21	0.636
320.0	1.26e-20	0.620	321.0	1.53e-20	0.585	322.0	6.69e-21	0.550	323.0	3.45e-21	0.515	324.0	8.16e-21	0.480
325.0	1.85e-20	0.445	326.0	5.95e-20	0.410	327.0	3.49e-20	0.375	328.0	1.09e-20	0.340	329.0	3.35e-20	0.305
330.0	3.32e-20	0.270	331.0	1.07e-20	0.243	332.0	2.89e-21	0.216	333.0	2.15e-21	0.189	334.0	1.71e-21	0.162
335.0	1.43e-21	0.135	336.0	1.94e-21	0.108	337.0	4.17e-21	0.081	338.0	2.36e-20	0.054	339.0	4.71e-20	0.027
340.0	2.48e-20	0.000												
							HCHO_M							
240.0	6.40e-22	0.490	241.0	5.60e-22	0.490	242.0	1.05e-21	0.490	243.0	1.15e-21	0.490	244.0	8.20e-22	0.490
245.0	1.03e-21	0.490	246.0	9.80e-22	0.490	247.0	1.35e-21	0.490	248.0	1.91e-21	0.490	249.0	2.82e-21	0.490
250.0	2.05e-21	0.490	251.0	1.70e-21	0.490	252.0	2.88e-21	0.490	253.0	2.55e-21	0.490	254.0	2.55e-21	0.490
255.0	3.60e-21	0.490	256.0	5.09e-21	0.490	257.0	3.39e-21	0.490	258.0	2.26e-21	0.490	259.0	5.04e-21	0.490
260.0	5.05e-21	0.490	261.0	5.49e-21	0.484	262.0	5.20e-21	0.478	263.0	9.33e-21	0.472	264.0	8.23e-21	0.466
265.0	4.30e-21	0.460	266.0	4.95e-21	0.454	267.0	1.24e-20	0.448	268.0	1.11e-20	0.442	269.0	8.78e-21	0.436
270.0	9.36e-21	0.430	271.0	1.79e-20	0.419	272.0	1.23e-20	0.408	273.0	6.45e-21	0.397	274.0	6.56e-21	0.386
275.0	2.23e-20	0.375	276.0	2.42e-20	0.364	277.0	1.40e-20	0.353	278.0	1.05e-20	0.342	279.0	2.55e-20	0.331
280.0	2.08e-20	0.320	281.0	1.48e-20	0.312	282.0	8.81e-21	0.304	283.0	1.07e-20	0.296	284.0	4.49e-20	0.288
285.0	3.59e-20	0.280	286.0	1.96e-20	0.272	287.0	1.30e-20	0.264	288.0	3.36e-20	0.256	289.0	2.84e-20	0.248
290.0	1.30e-20	0.240	291.0	1.75e-20	0.237	292.0	8.32e-21	0.234	293.0	3.73e-20	0.231	294.0	6.54e-20	0.228
295.0	3.95e-20	0.225	296.0	2.33e-20	0.222	297.0	1.51e-20	0.219	298.0	4.04e-20	0.216	299.0	2.87e-20	0.213
300.0	8.71e-21	0.210	301.0	1.72e-20	0.211	302.0	1.06e-20	0.212	303.0	3.20e-20	0.213	304.0	6.90e-20	0.214
305.0	4.91e-20	0.215	306.0	4.63e-20	0.216	307.0	2.10e-20	0.217	308.0	1.49e-20	0.218	309.0	3.41e-20	0.219
310.0	1.95e-20	0.220	311.0	5.21e-21	0.236	312.0	1.12e-20	0.252	313.0	1.12e-20	0.268	314.0	4.75e-20	0.284
315.0	5.25e-20	0.300	316.0	2.90e-20	0.316	317.0	5.37e-20	0.332	318.0	2.98e-20	0.348	319.0	9.18e-21	0.364
320.0	1.26e-20	0.380	321.0	1.53e-20	0.408	322.0	6.69e-21	0.436	323.0	3.45e-21	0.464	324.0	8.16e-21	0.492
325.0	1.85e-20	0.520	326.0	5.95e-20	0.548	327.0	3.49e-20	0.576	328.0	1.09e-20	0.604	329.0	3.35e-20	0.632
330.0	3.32e-20	0.660	331.0	1.07e-20	0.650	332.0	2.89e-21	0.640	333.0	2.15e-21	0.630	334.0	1.71e-21	0.620
335.0	1.43e-21	0.610	336.0	1.94e-21	0.600	337.0	4.17e-21	0.590	338.0	2.36e-20	0.580	339.0	4.71e-20	0.570
340.0	2.48e-20	0.560	341.0	7.59e-21	0.525	342.0	6.81e-21	0.490	343.0	1.95e-20	0.455	344.0	1.14e-20	0.420
345.0	3.23e-21	0.385	346.0	1.13e-21	0.350	347.0	6.60e-22	0.315	348.0	1.22e-21	0.280	349.0	3.20e-22	0.245

Table A-3 (continued)

WL (nm)	Abs (cm^2)	QY	WL (nm)	Abs (cm^2)	QY	WL (nm)	Abs (cm^2)	QY	WL (nm)	Abs (cm^2)	QY	WL (nm)	Abs (cm^2)	QY
350.0	3.80e-22	0.210	351.0	1.04e-21	0.192	352.0	7.13e-21	0.174	353.0	2.21e-20	0.156	354.0	1.54e-20	0.138
355.0	6.76e-21	0.120	356.0	1.35e-21	0.102	357.0	3.60e-22	0.084	358.0	5.70e-23	0.066	359.0	5.80e-22	0.048
360.0	8.20e-22	0.000												
							CCHO_R							
262.0	2.44e-20	0.326	266.0	3.05e-20	0.358	270.0	3.42e-20	0.390	274.0	4.03e-20	0.466	278.0	4.19e-20	0.542
280.0	4.50e-20	0.580	281.0	4.69e-20	0.575	282.0	4.72e-20	0.570	283.0	4.75e-20	0.565	284.0	4.61e-20	0.560
285.0	4.49e-20	0.555	286.0	4.44e-20	0.550	287.0	4.59e-20	0.545	288.0	4.72e-20	0.540	289.0	4.77e-20	0.535
290.0	4.89e-20	0.530	291.0	4.78e-20	0.520	292.0	4.68e-20	0.510	293.0	4.53e-20	0.500	294.0	4.33e-20	0.490
295.0	4.27e-20	0.480	296.0	4.24e-20	0.470	297.0	4.38e-20	0.460	298.0	4.41e-20	0.450	299.0	4.26e-20	0.440
300.0	4.16e-20	0.430	301.0	3.99e-20	0.418	302.0	3.86e-20	0.406	303.0	3.72e-20	0.394	304.0	3.48e-20	0.382
305.0	3.42e-20	0.370	306.0	3.42e-20	0.354	307.0	3.36e-20	0.338	308.0	3.33e-20	0.322	309.0	3.14e-20	0.306
310.0	2.93e-20	0.290	311.0	2.76e-20	0.266	312.0	2.53e-20	0.242	313.0	2.47e-20	0.218	314.0	2.44e-20	0.194
315.0	2.20e-20	0.170	316.0	2.04e-20	0.156	317.0	2.07e-20	0.142	318.0	1.98e-20	0.128	319.0	1.87e-20	0.114
320.0	1.72e-20	0.100	321.0	1.48e-20	0.088	322.0	1.40e-20	0.076	323.0	1.24e-20	0.064	324.0	1.09e-20	0.052
325.0	1.14e-20	0.040	326.0	1.07e-20	0.032	327.0	8.58e-21	0.024	328.0	7.47e-21	0.016	329.0	7.07e-21	0.008
							C2CHO							
294.0	5.80e-20	0.890	295.0	5.57e-20	0.885	296.0	5.37e-20	0.880	297.0	5.16e-20	0.875	298.0	5.02e-20	0.870
299.0	5.02e-20	0.865	300.0	5.04e-20	0.860	301.0	5.09e-20	0.855	302.0	5.07e-20	0.850	303.0	4.94e-20	0.818
304.0	4.69e-20	0.786	305.0	4.32e-20	0.755	306.0	4.04e-20	0.723	307.0	3.81e-20	0.691	308.0	3.65e-20	0.659
309.0	3.62e-20	0.627	310.0	3.60e-20	0.596	311.0	3.53e-20	0.564	312.0	3.50e-20	0.532	313.0	3.32e-20	0.500
314.0	3.06e-20	0.480	315.0	2.77e-20	0.460	316.0	2.43e-20	0.440	317.0	2.18e-20	0.420	318.0	2.00e-20	0.400
319.0	1.86e-20	0.380	320.0	1.83e-20	0.360	321.0	1.78e-20	0.340	322.0	1.66e-20	0.320	323.0	1.58e-20	0.300
324.0	1.49e-20	0.280	325.0	1.30e-20	0.260	326.0	1.13e-20	0.248	327.0	9.96e-21	0.236	328.0	8.28e-21	0.223
329.0	6.85e-21	0.211	330.0	5.75e-21	0.199	331.0	4.94e-21	0.187	332.0	4.66e-21	0.174	333.0	4.30e-21	0.162
334.0	3.73e-21	0.150	335.0	3.25e-21	0.133	336.0	2.80e-21	0.117	337.0	2.30e-21	0.100	338.0	1.85e-21	0.083
339.0	1.66e-21	0.067	340.0	1.55e-21	0.050	341.0	1.19e-21	0.033	342.0	7.60e-22	0.017	343.0	4.50e-22	0.000
							ACETONE							
250.0	2.47e-20	0.760	254.0	3.04e-20	0.776	258.0	3.61e-20	0.792	262.0	4.15e-20	0.768	266.0	4.58e-20	0.704
270.0	4.91e-20	0.640	274.0	5.06e-20	0.604	278.0	5.07e-20	0.568	280.0	5.05e-20	0.550	281.0	5.01e-20	0.525
282.0	4.94e-20	0.500	283.0	4.86e-20	0.475	284.0	4.76e-20	0.450	285.0	4.68e-20	0.425	286.0	4.58e-20	0.400
287.0	4.50e-20	0.375	288.0	4.41e-20	0.350	289.0	4.29e-20	0.325	290.0	4.19e-20	0.302	291.0	4.08e-20	0.284
292.0	3.94e-20	0.266	293.0	3.81e-20	0.249	294.0	3.67e-20	0.232	295.0	3.52e-20	0.217	296.0	3.35e-20	0.201
297.0	3.20e-20	0.187	298.0	3.07e-20	0.173	299.0	2.91e-20	0.160	300.0	2.77e-20	0.147	301.0	2.66e-20	0.135
302.0	2.53e-20	0.124	303.0	2.37e-20	0.114	304.0	2.24e-20	0.104	305.0	2.11e-20	0.095	306.0	1.95e-20	0.086
307.0	1.80e-20	0.078	308.0	1.66e-20	0.071	309.0	1.54e-20	0.064	310.0	1.41e-20	0.057	311.0	1.28e-20	0.052
312.0	1.17e-20	0.046	313.0	1.08e-20	0.042	314.0	9.67e-21	0.037	315.0	8.58e-21	0.033	316.0	7.77e-21	0.029
317.0	6.99e-21	0.026	318.0	6.08e-21	0.023	319.0	5.30e-21	0.020	320.0	4.67e-21	0.018	321.0	4.07e-21	0.016
322.0	3.44e-21	0.014	323.0	2.87e-21	0.012	324.0	2.43e-21	0.011	325.0	2.05e-21	0.009	326.0	1.68e-21	0.008
327.0	1.35e-21	0.007	328.0	1.08e-21	0.006	329.0	8.60e-22	0.005	330.0	6.70e-22	0.005	331.0	5.10e-22	0.004
332.0	4.00e-22	0.003	333.0	3.10e-22	0.003	334.0	2.60e-22	0.002	335.0	1.70e-22	0.002	336.0	1.40e-22	0.002
337.0	1.10e-22	0.002	338.0	9.00e-23	0.001	339.0	6.00e-23	0.001	340.0	5.00e-23	0.001	341.0	5.00e-23	0.001
342.0	3.00e-23	0.001	343.0	4.00e-23	0.001	344.0	2.00e-23	0.000						
							KETONE							
198.5	3.95e-19	1.000	199.0	1.61e-19	1.000	199.5	7.75e-20	1.000	200.0	3.76e-20	1.000	200.5	2.51e-20	1.000
201.0	1.83e-20	1.000	201.5	1.36e-20	1.000	202.0	1.16e-20	1.000	202.5	8.97e-21	1.000	203.0	4.62e-21	1.000
203.5	3.18e-21	1.000	204.0	2.42e-21	1.000	204.5	2.01e-21	1.000	205.0	1.77e-21	1.000	205.5	1.64e-21	1.000
206.0	1.54e-21	1.000	206.5	1.52e-21	1.000	207.0	1.54e-21	1.000	207.5	1.62e-21	1.000	208.0	1.64e-21	1.000
208.5	1.60e-21	1.000	209.0	1.57e-21	1.000	209.5	1.49e-21	1.000	210.0	1.47e-21	1.000	210.5	1.52e-21	1.000
211.0	1.50e-21	1.000	211.5	1.62e-21	1.000	212.0	1.81e-21	1.000	212.5	2.10e-21	1.000	213.0	2.23e-21	1.000
213.5	2.06e-21	1.000	214.0	1.69e-21	1.000	214.5	1.49e-21	1.000	215.0	1.42e-21	1.000	215.5	1.42e-21	1.000
216.0	1.42e-21	1.000	216.5	1.48e-21	1.000	217.0	1.48e-21	1.000	217.5	1.53e-21	1.000	218.0	1.56e-21	1.000
218.5	1.67e-21	1.000	219.0	1.68e-21	1.000	219.5	1.78e-21	1.000	220.0	1.85e-21	1.000	220.5	1.92e-21	1.000
221.0	2.01e-21	1.000	221.5	2.11e-21	1.000	222.0	2.23e-21	1.000	222.5	2.33e-21	1.000	223.0	2.48e-21	1.000
223.5	2.60e-21	1.000	224.0	2.74e-21	1.000	224.5	2.85e-21	1.000	225.0	3.04e-21	1.000	225.5	3.15e-21	1.000
226.0	3.33e-21	1.000	226.5	3.55e-21	1.000	227.0	3.73e-21	1.000	227.5	3.93e-21	1.000	228.0	4.11e-21	1.000
228.5	4.34e-21	1.000	229.0	4.56e-21	1.000	229.5	4.75e-21	1.000	230.0	5.01e-21	1.000	230.5	5.27e-21	1.000
231.0	5.53e-21	1.000	231.5	5.83e-21	1.000	232.0	6.15e-21	1.000	232.5	6.45e-21	1.000	233.0	6.73e-21	1.000
233.5	7.02e-21	1.000	234.0	7.42e-21	1.000	234.5	7.83e-21	1.000	235.0	8.11e-21	1.000	235.5	8.45e-21	1.000
236.0	8.82e-21	1.000	236.5	9.21e-21	1.000	237.0	9.65e-21	1.000	237.5	1.00e-20	1.000	238.0	1.05e-20	1.000
238.5	1.10e-20	1.000	239.0	1.15e-20	1.000	239.5	1.20e-20	1.000	240.0	1.23e-20	1.000	240.5	1.28e-20	1.000
241.0	1.32e-20	1.000	241.5	1.38e-20	1.000	242.0	1.44e-20	1.000	242.5	1.50e-20	1.000	243.0	1.57e-20	1.000
243.5	1.63e-20	1.000	244.0	1.68e-20	1.000	244.5	1.75e-20	1.000	245.0	1.81e-20	1.000	245.5	1.88e-20	1.000
246.0	1.96e-20	1.000	246.5	2.03e-20	1.000	247.0	2.11e-20	1.000	247.5	2.19e-20	1.000	248.0	2.25e-20	1.000
248.5	2.33e-20	1.000	249.0	2.40e-20	1.000	249.5	2.48e-20	1.000	250.0	2.56e-20	1.000	250.5	2.64e-20	1.000
251.0	2.73e-20	1.000	251.5	2.81e-20	1.000	252.0	2.88e-20	1.000	252.5	2.98e-20	1.000	253.0	3.07e-20	1.000
253.5	3.16e-20	1.000	254.0	3.25e-20	1.000	254.5	3.34e-20	1.000	255.0	3.43e-20	1.000	255.5	3.51e-20	1.000
256.0	3.59e-20	1.000	256.5	3.67e-20	1.000	257.0	3.75e-20	1.000	257.5	3.84e-20	1.000	258.0	3.94e-20	1.000
258.5	4.03e-20	1.000	259.0	4.13e-20	1.000	259.5	4.22e-20	1.000	260.0	4.28e-20	1.000	260.5	4.33e-20	1.000
261.0	4.41e-20	1.000	261.5	4.49e-20	1.000	262.0	4.57e-20	1.000	262.5	4.65e-20	1.000	263.0	4.72e-20	1.000
263.5	4.78e-20	1.000	264.0	4.85e-20	1.000	264.5	4.92e-20	1.000	265.0	4.99e-20	1.000	265.5	5.04e-20	1.000
266.0	5.12e-20	1.000	266.5	5.22e-20	1.000	267.0	5.28e-20	1.000	267.5	5.34e-20	1.000	268.0	5.41e-20	1.000

Table A-3 (continued)

WL (nm)	Abs (cm^2)	QY	WL (nm)	Abs (cm^2)	QY	WL (nm)	Abs (cm^2)	QY	WL (nm)	Abs (cm^2)	QY	WL (nm)	Abs (cm^2)	QY
268.5	5.46e-20	1.000	269.0	5.51e-20	1.000	269.5	5.55e-20	1.000	270.0	5.59e-20	1.000	270.5	5.63e-20	1.000
271.0	5.66e-20	1.000	271.5	5.70e-20	1.000	272.0	5.74e-20	1.000	272.5	5.78e-20	1.000	273.0	5.81e-20	1.000
273.5	5.86e-20	1.000	274.0	5.90e-20	1.000	274.5	5.93e-20	1.000	275.0	5.96e-20	1.000	275.5	5.97e-20	1.000
276.0	5.98e-20	1.000	276.5	5.98e-20	1.000	277.0	5.99e-20	1.000	277.5	5.99e-20	1.000	278.0	5.98e-20	1.000
278.5	5.96e-20	1.000	279.0	5.96e-20	1.000	279.5	5.95e-20	1.000	280.0	5.94e-20	1.000	280.5	5.92e-20	1.000
281.0	5.90e-20	1.000	281.5	5.88e-20	1.000	282.0	5.86e-20	1.000	282.5	5.83e-20	1.000	283.0	5.79e-20	1.000
283.5	5.75e-20	1.000	284.0	5.71e-20	1.000	284.5	5.67e-20	1.000	285.0	5.61e-20	1.000	285.5	5.56e-20	1.000
286.0	5.51e-20	1.000	286.5	5.45e-20	1.000	287.0	5.41e-20	1.000	287.5	5.37e-20	1.000	288.0	5.33e-20	1.000
288.5	5.27e-20	1.000	289.0	5.21e-20	1.000	289.5	5.15e-20	1.000	290.0	5.08e-20	1.000	290.5	4.99e-20	1.000
291.0	4.89e-20	1.000	291.5	4.82e-20	1.000	292.0	4.73e-20	1.000	292.5	4.62e-20	1.000	293.0	4.53e-20	1.000
293.5	4.41e-20	1.000	294.0	4.32e-20	1.000	294.5	4.23e-20	1.000	295.0	4.15e-20	1.000	295.5	4.11e-20	1.000
296.0	4.01e-20	1.000	296.5	3.94e-20	1.000	297.0	3.88e-20	1.000	297.5	3.77e-20	1.000	298.0	3.69e-20	1.000
298.5	3.63e-20	1.000	299.0	3.54e-20	1.000	299.5	3.46e-20	1.000	300.0	3.36e-20	1.000	300.5	3.24e-20	1.000
301.0	3.16e-20	1.000	301.5	3.06e-20	1.000	302.0	2.95e-20	1.000	302.5	2.82e-20	1.000	303.0	2.70e-20	1.000
303.5	2.59e-20	1.000	304.0	2.49e-20	1.000	304.5	2.42e-20	1.000	305.0	2.34e-20	1.000	305.5	2.28e-20	1.000
306.0	2.19e-20	1.000	306.5	2.11e-20	1.000	307.0	2.04e-20	1.000	307.5	1.93e-20	1.000	308.0	1.88e-20	1.000
308.5	1.80e-20	1.000	309.0	1.73e-20	1.000	309.5	1.66e-20	1.000	310.0	1.58e-20	1.000	310.5	1.48e-20	1.000
311.0	1.42e-20	1.000	311.5	1.34e-20	1.000	312.0	1.26e-20	1.000	312.5	1.17e-20	1.000	313.0	1.13e-20	1.000
313.5	1.08e-20	1.000	314.0	1.04e-20	1.000	314.5	9.69e-21	1.000	315.0	8.91e-21	1.000	315.5	8.61e-21	1.000
316.0	7.88e-21	1.000	316.5	7.25e-21	1.000	317.0	6.92e-21	1.000	317.5	6.43e-21	1.000	318.0	6.07e-21	1.000
318.5	5.64e-21	1.000	319.0	5.19e-21	1.000	319.5	4.66e-21	1.000	320.0	4.36e-21	1.000	320.5	3.95e-21	1.000
321.0	3.64e-21	1.000	321.5	3.38e-21	1.000	322.0	3.17e-21	1.000	322.5	2.80e-21	1.000	323.0	2.62e-21	1.000
323.5	2.29e-21	1.000	324.0	2.13e-21	1.000	324.5	1.93e-21	1.000	325.0	1.70e-21	1.000	325.5	1.58e-21	1.000
326.0	1.48e-21	1.000	326.5	1.24e-21	1.000	327.0	1.20e-21	1.000	327.5	1.04e-21	1.000	328.0	9.51e-22	1.000
328.5	8.44e-22	1.000	329.0	7.26e-22	1.000	329.5	6.70e-22	1.000	330.0	6.08e-22	1.000	330.5	5.15e-22	1.000
331.0	4.56e-22	1.000	331.5	4.13e-22	1.000	332.0	3.56e-22	1.000	332.5	3.30e-22	1.000	333.0	2.97e-22	1.000
333.5	2.67e-22	1.000	334.0	2.46e-22	1.000	334.5	2.21e-22	1.000	335.0	1.93e-22	1.000	335.5	1.56e-22	1.000
336.0	1.47e-22	1.000	336.5	1.37e-22	1.000	337.0	1.27e-22	1.000	337.5	1.19e-22	1.000	338.0	1.09e-22	1.000
338.5	1.01e-22	1.000	339.0	9.09e-23	1.000	339.5	8.22e-23	1.000	340.0	7.66e-23	1.000	340.5	7.43e-23	1.000
341.0	6.83e-23	1.000	341.5	6.72e-23	1.000	342.0	6.04e-23	1.000	342.5	4.78e-23	1.000	343.0	0.00e+00	1.000
							COOH							
210.0	3.12e-19	1.000	215.0	2.09e-19	1.000	220.0	1.54e-19	1.000	225.0	1.22e-19	1.000	230.0	9.62e-20	1.000
235.0	7.61e-20	1.000	240.0	6.05e-20	1.000	245.0	4.88e-20	1.000	250.0	3.98e-20	1.000	255.0	3.23e-20	1.000
260.0	2.56e-20	1.000	265.0	2.11e-20	1.000	270.0	1.70e-20	1.000	275.0	1.39e-20	1.000	280.0	1.09e-20	1.000
285.0	8.63e-21	1.000	290.0	6.91e-21	1.000	295.0	5.51e-21	1.000	300.0	4.13e-21	1.000	305.0	3.13e-21	1.000
310.0	2.39e-21	1.000	315.0	1.82e-21	1.000	320.0	1.37e-21	1.000	325.0	1.05e-21	1.000	330.0	7.90e-22	1.000
335.0	6.10e-22	1.000	340.0	4.70e-22	1.000	345.0	3.50e-22	1.000	350.0	2.70e-22	1.000	355.0	2.10e-22	1.000
360.0	1.60e-22	1.000	365.0	1.20e-22	1.000	370.0	0.00e+00	1.000						
							GLY_R							
230.0	2.87e-21	1.000	235.0	2.87e-21	1.000	240.0	4.30e-21	1.000	245.0	5.73e-21	1.000	250.0	8.60e-21	1.000
255.0	1.15e-20	1.000	260.0	1.43e-20	1.000	265.0	1.86e-20	1.000	270.0	2.29e-20	1.000	275.0	2.58e-20	1.000
280.0	2.87e-20	1.000	285.0	3.30e-20	1.000	290.0	3.15e-20	1.000	295.0	3.30e-20	1.000	300.0	3.58e-20	1.000
305.0	2.72e-20	1.000	310.0	2.72e-20	1.000	312.5	2.87e-20	1.000	315.0	2.29e-20	1.000	320.0	1.43e-20	1.000
325.0	1.15e-20	1.000	327.5	1.43e-20	1.000	330.0	1.15e-20	1.000	335.0	2.87e-21	1.000	340.0	0.00e+00	1.000
345.0	0.00e+00	1.000	350.0	0.00e+00	1.000	355.0	0.00e+00	1.000	360.0	2.29e-21	1.000	365.0	2.87e-21	1.000
370.0	8.03e-21	1.000	375.0	1.00e-20	1.000	380.0	1.72e-20	0.972	382.0	1.58e-20	0.855	384.0	1.49e-20	0.737
386.0	1.49e-20	0.619	388.0	2.87e-20	0.502	390.0	3.15e-20	0.384	391.0	3.24e-20	0.326	392.0	3.04e-20	0.267
393.0	2.23e-20	0.208	394.0	2.63e-20	0.149	395.0	3.04e-20	0.090	396.0	2.63e-20	0.032	397.0	2.43e-20	0.000
398.0	3.24e-20	0.000	399.0	3.04e-20	0.000	400.0	2.84e-20	0.000	401.0	3.24e-20	0.000	402.0	4.46e-20	0.000
403.0	5.27e-20	0.000	404.0	4.26e-20	0.000	405.0	3.04e-20	0.000	406.0	3.04e-20	0.000	407.0	2.84e-20	0.000
408.0	2.43e-20	0.000	409.0	2.84e-20	0.000	410.0	6.08e-20	0.000	411.0	5.07e-20	0.000	411.5	6.08e-20	0.000
412.0	4.86e-20	0.000	413.0	8.31e-20	0.000	413.5	6.48e-20	0.000	414.0	7.50e-20	0.000	414.5	8.11e-20	0.000
415.0	8.11e-20	0.000	415.5	6.89e-20	0.000	416.0	4.26e-20	0.000	417.0	4.86e-20	0.000	418.0	5.88e-20	0.000
							GLY_ABS							
230.0	2.87e-21	1.000	235.0	2.87e-21	1.000	240.0	4.30e-21	1.000	245.0	5.73e-21	1.000	250.0	8.60e-21	1.000
255.0	1.15e-20	1.000	260.0	1.43e-20	1.000	265.0	1.86e-20	1.000	270.0	2.29e-20	1.000	275.0	2.58e-20	1.000
280.0	2.87e-20	1.000	285.0	3.30e-20	1.000	290.0	3.15e-20	1.000	295.0	3.30e-20	1.000	300.0	3.58e-20	1.000
305.0	2.72e-20	1.000	310.0	2.72e-20	1.000	312.5	2.87e-20	1.000	315.0	2.29e-20	1.000	320.0	1.43e-20	1.000
325.0	1.15e-20	1.000	327.5	1.43e-20	1.000	330.0	1.15e-20	1.000	335.0	2.87e-21	1.000	340.0	0.00e+00	1.000
355.0	0.00e+00	1.000	360.0	2.29e-21	1.000	365.0	2.87e-21	1.000	370.0	8.03e-21	1.000	375.0	1.00e-20	1.000
380.0	1.72e-20	1.000	382.0	1.58e-20	1.000	384.0	1.49e-20	1.000	386.0	1.49e-20	1.000	388.0	2.87e-20	1.000
390.0	3.15e-20	1.000	391.0	3.24e-20	1.000	392.0	3.04e-20	1.000	393.0	2.23e-20	1.000	394.0	2.63e-20	1.000
395.0	3.04e-20	1.000	396.0	2.63e-20	1.000	397.0	2.43e-20	1.000	398.0	3.24e-20	1.000	399.0	3.04e-20	1.000
400.0	2.84e-20	1.000	401.0	3.24e-20	1.000	402.0	4.46e-20	1.000	403.0	5.27e-20	1.000	404.0	4.26e-20	1.000
405.0	3.04e-20	1.000	406.0	3.04e-20	1.000	407.0	2.84e-20	1.000	408.0	2.43e-20	1.000	409.0	2.84e-20	1.000
410.0	6.08e-20	1.000	411.0	5.07e-20	1.000	411.5	6.08e-20	1.000	412.0	4.86e-20	1.000	413.0	8.31e-20	1.000
413.5	6.48e-20	1.000	414.0	7.50e-20	1.000	414.5	8.11e-20	1.000	415.0	8.11e-20	1.000	415.5	6.89e-20	1.000
416.0	4.26e-20	1.000	417.0	4.86e-20	1.000	418.0	5.88e-20	1.000	419.0	6.69e-20	1.000	420.0	3.85e-20	1.000
421.0	5.67e-20	1.000	421.5	4.46e-20	1.000	422.0	5.27e-20	1.000	422.5	1.05e-19	1.000	423.0	8.51e-20	1.000
424.0	6.08e-20	1.000	425.0	7.29e-20	1.000	426.0	1.18e-19	1.000	426.5	1.30e-19	1.000	427.0	1.07e-19	1.000
428.0	1.66e-19	1.000	429.0	4.05e-20	1.000	430.0	5.07e-20	1.000	431.0	4.86e-20	1.000	432.0	4.05e-20	1.000

Table A-3 (continued)

WL (nm)	Abs (cm^2)	QY	WL (nm)	Abs (cm^2)	QY	WL (nm)	Abs (cm^2)	QY	WL (nm)	Abs (cm^2)	QY	WL (nm)	Abs (cm^2)	QY
433.0	3.65e-20	1.000	434.0	4.05e-20	1.000	434.5	6.08e-20	1.000	435.0	5.07e-20	1.000	436.0	8.11e-20	1.000
436.5	1.13e-19	1.000	437.0	5.27e-20	1.000	438.0	1.01e-19	1.000	438.5	1.38e-19	1.000	439.0	7.70e-20	1.000
440.0	2.47e-19	1.000	441.0	8.11e-20	1.000	442.0	6.08e-20	1.000	443.0	7.50e-20	1.000	444.0	9.32e-20	1.000
445.0	1.13e-19	1.000	446.0	5.27e-20	1.000	447.0	2.43e-20	1.000	448.0	2.84e-20	1.000	449.0	3.85e-20	1.000
450.0	6.08e-20	1.000	451.0	1.09e-19	1.000	451.5	9.32e-20	1.000	452.0	1.22e-19	1.000	453.0	2.39e-19	1.000
454.0	1.70e-19	1.000	455.0	3.40e-19	1.000	455.5	4.05e-19	1.000	456.0	1.01e-19	1.000	457.0	1.62e-20	1.000
458.0	1.22e-20	1.000	458.5	1.42e-20	1.000	459.0	4.05e-21	1.000	460.0	4.05e-21	1.000	460.5	6.08e-21	1.000
461.0	2.03e-21	1.000	462.0	0.00e+00	1.000									
						MGLY_ADJ								
219.0	9.84e-21	1.000	219.5	1.04e-20	1.000	220.0	1.06e-20	1.000	220.5	1.11e-20	1.000	221.0	1.15e-20	1.000
221.5	1.18e-20	1.000	222.0	1.22e-20	1.000	222.5	1.24e-20	1.000	223.0	1.26e-20	1.000	223.5	1.26e-20	1.000
224.0	1.25e-20	1.000	224.5	1.24e-20	1.000	225.0	1.25e-20	1.000	225.5	1.27e-20	1.000	226.0	1.27e-20	1.000
226.5	1.29e-20	1.000	227.0	1.31e-20	1.000	227.5	1.32e-20	1.000	228.0	1.35e-20	1.000	228.5	1.37e-20	1.000
229.0	1.40e-20	1.000	229.5	1.42e-20	1.000	230.0	1.48e-20	1.000	230.5	1.53e-20	1.000	231.0	1.57e-20	1.000
231.5	1.59e-20	1.000	232.0	1.61e-20	1.000	232.5	1.62e-20	1.000	233.0	1.61e-20	1.000	233.5	1.68e-20	1.000
234.0	1.74e-20	1.000	234.5	1.80e-20	1.000	235.0	1.84e-20	1.000	235.5	1.87e-20	1.000	236.0	1.89e-20	1.000
236.5	1.91e-20	1.000	237.0	1.93e-20	1.000	237.5	1.94e-20	1.000	238.0	1.96e-20	1.000	238.5	1.96e-20	1.000
239.0	2.01e-20	1.000	239.5	2.04e-20	1.000	240.0	2.08e-20	1.000	240.5	2.10e-20	1.000	241.0	2.14e-20	1.000
241.5	2.16e-20	1.000	242.0	2.19e-20	1.000	242.5	2.20e-20	1.000	243.0	2.23e-20	1.000	243.5	2.26e-20	1.000
244.0	2.28e-20	1.000	244.5	2.29e-20	1.000	245.0	2.30e-20	1.000	245.5	2.32e-20	1.000	246.0	2.33e-20	1.000
246.5	2.35e-20	1.000	247.0	2.38e-20	1.000	247.5	2.41e-20	1.000	248.0	2.46e-20	1.000	248.5	2.51e-20	1.000
249.0	2.57e-20	1.000	249.5	2.61e-20	1.000	250.0	2.65e-20	1.000	250.5	2.67e-20	1.000	251.0	2.69e-20	1.000
251.5	2.69e-20	1.000	252.0	2.71e-20	1.000	252.5	2.72e-20	1.000	253.0	2.73e-20	1.000	253.5	2.74e-20	1.000
254.0	2.76e-20	1.000	254.5	2.78e-20	1.000	255.0	2.82e-20	1.000	255.5	2.87e-20	1.000	256.0	2.93e-20	1.000
256.5	2.98e-20	1.000	257.0	3.07e-20	1.000	257.5	3.12e-20	1.000	258.0	3.17e-20	1.000	258.5	3.21e-20	1.000
259.0	3.26e-20	1.000	259.5	3.28e-20	1.000	260.0	3.29e-20	1.000	260.5	3.31e-20	1.000	261.0	3.33e-20	1.000
261.5	3.34e-20	1.000	262.0	3.36e-20	1.000	262.5	3.38e-20	1.000	263.0	3.42e-20	1.000	263.5	3.44e-20	1.000
264.0	3.48e-20	1.000	264.5	3.54e-20	1.000	265.0	3.59e-20	1.000	265.5	3.65e-20	1.000	266.0	3.73e-20	1.000
266.5	3.80e-20	1.000	267.0	3.87e-20	1.000	267.5	3.95e-20	1.000	268.0	4.02e-20	1.000	268.5	4.08e-20	1.000
269.0	4.13e-20	1.000	269.5	4.17e-20	1.000	270.0	4.20e-20	1.000	270.5	4.22e-20	1.000	271.0	4.22e-20	1.000
271.5	4.22e-20	1.000	272.0	4.23e-20	1.000	272.5	4.24e-20	1.000	273.0	4.27e-20	1.000	273.5	4.29e-20	1.000
274.0	4.31e-20	1.000	274.5	4.33e-20	1.000	275.0	4.37e-20	1.000	275.5	4.42e-20	1.000	276.0	4.48e-20	1.000
276.5	4.56e-20	1.000	277.0	4.64e-20	1.000	277.5	4.71e-20	1.000	278.0	4.78e-20	1.000	278.5	4.83e-20	1.000
279.0	4.87e-20	1.000	279.5	4.90e-20	1.000	280.0	4.92e-20	1.000	280.5	4.93e-20	1.000	281.0	4.94e-20	1.000
281.5	4.92e-20	1.000	282.0	4.90e-20	1.000	282.5	4.86e-20	1.000	283.0	4.83e-20	1.000	283.5	4.79e-20	1.000
284.0	4.76e-20	1.000	284.5	4.72e-20	1.000	285.0	4.70e-20	1.000	285.5	4.68e-20	1.000	286.0	4.66e-20	1.000
286.5	4.65e-20	1.000	287.0	4.65e-20	1.000	287.5	4.68e-20	1.000	288.0	4.73e-20	1.000	288.5	4.78e-20	1.000
289.0	4.84e-20	1.000	289.5	4.89e-20	1.000	290.0	4.92e-20	1.000	290.5	4.92e-20	1.000	291.0	4.90e-20	1.000
291.5	4.86e-20	1.000	292.0	4.81e-20	1.000	292.5	4.75e-20	1.000	293.0	4.70e-20	1.000	293.5	4.65e-20	1.000
294.0	4.58e-20	1.000	294.5	4.48e-20	1.000	295.0	4.38e-20	1.000	295.5	4.27e-20	1.000	296.0	4.17e-20	1.000
296.5	4.07e-20	1.000	297.0	3.99e-20	1.000	297.5	3.94e-20	1.000	298.0	3.88e-20	1.000	298.5	3.82e-20	1.000
299.0	3.76e-20	1.000	299.5	3.72e-20	1.000	300.0	3.69e-20	1.000	300.5	3.68e-20	1.000	301.0	3.70e-20	1.000
301.5	3.72e-20	1.000	302.0	3.74e-20	1.000	302.5	3.74e-20	1.000	303.0	3.75e-20	1.000	303.5	3.71e-20	1.000
304.0	3.62e-20	1.000	304.5	3.51e-20	1.000	305.0	3.38e-20	1.000	305.5	3.25e-20	1.000	306.0	3.15e-20	1.000
306.5	3.04e-20	1.000	307.0	2.92e-20	1.000	307.5	2.80e-20	1.000	308.0	2.71e-20	1.000	308.5	2.63e-20	1.000
309.0	2.52e-20	1.000	309.5	2.43e-20	1.000	310.0	2.34e-20	1.000	310.5	2.25e-20	1.000	311.0	2.19e-20	1.000
311.5	2.12e-20	1.000	312.0	2.06e-20	1.000	312.5	2.02e-20	1.000	313.0	1.96e-20	1.000	313.5	1.92e-20	1.000
314.0	1.91e-20	1.000	314.5	1.88e-20	1.000	315.0	1.86e-20	1.000	315.5	1.85e-20	1.000	316.0	1.86e-20	1.000
316.5	1.87e-20	1.000	317.0	1.87e-20	1.000	317.5	1.87e-20	1.000	318.0	1.83e-20	1.000	318.5	1.75e-20	1.000
319.0	1.69e-20	1.000	319.5	1.60e-20	1.000	320.0	1.50e-20	1.000	320.5	1.41e-20	1.000	321.0	1.34e-20	1.000
321.5	1.27e-20	1.000	322.0	1.21e-20	1.000	322.5	1.18e-20	1.000	323.0	1.14e-20	1.000	323.5	1.08e-20	1.000
324.0	1.01e-20	1.000	324.5	9.62e-21	1.000	325.0	9.28e-21	1.000	325.5	8.75e-21	1.000	326.0	8.49e-21	1.000
326.5	8.21e-21	1.000	327.0	7.71e-21	1.000	327.5	7.38e-21	1.000	328.0	7.18e-21	1.000	328.5	6.86e-21	1.000
329.0	6.71e-21	1.000	329.5	6.63e-21	1.000	330.0	6.46e-21	1.000	330.5	6.29e-21	1.000	331.0	6.21e-21	1.000
331.5	6.18e-21	1.000	332.0	6.20e-21	1.000	332.5	5.49e-21	1.000	333.0	5.21e-21	1.000	333.5	5.38e-21	1.000
334.0	5.35e-21	1.000	334.5	5.04e-21	1.000	335.0	4.94e-21	1.000	335.5	4.90e-21	1.000	336.0	4.52e-21	1.000
336.5	4.26e-21	1.000	337.0	4.11e-21	1.000	337.5	3.76e-21	1.000	338.0	3.61e-21	1.000	338.5	3.58e-21	1.000
339.0	3.47e-21	1.000	339.5	3.32e-21	1.000	340.0	3.22e-21	1.000	340.5	3.10e-21	1.000	341.0	3.00e-21	1.000
341.5	2.94e-21	1.000	342.0	2.89e-21	1.000	342.5	2.86e-21	1.000	343.0	2.88e-21	1.000	343.5	2.88e-21	1.000
344.0	2.89e-21	0.992	344.5	2.91e-21	0.984	345.0	2.95e-21	0.976	345.5	3.00e-21	0.968	346.0	3.08e-21	0.960
346.5	3.18e-21	0.953	347.0	3.25e-21	0.945	347.5	3.30e-21	0.937	348.0	3.39e-21	0.929	348.5	3.51e-21	0.921
349.0	3.63e-21	0.913	349.5	3.73e-21	0.905	350.0	3.85e-21	0.897	350.5	3.99e-21	0.889	351.0	4.27e-21	0.881
351.5	4.47e-21	0.873	352.0	4.63e-21	0.865	352.5	4.78e-21	0.858	353.0	4.92e-21	0.850	353.5	5.07e-21	0.842
354.0	5.23e-21	0.834	354.5	5.39e-21	0.826	355.0	5.56e-21	0.818	355.5	5.77e-21	0.810	356.0	5.97e-21	0.802
356.5	6.15e-21	0.794	357.0	6.35e-21	0.786	357.5	6.56e-21	0.778	358.0	6.76e-21	0.770	358.5	6.95e-21	0.763
359.0	7.20e-21	0.755	359.5	7.44e-21	0.747	360.0	7.64e-21	0.739	360.5	7.89e-21	0.731	361.0	8.15e-21	0.723
361.5	8.43e-21	0.715	362.0	8.71e-21	0.707	362.5	9.02e-21	0.699	363.0	9.33e-21	0.691	363.5	9.65e-21	0.683
364.0	1.00e-20	0.675	364.5	1.04e-20	0.668	365.0	1.08e-20	0.660	365.5	1.11e-20	0.652	366.0	1.15e-20	0.644
366.5	1.19e-20	0.636	367.0	1.23e-20	0.628	367.5	1.27e-20	0.620	368.0	1.31e-20	0.612	368.5	1.35e-20	0.604
369.0	1.40e-20	0.596	369.5	1.44e-20	0.588	370.0	1.47e-20	0.580	370.5	1.51e-20	0.573	371.0	1.55e-20	0.565
371.5	1.59e-20	0.557	372.0	1.64e-20	0.549	372.5	1.70e-20	0.541	373.0	1.73e-20	0.533	373.5	1.77e-20	0.525
374.0	1.81e-20	0.517	374.5	1.86e-20	0.509	375.0	1.90e-20	0.501	375.5	1.96e-20	0.493	376.0	2.02e-20	0.486

Table A-3 (continued)

WL (nm)	Abs (cm^2)	QY	WL (nm)	Abs (cm^2)	QY	WL (nm)	Abs (cm^2)	QY	WL (nm)	Abs (cm^2)	QY	WL (nm)	Abs (cm^2)	QY
376.5	2.06e-20	0.478	377.0	2.10e-20	0.470	377.5	2.14e-20	0.462	378.0	2.18e-20	0.454	378.5	2.24e-20	0.446
379.0	2.30e-20	0.438	379.5	2.37e-20	0.430	380.0	2.42e-20	0.422	380.5	2.47e-20	0.414	381.0	2.54e-20	0.406
381.5	2.62e-20	0.398	382.0	2.69e-20	0.391	382.5	2.79e-20	0.383	383.0	2.88e-20	0.375	383.5	2.96e-20	0.367
384.0	3.02e-20	0.359	384.5	3.10e-20	0.351	385.0	3.20e-20	0.343	385.5	3.29e-20	0.335	386.0	3.39e-20	0.327
386.5	3.51e-20	0.319	387.0	3.62e-20	0.311	387.5	3.69e-20	0.303	388.0	3.70e-20	0.296	388.5	3.77e-20	0.288
389.0	3.88e-20	0.280	389.5	3.97e-20	0.272	390.0	4.03e-20	0.264	390.5	4.12e-20	0.256	391.0	4.22e-20	0.248
391.5	4.29e-20	0.240	392.0	4.30e-20	0.232	392.5	4.38e-20	0.224	393.0	4.47e-20	0.216	393.5	4.55e-20	0.208
394.0	4.56e-20	0.201	394.5	4.59e-20	0.193	395.0	4.67e-20	0.185	395.5	4.80e-20	0.177	396.0	4.87e-20	0.169
396.5	4.96e-20	0.161	397.0	5.08e-20	0.153	397.5	5.19e-20	0.145	398.0	5.23e-20	0.137	398.5	5.39e-20	0.129
399.0	5.46e-20	0.121	399.5	5.54e-20	0.113	400.0	5.59e-20	0.106	400.5	5.77e-20	0.098	401.0	5.91e-20	0.090
401.5	5.99e-20	0.082	402.0	6.06e-20	0.074	402.5	6.20e-20	0.066	403.0	6.35e-20	0.058	403.5	6.52e-20	0.050
404.0	6.54e-20	0.042	404.5	6.64e-20	0.034	405.0	6.93e-20	0.026	405.5	7.15e-20	0.018	406.0	7.19e-20	0.011
406.5	7.32e-20	0.003	407.0	7.58e-20	0.000	407.5	7.88e-20	0.000	408.0	7.97e-20	0.000	408.5	7.91e-20	0.000
409.0	8.11e-20	0.000	409.5	8.41e-20	0.000	410.0	8.53e-20	0.000	410.5	8.59e-20	0.000	411.0	8.60e-20	0.000
411.5	8.80e-20	0.000	412.0	9.04e-20	0.000	412.5	9.45e-20	0.000	413.0	9.34e-20	0.000	413.5	9.37e-20	0.000
414.0	9.63e-20	0.000	414.5	9.71e-20	0.000	415.0	9.70e-20	0.000	415.5	9.65e-20	0.000	416.0	9.69e-20	0.000
416.5	9.89e-20	0.000	417.0	1.00e-19	0.000	417.5	1.02e-19	0.000	418.0	1.00e-19	0.000	418.5	1.02e-19	0.000
419.0	1.01e-19	0.000	419.5	1.01e-19	0.000	420.0	1.03e-19	0.000	420.5	1.01e-19	0.000	421.0	1.04e-19	0.000
							BACL_ADJ							
230.0	1.30e-20	1.000	232.5	1.46e-20	1.000	235.0	1.68e-20	1.000	237.5	1.84e-20	1.000	240.0	2.16e-20	1.000
242.5	2.49e-20	1.000	245.0	2.65e-20	1.000	247.5	2.71e-20	1.000	250.0	3.03e-20	1.000	252.5	3.46e-20	1.000
255.0	3.46e-20	1.000	257.5	3.57e-20	1.000	260.0	3.95e-20	1.000	262.5	4.17e-20	1.000	265.0	4.17e-20	1.000
267.5	4.22e-20	1.000	270.0	4.60e-20	1.000	272.5	4.54e-20	1.000	275.0	4.33e-20	1.000	277.5	4.22e-20	1.000
280.0	4.44e-20	1.000	282.5	4.33e-20	1.000	285.0	3.90e-20	1.000	287.5	3.57e-20	1.000	290.0	3.25e-20	1.000
292.5	2.92e-20	1.000	295.0	2.60e-20	1.000	297.5	2.16e-20	1.000	300.0	1.79e-20	1.000	302.5	1.73e-20	1.000
305.0	1.46e-20	1.000	307.5	1.08e-20	1.000	310.0	9.20e-21	1.000	312.5	7.03e-21	1.000	315.0	6.49e-21	1.000
317.5	5.41e-21	1.000	320.0	5.41e-21	1.000	322.5	5.41e-21	1.000	325.0	4.33e-21	1.000	327.5	3.25e-21	1.000
330.0	3.79e-21	1.000	332.5	3.79e-21	1.000	335.0	4.33e-21	1.000	337.5	4.87e-21	1.000	340.0	5.41e-21	1.000
342.5	5.95e-21	1.000	345.0	6.49e-21	1.000	347.5	7.03e-21	1.000	350.0	8.12e-21	0.995	352.5	7.57e-21	0.960
355.0	9.20e-21	0.925	357.5	9.74e-21	0.890	360.0	1.08e-20	0.855	362.5	1.19e-20	0.820	365.0	1.41e-20	0.785
367.5	1.51e-20	0.750	370.0	1.79e-20	0.715	372.5	2.00e-20	0.680	375.0	2.11e-20	0.645	377.5	2.33e-20	0.610
380.0	2.60e-20	0.575	382.5	2.81e-20	0.540	385.0	3.14e-20	0.505	387.5	3.46e-20	0.470	390.0	3.90e-20	0.435
392.5	4.11e-20	0.399	395.0	4.33e-20	0.364	397.5	4.38e-20	0.329	400.0	4.65e-20	0.294	402.5	4.81e-20	0.259
405.0	5.19e-20	0.224	407.5	5.84e-20	0.189	410.0	6.06e-20	0.154	412.5	6.49e-20	0.119	415.0	6.92e-20	0.084
417.5	6.87e-20	0.049	420.0	6.82e-20	0.014	422.5	6.71e-20	0.000	425.0	6.49e-20	0.000	427.5	5.95e-20	0.000
430.0	5.73e-20	0.000	432.5	6.28e-20	0.000	435.0	6.01e-20	0.000	437.5	5.84e-20	0.000	440.0	5.95e-20	0.000
442.5	6.49e-20	0.000	445.0	5.95e-20	0.000	447.5	4.98e-20	0.000	450.0	3.79e-20	0.000	452.5	2.81e-20	0.000
455.0	1.73e-20	0.000	457.5	1.08e-20	0.000	460.0	5.41e-21	0.000	462.5	3.79e-21	0.000	465.0	2.16e-21	0.000
467.5	1.08e-21	0.000	470.0	1.08e-21	0.000	472.5	0.00e+00	0.000						
							BZCHO							
299.0	1.78e-19	1.000	304.0	7.40e-20	1.000	306.0	6.91e-20	1.000	309.0	6.41e-20	1.000	313.0	6.91e-20	1.000
314.0	6.91e-20	1.000	318.0	6.41e-20	1.000	325.0	8.39e-20	1.000	332.0	7.65e-20	1.000	338.0	8.88e-20	1.000
342.0	8.88e-20	1.000	346.0	7.89e-20	1.000	349.0	7.89e-20	1.000	354.0	9.13e-20	1.000	355.0	8.14e-20	1.000
364.0	5.67e-20	1.000	368.0	6.66e-20	1.000	369.0	8.39e-20	1.000	370.0	8.39e-20	1.000	372.0	3.45e-20	1.000
374.0	3.21e-20	1.000	376.0	2.47e-20	1.000	377.0	2.47e-20	1.000	380.0	3.58e-20	1.000	382.0	9.90e-21	1.000
386.0	0.00e+00	1.000												
							ACROLEIN							
250.0	1.80e-21	1.000	252.0	2.05e-21	1.000	253.0	2.20e-21	1.000	254.0	2.32e-21	1.000	255.0	2.45e-21	1.000
256.0	2.56e-21	1.000	257.0	2.65e-21	1.000	258.0	2.74e-21	1.000	259.0	2.83e-21	1.000	260.0	2.98e-21	1.000
261.0	3.24e-21	1.000	262.0	3.47e-21	1.000	263.0	3.58e-21	1.000	264.0	3.93e-21	1.000	265.0	4.67e-21	1.000
266.0	5.10e-21	1.000	267.0	5.38e-21	1.000	268.0	5.73e-21	1.000	269.0	6.13e-21	1.000	270.0	6.64e-21	1.000
271.0	7.20e-21	1.000	272.0	7.77e-21	1.000	273.0	8.37e-21	1.000	274.0	8.94e-21	1.000	275.0	9.55e-21	1.000
276.0	1.04e-20	1.000	277.0	1.12e-20	1.000	278.0	1.19e-20	1.000	279.0	1.27e-20	1.000	280.0	1.27e-20	1.000
281.0	1.26e-20	1.000	282.0	1.26e-20	1.000	283.0	1.28e-20	1.000	284.0	1.33e-20	1.000	285.0	1.38e-20	1.000
286.0	1.44e-20	1.000	287.0	1.50e-20	1.000	288.0	1.57e-20	1.000	289.0	1.63e-20	1.000	290.0	1.71e-20	1.000
291.0	1.78e-20	1.000	292.0	1.86e-20	1.000	293.0	1.95e-20	1.000	294.0	2.05e-20	1.000	295.0	2.15e-20	1.000
296.0	2.26e-20	1.000	297.0	2.37e-20	1.000	298.0	2.48e-20	1.000	299.0	2.60e-20	1.000	300.0	2.73e-20	1.000
301.0	2.85e-20	1.000	302.0	2.99e-20	1.000	303.0	3.13e-20	1.000	304.0	3.27e-20	1.000	305.0	3.39e-20	1.000
306.0	3.51e-20	1.000	307.0	3.63e-20	1.000	308.0	3.77e-20	1.000	309.0	3.91e-20	1.000	310.0	4.07e-20	1.000
311.0	4.25e-20	1.000	312.0	4.39e-20	1.000	313.0	4.44e-20	1.000	314.0	4.50e-20	1.000	315.0	4.59e-20	1.000
316.0	4.75e-20	1.000	317.0	4.90e-20	1.000	318.0	5.05e-20	1.000	319.0	5.19e-20	1.000	320.0	5.31e-20	1.000
321.0	5.43e-20	1.000	322.0	5.52e-20	1.000	323.0	5.60e-20	1.000	324.0	5.67e-20	1.000	325.0	5.67e-20	1.000
326.0	5.62e-20	1.000	327.0	5.63e-20	1.000	328.0	5.71e-20	1.000	329.0	5.76e-20	1.000	330.0	5.80e-20	1.000
331.0	5.95e-20	1.000	332.0	6.23e-20	1.000	333.0	6.39e-20	1.000	334.0	6.38e-20	1.000	335.0	6.24e-20	1.000
336.0	6.01e-20	1.000	337.0	5.79e-20	1.000	338.0	5.63e-20	1.000	339.0	5.56e-20	1.000	340.0	5.52e-20	1.000
341.0	5.54e-20	1.000	342.0	5.53e-20	1.000	343.0	5.47e-20	1.000	344.0	5.41e-20	1.000	345.0	5.40e-20	1.000
346.0	5.48e-20	1.000	347.0	5.90e-20	1.000	348.0	6.08e-20	1.000	349.0	6.00e-20	1.000	350.0	5.53e-20	1.000
351.0	5.03e-20	1.000	352.0	4.50e-20	1.000	353.0	4.03e-20	1.000	354.0	3.75e-20	1.000	355.0	3.55e-20	1.000
356.0	3.45e-20	1.000	357.0	3.46e-20	1.000	358.0	3.49e-20	1.000	359.0	3.41e-20	1.000	360.0	3.23e-20	1.000
361.0	2.95e-20	1.000	362.0	2.81e-20	1.000	363.0	2.91e-20	1.000	364.0	3.25e-20	1.000	365.0	3.54e-20	1.000
366.0	3.30e-20	1.000	367.0	2.78e-20	1.000	368.0	2.15e-20	1.000	369.0	1.59e-20	1.000	370.0	1.19e-20	1.000

Table A-3 (continued)

WL (nm)	Abs (cm^2)	QY	WL (nm)	Abs (cm^2)	QY	WL (nm)	Abs (cm^2)	QY	WL (nm)	Abs (cm^2)	QY	WL (nm)	Abs (cm^2)	QY
371.0	8.99e-21	1.000	372.0	7.22e-21	1.000	373.0	5.86e-21	1.000	374.0	4.69e-21	1.000	375.0	3.72e-21	1.000
376.0	3.57e-21	1.000	377.0	3.55e-21	1.000	378.0	2.83e-21	1.000	379.0	1.69e-21	1.000	380.0	8.29e-24	1.000
381.0	0.00e+00	1.000												
							IC3ONO2							
185.0	1.79e-17	1.000	188.0	1.81e-17	1.000	190.0	1.79e-17	1.000	195.0	1.61e-17	1.000	200.0	1.26e-17	1.000
205.0	8.67e-18	1.000	210.0	4.98e-18	1.000	215.0	2.47e-18	1.000	220.0	1.17e-18	1.000	225.0	5.80e-19	1.000
230.0	3.10e-19	1.000	235.0	1.80e-19	1.000	240.0	1.10e-19	1.000	245.0	7.00e-20	1.000	250.0	5.70e-20	1.000
255.0	5.20e-20	1.000	260.0	4.90e-20	1.000	265.0	4.60e-20	1.000	270.0	4.10e-20	1.000	275.0	3.60e-20	1.000
280.0	2.90e-20	1.000	285.0	2.30e-20	1.000	290.0	1.70e-20	1.000	295.0	1.20e-20	1.000	300.0	8.10e-21	1.000
305.0	5.20e-21	1.000	310.0	3.20e-21	1.000	315.0	1.90e-21	1.000	320.0	1.10e-21	1.000	325.0	6.10e-22	1.000
330.0	3.70e-22	1.000	335.0	0.00e+00	1.000									
							MGLY_ABS							
219.0	9.84e-21	1.000	219.5	1.04e-20	1.000	220.0	1.06e-20	1.000	220.5	1.11e-20	1.000	221.0	1.15e-20	1.000
221.5	1.18e-20	1.000	222.0	1.22e-20	1.000	222.5	1.24e-20	1.000	223.0	1.26e-20	1.000	223.5	1.26e-20	1.000
224.0	1.25e-20	1.000	224.5	1.24e-20	1.000	225.0	1.25e-20	1.000	225.5	1.27e-20	1.000	226.0	1.27e-20	1.000
226.5	1.29e-20	1.000	227.0	1.31e-20	1.000	227.5	1.32e-20	1.000	228.0	1.35e-20	1.000	228.5	1.37e-20	1.000
229.0	1.40e-20	1.000	229.5	1.42e-20	1.000	230.0	1.48e-20	1.000	230.5	1.53e-20	1.000	231.0	1.57e-20	1.000
231.5	1.59e-20	1.000	232.0	1.61e-20	1.000	232.5	1.62e-20	1.000	233.0	1.61e-20	1.000	233.5	1.68e-20	1.000
234.0	1.74e-20	1.000	234.5	1.80e-20	1.000	235.0	1.84e-20	1.000	235.5	1.87e-20	1.000	236.0	1.89e-20	1.000
236.5	1.91e-20	1.000	237.0	1.93e-20	1.000	237.5	1.94e-20	1.000	238.0	1.96e-20	1.000	238.5	1.96e-20	1.000
239.0	2.01e-20	1.000	239.5	2.04e-20	1.000	240.0	2.08e-20	1.000	240.5	2.10e-20	1.000	241.0	2.14e-20	1.000
241.5	2.16e-20	1.000	242.0	2.19e-20	1.000	242.5	2.20e-20	1.000	243.0	2.23e-20	1.000	243.5	2.26e-20	1.000
244.0	2.28e-20	1.000	244.5	2.29e-20	1.000	245.0	2.30e-20	1.000	245.5	2.32e-20	1.000	246.0	2.33e-20	1.000
246.5	2.35e-20	1.000	247.0	2.38e-20	1.000	247.5	2.41e-20	1.000	248.0	2.46e-20	1.000	248.5	2.51e-20	1.000
249.0	2.57e-20	1.000	249.5	2.61e-20	1.000	250.0	2.65e-20	1.000	250.5	2.67e-20	1.000	251.0	2.69e-20	1.000
251.5	2.69e-20	1.000	252.0	2.71e-20	1.000	252.5	2.72e-20	1.000	253.0	2.73e-20	1.000	253.5	2.74e-20	1.000
254.0	2.76e-20	1.000	254.5	2.78e-20	1.000	255.0	2.82e-20	1.000	255.5	2.87e-20	1.000	256.0	2.93e-20	1.000
256.5	2.98e-20	1.000	257.0	3.07e-20	1.000	257.5	3.12e-20	1.000	258.0	3.17e-20	1.000	258.5	3.21e-20	1.000
259.0	3.26e-20	1.000	259.5	3.28e-20	1.000	260.0	3.29e-20	1.000	260.5	3.31e-20	1.000	261.0	3.33e-20	1.000
261.5	3.34e-20	1.000	262.0	3.36e-20	1.000	262.5	3.38e-20	1.000	263.0	3.42e-20	1.000	263.5	3.44e-20	1.000
264.0	3.48e-20	1.000	264.5	3.54e-20	1.000	265.0	3.59e-20	1.000	265.5	3.65e-20	1.000	266.0	3.73e-20	1.000
266.5	3.80e-20	1.000	267.0	3.87e-20	1.000	267.5	3.95e-20	1.000	268.0	4.02e-20	1.000	268.5	4.08e-20	1.000
269.0	4.13e-20	1.000	269.5	4.17e-20	1.000	270.0	4.20e-20	1.000	270.5	4.22e-20	1.000	271.0	4.22e-20	1.000
271.5	4.22e-20	1.000	272.0	4.23e-20	1.000	272.5	4.24e-20	1.000	273.0	4.27e-20	1.000	273.5	4.29e-20	1.000
274.0	4.31e-20	1.000	274.5	4.33e-20	1.000	275.0	4.37e-20	1.000	275.5	4.42e-20	1.000	276.0	4.48e-20	1.000
276.5	4.56e-20	1.000	277.0	4.64e-20	1.000	277.5	4.71e-20	1.000	278.0	4.78e-20	1.000	278.5	4.83e-20	1.000
279.0	4.87e-20	1.000	279.5	4.90e-20	1.000	280.0	4.92e-20	1.000	280.5	4.93e-20	1.000	281.0	4.94e-20	1.000
281.5	4.92e-20	1.000	282.0	4.90e-20	1.000	282.5	4.86e-20	1.000	283.0	4.83e-20	1.000	283.5	4.79e-20	1.000
284.0	4.76e-20	1.000	284.5	4.72e-20	1.000	285.0	4.70e-20	1.000	285.5	4.68e-20	1.000	286.0	4.66e-20	1.000
286.5	4.65e-20	1.000	287.0	4.65e-20	1.000	287.5	4.68e-20	1.000	288.0	4.73e-20	1.000	288.5	4.78e-20	1.000
289.0	4.84e-20	1.000	289.5	4.89e-20	1.000	290.0	4.92e-20	1.000	290.5	4.92e-20	1.000	291.0	4.90e-20	1.000
291.5	4.86e-20	1.000	292.0	4.81e-20	1.000	292.5	4.75e-20	1.000	293.0	4.70e-20	1.000	293.5	4.65e-20	1.000
294.0	4.58e-20	1.000	294.5	4.48e-20	1.000	295.0	4.38e-20	1.000	295.5	4.27e-20	1.000	296.0	4.17e-20	1.000
296.5	4.07e-20	1.000	297.0	3.99e-20	1.000	297.5	3.94e-20	1.000	298.0	3.88e-20	1.000	298.5	3.82e-20	1.000
299.0	3.76e-20	1.000	299.5	3.72e-20	1.000	300.0	3.69e-20	1.000	300.5	3.68e-20	1.000	301.0	3.70e-20	1.000
301.5	3.72e-20	1.000	302.0	3.74e-20	1.000	302.5	3.74e-20	1.000	303.0	3.75e-20	1.000	303.5	3.71e-20	1.000
304.0	3.62e-20	1.000	304.5	3.51e-20	1.000	305.0	3.38e-20	1.000	305.5	3.25e-20	1.000	306.0	3.15e-20	1.000
306.5	3.04e-20	1.000	307.0	2.92e-20	1.000	307.5	2.80e-20	1.000	308.0	2.71e-20	1.000	308.5	2.63e-20	1.000
309.0	2.52e-20	1.000	309.5	2.43e-20	1.000	310.0	2.34e-20	1.000	310.5	2.25e-20	1.000	311.0	2.19e-20	1.000
311.5	2.12e-20	1.000	312.0	2.06e-20	1.000	312.5	2.02e-20	1.000	313.0	1.96e-20	1.000	313.5	1.92e-20	1.000
314.0	1.91e-20	1.000	314.5	1.88e-20	1.000	315.0	1.86e-20	1.000	315.5	1.85e-20	1.000	316.0	1.86e-20	1.000
316.5	1.87e-20	1.000	317.0	1.87e-20	1.000	317.5	1.87e-20	1.000	318.0	1.83e-20	1.000	318.5	1.75e-20	1.000
319.0	1.69e-20	1.000	319.5	1.60e-20	1.000	320.0	1.50e-20	1.000	320.5	1.41e-20	1.000	321.0	1.34e-20	1.000
321.5	1.27e-20	1.000	322.0	1.21e-20	1.000	322.5	1.18e-20	1.000	323.0	1.14e-20	1.000	323.5	1.08e-20	1.000
324.0	1.01e-20	1.000	324.5	9.62e-21	1.000	325.0	9.28e-21	1.000	325.5	8.75e-21	1.000	326.0	8.49e-21	1.000
326.5	8.21e-21	1.000	327.0	7.71e-21	1.000	327.5	7.38e-21	1.000	328.0	7.18e-21	1.000	328.5	6.86e-21	1.000
329.0	6.71e-21	1.000	329.5	6.63e-21	1.000	330.0	6.46e-21	1.000	330.5	6.29e-21	1.000	331.0	6.21e-21	1.000
331.5	6.18e-21	1.000	332.0	6.20e-21	1.000	332.5	5.49e-21	1.000	333.0	5.21e-21	1.000	333.5	5.38e-21	1.000
334.0	5.35e-21	1.000	334.5	5.04e-21	1.000	335.0	4.94e-21	1.000	335.5	4.90e-21	1.000	336.0	4.52e-21	1.000
336.5	4.26e-21	1.000	337.0	4.11e-21	1.000	337.5	3.76e-21	1.000	338.0	3.61e-21	1.000	338.5	3.58e-21	1.000
339.0	3.47e-21	1.000	339.5	3.32e-21	1.000	340.0	3.22e-21	1.000	340.5	3.10e-21	1.000	341.0	3.00e-21	1.000
341.5	2.94e-21	1.000	342.0	2.89e-21	1.000	342.5	2.86e-21	1.000	343.0	2.88e-21	1.000	343.5	2.88e-21	1.000
344.0	2.89e-21	1.000	344.5	2.91e-21	1.000	345.0	2.95e-21	1.000	345.5	3.00e-21	1.000	346.0	3.08e-21	1.000
346.5	3.18e-21	1.000	347.0	3.25e-21	1.000	347.5	3.30e-21	1.000	348.0	3.39e-21	1.000	348.5	3.51e-21	1.000
349.0	3.63e-21	1.000	349.5	3.73e-21	1.000	350.0	3.85e-21	1.000	350.5	3.99e-21	1.000	351.0	4.27e-21	1.000
351.5	4.47e-21	1.000	352.0	4.63e-21	1.000	352.5	4.78e-21	1.000	353.0	4.92e-21	1.000	353.5	5.07e-21	1.000
354.0	5.23e-21	1.000	354.5	5.39e-21	1.000	355.0	5.56e-21	1.000	355.5	5.77e-21	1.000	356.0	5.97e-21	1.000
356.5	6.15e-21	1.000	357.0	6.35e-21	1.000	357.5	6.56e-21	1.000	358.0	6.76e-21	1.000	358.5	6.95e-21	1.000
359.0	7.20e-21	1.000	359.5	7.44e-21	1.000	360.0	7.64e-21	1.000	360.5	7.89e-21	1.000	361.0	8.15e-21	1.000
361.5	8.43e-21	1.000	362.0	8.71e-21	1.000	362.5	9.02e-21	1.000	363.0	9.33e-21	1.000	363.5	9.65e-21	1.000
364.0	1.00e-20	1.000	364.5	1.04e-20	1.000	365.0	1.08e-20	1.000	365.5	1.11e-20	1.000	366.0	1.15e-20	1.000

Table A-3 (continued)

WL (nm)	Abs (cm^2)	QY	WL (nm)	Abs (cm^2)	QY	WL (nm)	Abs (cm^2)	QY	WL (nm)	Abs (cm^2)	QY	WL (nm)	Abs (cm^2)	QY
366.5	1.19e-20	1.000	367.0	1.23e-20	1.000	367.5	1.27e-20	1.000	368.0	1.31e-20	1.000	368.5	1.35e-20	1.000
369.0	1.40e-20	1.000	369.5	1.44e-20	1.000	370.0	1.47e-20	1.000	370.5	1.51e-20	1.000	371.0	1.55e-20	1.000
371.5	1.59e-20	1.000	372.0	1.64e-20	1.000	372.5	1.70e-20	1.000	373.0	1.73e-20	1.000	373.5	1.77e-20	1.000
374.0	1.81e-20	1.000	374.5	1.86e-20	1.000	375.0	1.90e-20	1.000	375.5	1.96e-20	1.000	376.0	2.02e-20	1.000
376.5	2.06e-20	1.000	377.0	2.10e-20	1.000	377.5	2.14e-20	1.000	378.0	2.18e-20	1.000	378.5	2.24e-20	1.000
379.0	2.30e-20	1.000	379.5	2.37e-20	1.000	380.0	2.42e-20	1.000	380.5	2.47e-20	1.000	381.0	2.54e-20	1.000
381.5	2.62e-20	1.000	382.0	2.69e-20	1.000	382.5	2.79e-20	1.000	383.0	2.88e-20	1.000	383.5	2.96e-20	1.000
384.0	3.02e-20	1.000	384.5	3.10e-20	1.000	385.0	3.20e-20	1.000	385.5	3.29e-20	1.000	386.0	3.39e-20	1.000
386.5	3.51e-20	1.000	387.0	3.62e-20	1.000	387.5	3.69e-20	1.000	388.0	3.70e-20	1.000	388.5	3.77e-20	1.000
389.0	3.88e-20	1.000	389.5	3.97e-20	1.000	390.0	4.03e-20	1.000	390.5	4.12e-20	1.000	391.0	4.22e-20	1.000
391.5	4.29e-20	1.000	392.0	4.30e-20	1.000	392.5	4.38e-20	1.000	393.0	4.47e-20	1.000	393.5	4.55e-20	1.000
394.0	4.56e-20	1.000	394.5	4.59e-20	1.000	395.0	4.67e-20	1.000	395.5	4.80e-20	1.000	396.0	4.87e-20	1.000
396.5	4.96e-20	1.000	397.0	5.08e-20	1.000	397.5	5.19e-20	1.000	398.0	5.23e-20	1.000	398.5	5.39e-20	1.000
399.0	5.46e-20	1.000	399.5	5.54e-20	1.000	400.0	5.59e-20	1.000	400.5	5.77e-20	1.000	401.0	5.91e-20	1.000
401.5	5.99e-20	1.000	402.0	6.06e-20	1.000	402.5	6.20e-20	1.000	403.0	6.35e-20	1.000	403.5	6.52e-20	1.000
404.0	6.54e-20	1.000	404.5	6.64e-20	1.000	405.0	6.93e-20	1.000	405.5	7.15e-20	1.000	406.0	7.19e-20	1.000
406.5	7.32e-20	1.000	407.0	7.58e-20	1.000	407.5	7.88e-20	1.000	408.0	7.97e-20	1.000	408.5	7.91e-20	1.000
409.0	8.11e-20	1.000	409.5	8.41e-20	1.000	410.0	8.53e-20	1.000	410.5	8.59e-20	1.000	411.0	8.60e-20	1.000
411.5	8.80e-20	1.000	412.0	9.04e-20	1.000	412.5	9.45e-20	1.000	413.0	9.34e-20	1.000	413.5	9.37e-20	1.000
414.0	9.63e-20	1.000	414.5	9.71e-20	1.000	415.0	9.70e-20	1.000	415.5	9.65e-20	1.000	416.0	9.69e-20	1.000
416.5	9.89e-20	1.000	417.0	1.00e-19	1.000	417.5	1.02e-19	1.000	418.0	1.00e-19	1.000	418.5	1.02e-19	1.000
419.0	1.01e-19	1.000	419.5	1.01e-19	1.000	420.0	1.03e-19	1.000	420.5	1.01e-19	1.000	421.0	1.04e-19	1.000
421.5	1.05e-19	1.000	422.0	1.06e-19	1.000	422.5	1.04e-19	1.000	423.0	1.05e-19	1.000	423.5	1.05e-19	1.000
424.0	1.01e-19	1.000	424.5	1.01e-19	1.000	425.0	1.05e-19	1.000	425.5	1.03e-19	1.000	426.0	1.02e-19	1.000
426.5	1.01e-19	1.000	427.0	9.77e-20	1.000	427.5	9.81e-20	1.000	428.0	1.00e-19	1.000	428.5	1.02e-19	1.000
429.0	9.89e-20	1.000	429.5	9.85e-20	1.000	430.0	1.04e-19	1.000	430.5	1.08e-19	1.000	431.0	1.05e-19	1.000
431.5	1.02e-19	1.000	432.0	9.64e-20	1.000	432.5	1.01e-19	1.000	433.0	1.06e-19	1.000	433.5	1.09e-19	1.000
434.0	1.04e-19	1.000	434.5	1.03e-19	1.000	435.0	1.07e-19	1.000	435.5	1.16e-19	1.000	436.0	1.09e-19	1.000
436.5	1.11e-19	1.000	437.0	9.81e-20	1.000	437.5	9.71e-20	1.000	438.0	1.06e-19	1.000	438.5	1.16e-19	1.000
439.0	1.08e-19	1.000	439.5	1.05e-19	1.000	440.0	9.70e-20	1.000	440.5	1.01e-19	1.000	441.0	1.04e-19	1.000
441.5	1.07e-19	1.000	442.0	1.02e-19	1.000	442.5	9.68e-20	1.000	443.0	1.00e-19	1.000	443.5	1.14e-19	1.000
444.0	1.13e-19	1.000	444.5	1.03e-19	1.000	445.0	9.74e-20	1.000	445.5	8.46e-20	1.000	446.0	8.70e-20	1.000
446.5	9.97e-20	1.000	447.0	1.01e-19	1.000	447.5	9.15e-20	1.000	448.0	9.41e-20	1.000	448.5	8.99e-20	1.000
449.0	1.10e-19	1.000	449.5	9.12e-20	1.000	450.0	8.56e-20	1.000	450.5	8.28e-20	1.000	451.0	6.15e-20	1.000
451.5	5.56e-20	1.000	452.0	6.47e-20	1.000	452.5	7.27e-20	1.000	453.0	5.75e-20	1.000	453.5	5.08e-20	1.000
454.0	4.38e-20	1.000	454.5	3.81e-20	1.000	455.0	3.61e-20	1.000	455.5	3.61e-20	1.000	456.0	3.13e-20	1.000
456.5	2.72e-20	1.000	457.0	2.44e-20	1.000	457.5	2.22e-20	1.000	458.0	1.82e-20	1.000	458.5	1.43e-20	1.000
459.0	1.32e-20	1.000	459.5	1.05e-20	1.000	460.0	8.95e-21	1.000	460.5	8.90e-21	1.000	461.0	7.94e-21	1.000
461.5	7.04e-21	1.000	462.0	6.46e-21	1.000	462.5	5.63e-21	1.000	463.0	4.78e-21	1.000	463.5	3.94e-21	1.000
464.0	3.26e-21	1.000	464.5	2.97e-21	1.000	465.0	2.65e-21	1.000	465.5	2.46e-21	1.000	466.0	2.27e-21	1.000
466.5	2.08e-21	1.000	467.0	1.86e-21	1.000	467.5	1.76e-21	1.000	468.0	1.60e-21	1.000	468.5	1.44e-21	1.000
469.0	1.34e-21	1.000	469.5	1.20e-21	1.000	470.0	1.07e-21	1.000	470.5	1.02e-21	1.000	471.0	9.92e-22	1.000
471.5	9.97e-22	1.000	472.0	8.87e-22	1.000	472.5	8.27e-22	1.000	473.0	7.76e-22	1.000	473.5	7.15e-22	1.000
474.0	6.71e-22	1.000	474.5	6.67e-22	1.000	475.0	6.10e-22	1.000	475.5	6.17e-22	1.000	476.0	5.54e-22	1.000
476.5	5.22e-22	1.000	477.0	5.10e-22	1.000	477.5	5.17e-22	1.000	478.0	4.80e-22	1.000	478.5	4.71e-22	1.000
479.0	4.60e-22	1.000	479.5	4.35e-22	1.000	480.0	3.90e-22	1.000	480.5	3.71e-22	1.000	481.0	3.62e-22	1.000
481.5	3.52e-22	1.000	482.0	3.05e-22	1.000	482.5	3.05e-22	1.000	483.0	2.86e-22	1.000	483.5	2.53e-22	1.000
484.0	2.75e-22	1.000	484.5	2.59e-22	1.000	485.0	2.47e-22	1.000	485.5	2.36e-22	1.000	486.0	2.12e-22	1.000
486.5	1.89e-22	1.000	487.0	1.93e-22	1.000	487.5	1.86e-22	1.000	488.0	1.82e-22	1.000	488.5	1.75e-22	1.000
489.0	1.74e-22	1.000	489.5	1.72e-22	1.000	490.0	1.66e-22	1.000	490.5	1.75e-22	1.000	491.0	1.54e-22	1.000
491.5	1.74e-22	1.000	492.0	1.63e-22	1.000	492.5	1.53e-22	1.000	493.0	1.52e-22	1.000	493.5	5.85e-23	1.000
494.0	0.00e+00	1.000												

Table A-4. Chamber effect and background characterization parameters used in the environmental chamber model simulations for mechanism evaluation.

Cham.	Set [a]	Value	Discussion
NO_2 photolysis rate			Light intensity as measured by the NO_2 photolysis rate. The rate constants for the other photolysis reactions are calculated using the NO_2 photolysis rate assigned to the experiment and the photolysis rate constant ratios calculated using the relative spectral distribution for the light source.
DTC	704-779	0.161	Results of the actinometry experiments indicated that the light intensity was relatively constant for runs carried out during this period, and average light intensity values are used.
RN-I (ppb)			Ratio of the rate of wall + hν -> HONO to the NO_2 photolysis rate.
DTC	18	0.066	Average of value of RS-I that gave best fits to n-butane - NOx chamber experiments carried out in this chamber. The initial HONO was optimized at the same time. If a temperature dependence is shown, it was derived from the temperature dependence of the RN-I values that best fit characterization data in outdoor chamber experiments, with the same activation energy used in all cases. If a temperature dependence is not shown, then the temperature variation for experiments in this set is small compared to the run-to-run variability in the best fit RN-I values. Note that the radical source in Sets 3, 12, 13, and 16 runs was anomalously high. Any dependence of apparent radical source on initial NOx levels in Teflon bag chambers was found to be much less than the run-to-run variability.
HONO-F (unitless)			Ratio of the initial HONO concentration to the measured initial NO_2. [The initial NO_2 in the experiment is reduced by a factor of 1 - (HONO-F)]. Unless the characterization data indicate otherwise, it is assumed that the initial HONO is introduced with the NO2 injection, so is it is assumed to be proportional to the initial NO2 concentration.
DTC	18	0.8%	Average of value of initial HONO to initial NO2 that gave best fits to n-butane - NO_x chamber experiments carried out in this chamber. The RN-I parameter was optimized at the same time.
E-NO2/K1 (ppb)			Ratio of rate of NO2 offgasing from the walls to the NO2 photolysis rate.
All Teflon Bag Chambers		0	The NOx offgasing caused by representing the radical source by HONO offgasing appears to be sufficient for accounting for NOx offgasing effects in most cases. RN-I parameters adjusted to fit experiments sensitive to the radical source are consistent with NOx offgasing rates adjusted to fit pure air or aldehyde - air runs, to within the uncertainty and variability.
K(NO2W) (min^{-1})			Rate of unimolecular loss (or hydrolysis) of NO2 to the walls.
All Teflon Bag Chambers		1.6e-4	Based on dark NO_2 decay and HONO formation measured in the ETC by Pitts et al. (1984). Assumed to be the same in all Teflon bag chambers, regardless of volume.
YHONO			Yield of HONO in the unimolecular reaction (hydrolysis) of NO2 on the walls.
All Teflon Bag Chambers		0.2	Based on dark NO_2 decay and HONO formation measured in the ETC by Pitts et al. (1984). Assumed to be the same in all Teflon bag chambers, regardless of volume.

Table A-4 (continued)

Cham.	Set [a]	Value	Discussion
K(O3W) (min^{-1})			Unimolecular loss rate of O_3 to the walls.
DTC	All	1.5e-4	Based on results of O_3 decay in Teflon bag chambers experiments as discussed by Carter et al (1995c).
CTC	All	8.5e-5	Based on results of O_3 decay experiments in this chamber
k(N26I) (min^{-1})			Rate constant for N_2O_5 -> 2 Wall-NO_x. This represents the humidity-independent portion of the wall loss of N_2O_5, or the intercept of plots of rates of N_2O_5 loss against humidity.
All Teflon Bag Chambers		2.8e-3	Based on N_2O_5 decay rate measurements made by Tuazon et al (1983) for the ETC. Assumed to be independent of chamber size (Carter et al, 1995c).
k(N26S) (ppm^{-1} min^{-1})			Rate constant for N_2O_5 + H_2O -> 2 Wall-NO_x. This represents the humidity dependent portion of the wall loss of N_2O_5, or the slope of plots of rates of N_2O_5 loss against humidity.
All Teflon Bag Chambers		1.1e-6	Based on N_2O_5 decay rate measurements made by Tuazon et al (1983) for the ETC. Assumed to be independent of chamber size (Carter et al, 1995c).
k(XSHC) (min^{-1})			Rate constant for OH -> HO_2. This represents the effects of reaction of OH with reactive VOCs in the background air or offgased from the chamber walls. This parameter does not significantly affect model simulations of experiments other than pure air runs.
All Teflon Bag Chambers		250	Estimated from modeling several pure air in the ITC (Carter et al, 1996d), and also consistent with simulations of pure air runs in the ETC (Carter et al, 1997b).
H2O (ppm)			Default water vapor concentration for runs where no humidity data are available.
DTC	all	1.0e+3	Experiments in this chamber were carried out using dried purified air. The limited humidity data for such runs indicate that the humidity was less than 5%, probably no more than ~2.5%, and possibly much less than that. The default value corresponds to ~2.5 - 3% RH for the conditions of most experiments.

[a] Set refers to the characterization set, which refers to the group of experiments assumed to have the same run conditions and represented using the same chamber-dependent parameters. See Carter et al (1995) for more discussion. All experiments carried out for this program are assigned characterization set 18.